NOTICE

The quality of this microform is heavily dependent upon the quality of the original thesis submitted for microfilming. Every effort has been made to ensure the highest quality of reproduction possible.

If pages are missing, contact the university which granted the degree.

Some pages may have indistinct print especially if the original pages were typed with a poor typewriter ribbon or if the university sent us an inferior photocopy.

Reproduction in full or in part of this microform is governed by the Canadian Copyright Act, R.S.C. 1970, c. C-30, and subsequent amendments.

AVIS

La qualité de cette microforme dépend grandement de la qualité de la thèse soumise au microfilmage. Nous avons tout fait pour assurer une qualité supérieure de reproduction.

S'il manque des pages, veuillez communiquer avec l'université qui a conféré le grade.

La qualité d'impression de certaines pages peut laisser à désirer, surtout si les pages originales ont été dactylographiées à l'aide d'un ruban usé ou si l'université nous a fait parvenir une photocopie de qualité inférieure.

La reproduction, même partielle, de cette microforme est soumise à la Loi canadienne sur le droit d'auteur, SRC 1970, c. C-30, et ses amendements subséquents.

PERMEATION OF PURE GASES THROUGH POLYAMIDE MEMBRANES AND LAMINATED POLYAMIDE MEMBRANES

By

Frank Joseph Stanisic

A THESIS

SUBMITTED TO THE DEPARTMENT OF CHEMICAL ENGINEERING

AND THE SCHOOL OF GRADUATE STUDIES

OF THE UNIVERSITY OF OTTAWA

IN PARTIAL FULFILLMENT OF THE REQUIREMENTS

FOR THE DEGREE OF

MASTER OF APPLIED SCIENCE

IN

CHEMICAL ENGINEERING

NOTICE

The quality of this microform is heavily dependent upon the quality of the original thesis submitted for microfilming. Every effort has been made to ensure the highest quality of reproduction possible.

If pages are missing, contact the university which granted the degree.

Some pages may have indistinct print especially if the original pages were typed with a poor typewriter ribbon or if the university sent us an inferior photocopy.

Reproduction in full or in part of this microform is governed by the Canadian Copyright Act, R.S.C. 1970, c. C-30, and subsequent amendments.

AVIS

La qualité de cette microforme dépend grandement de la qualité de la thèse soumise au microfilmage. Nous avons tout fait pour assurer une qualité supérieure de reproduction.

S'il manque des pages, veuillez communiquer avec l'université qui a conféré le grade.

La qualité d'impression de certaines pages peut laisser à désirer, surtout si les pages originales ont été dactylographiées à l'aide d'un ruban usé ou si l'université nous a fait parvenir une photocopie de qualité inférieure.

La reproduction, même partielle, de cette microforme est soumise à la Loi canadienne sur le droit d'auteur, SRC 1970, c. C-30, et ses amendements subséquents.

ISBN 0-315-60574-X

UNIVERSITÉ D'OTTAWA
UNIVERSITY OF OTTAWA

Abstract

Asymmetric polyamide membranes of different porosities were prepared by varying the oven evaporation times. Permeation rates of hydrogen, helium, methane, nitrogen, oxygen, and carbon dioxide, for pressures between 345 and 2068 kPa, were measured for the above membranes and for the same membranes laminated with silicone rubber. The surface force pore flow model was employed to characterize and subsequently predict the permeation rates through the polyamide membranes; whereas, the modified resistance model was employed to analyze the experimental data of the laminated membranes. Membrane performance for various substrate porosities and lamination thicknesses were simulated by the modified resistance model.

Acknowledgement

I would like to express my gratitude to Dr. S. Sourirajan and Dr. T. Matsuura for their insight, guidance and assistance throughout the course of this work. I am also grateful to Dr. A. Fouda, from the National Research Council of Canada, whose knowledge of computer programing was very helpful.

I consider myself fortunate in being able to do my research at the Industrial Membrane Research Institute where the fellow students and researchers made my stay a most rewarding and enlightening experience - thank you.

Financial assistance provided by Shell Canada and NSERC is greatly appreciated. Their contributions enabled this work to be completed.

Nomenclature

0.1 Resistance Model

A_1	area of top layer which is over the substrate's membrane matrix (membrane matrix consists of network pores), m^2
$A_{1'}$	area of top layer which is over the substrates's pores (aggregate pores), m^2
A_2	area of substrate membrane matrix (composed of network pores), m^2
A_3	area of the pores (aggregate pores) on the surface of the substrate membrane, m^2
A_t	total area available for permeation, $A_t = A_2 + A_3 = A_1 + A_{1'}$, m^2
l_1,$l_{1'}$	thickness of top layer of section 1 and 1', m
l_2	effective thickness of substrate membrane, m
l_3	effective thickness of pores (aggregate pores) in substrate membrane, m
$P_{j,i}$	intrinsic permeability of section j for gas i where j = 1, 1', 2, 3 and i = H_2, He, N_2, O_2, CO_2, CH_4, mol.m/m^2.s.Pa
ΔP	pressure difference across the membrane, Pa
Q_i	permeation rate of component i, mol/s
$(R_j)_i$	resistance to flux for section j for gas i, Pa.s/mol
$(R_t)_i$	total resistance to flux for gas i through the substrate membrane, Pa.s/mol

$(R_t^L)_i$ total resistance to flux for gas i through the laminated membrane, Pa.s/mol

0.1.1 Greek Letters

α_j $= (R_j)_i/(R_j)_{H_2}$, resistance of gas i flux over the resistance of H_2 flux for section j

α_t $= (R_t)_i/(R_t)_{H_2}$, total resistance of gas i flux over the total resistance of H_2 flux for the substrate membrane

α_t^L $= (R_t^L)_i/(R_t^L)_{H_2}$, total resistance of gas i flux over the total resistance of H_2 flux for the composite membrane

0.2 Pore Flow Model

A_1	constant for a given membrane related to the porous structure, m^{-3}
A_2	constant related to surface transport, $kmol/m^3.s.Pa^2$
A_G	gas permeability coefficient, $kmol/m^2.s.Pa$
C_R	coefficient of resistance for transport of adsorbed molecules, $kg/s.m^2$
$\overline{c}$	mean speed of the gas molecules, m/s
d	collision diameter of gas molecules, m
G_1, G_2, G_3	a physicochemical constant
I_j	quantities defined in chapter 2, $j = 1$ to 5
k_H	Henry's adsorption constant
M	molecular weight of the gas, kg/kmol
N	Avogadro's number
$N(R)$	number of pores having a radius R, m^{-1}
N_t	total number of pores, having radii from zero to R_{max}
P	pressure, Pa
P_2	pressure (absolute) on the high pressure side of the membrane, Pa
ΔP	pressure differential across the membrane, Pa
$\overline{P}$	mean pressure across the membrane, Pa
Q_K, Q_v, Q_{sl}	quantity of gas transported in the gas phase by Knudsen, viscous, and slip mechanisms, respectively, kmol/s
Q_g	summation of Q_K, Q_v, Q_{sl}, kmol/s
Q_s	quantity of gas transported by surface flow mechanism, kmol/s
Q_t	total quantity of gas transported ie., summation of Q_g and Q_s, kmol/s

q_K, q_v, q_{sl}	quantity of gas transported through a single capillary by Knudsen, viscous, and slip mechanisms, respectively, kmol/s
R	pore radius, m
$\overline{R}$	mean pore radius, m
R_{max}	radius of the largest pore, m
$\mathbf{R}$	gas constant, m^3.Pa/K.kmol
S	membrane area, m^2
T	absolute temperature, K

0.2.1 Greek Letters

Δ_i	radius correction factor, a constant for gas i for a given membrane material, m
δ	equivalent thickness of the membrane, m
λ	mean free path of gases, m
ρ_{app}	apparent density of the membrane, kg/m^3
σ	standard deviation for the pore size distribution, m
τ	tortuosity factor for the pores
Φ_i	characteristic parameter, called the relative surface transport coefficient, related to gas-membrane interaction

Contents

List of Tables

List of Figures

Chapter 1

Introduction

1.1 Objective

This project involved the study of pure gas permeation through polyamide membranes with and without lamination of a second polymeric material (silicone rubber). The objective of this work was to gain a clearer understanding of how permeation occurs through the membrane and how separation factors may be improved by changing the lamination thickness and/or surface porosity of the polyamide.

This introduction deals solely with the important historical outcomes and current studies relevant to the gas separation field using membranes. More importantly only polymeric membrane materials will be discussed in this work. There are, of course, numerous other materials used for membranes today but polymeric materials (cellulose acetates, polyamides, polyimides, silicone rubbers, etc.) are still the most widely used and thus are deemed the most important.

1.2 Historical Overview

Gas separation using membranes in industry is a relatively new field even though knowledge of their potential was known back in 1866, when Thomas Graham noticed that various gases possessed different permeation velocities through a membrane. It was not until the 1940's that membranes were used industrially to enrich uranium 235 from approximately 0.71% to approximately 3% by weight, but this method was employed solely for the lack of an alternative process [55].

Membranes had one major obstacle to overcome before they could be truly integrated into industry; they had to be economically feasible when compared with the conventional separation methods such as absorption, adsorption and cryogenic processes. Prior to the 1960's, membranes lacked high permeability and separation efficiency. However, this problem was overcome when Loeb and Sourirajan [22] developed an asymmetric cellulose acetate membrane for water desalination by reverse osmosis. This major breakthrough heralded the onset of the golden age of membranology. Their membrane consisted of a thin dense skin supported on a highly porous substructure. The separation of differing components occurs in the skin layer, while the porous substructure provides the mechanical strength for the membrane.

This same membrane, when dried by Gantzel and Merten [11] in 1968, gave a high flux for helium when compared to nitrogen. Unfortunately their method of drying the membrane by quick freezing and vacuum sublimation was uneconomical for industrial use [32].

It was the early 1970's when an economical method of drying the wet reverse osmosis membrane was developed. A solvent exchange method was employed where the water in the membrane is replaced with a volatile solvent after which the membrane can be air dried. A number of researchers [52,49,25,24] were responsible

for the successful implementation of this drying method with Schell's [40] solvent exchange technique being the most widely used in industry.

Asymmetric membranes were first prepared from cellulose acetate, but can now be made from a variety of polymeric materials. However, it has been found that most polymers (other than cellulose acetate) are difficult to make into useful asymmetric membranes for gas separations. Membranes that are useful for liquid separations (reverse osmosis) are found to be inadequate for gas separations. Basically the pores of the RO membrane are too large thereby permitting viscous flow to occur and as a result low separation prevails. The difficulty in developing a straightforward process for producing large quantities of highly permselective membranes with sufficiently high permeation rates hampered membrane technology from entering into the competitive gas separation market.

It was in 1979, when Henis and Tripodi [15,13,14] developed a composite membrane with high permeation and selectivity, that membranes penetrated into the gas separation field. Their approach was to choose a polymer material which has good separation properties for a particular gas mixture. Make an asymmetric membrane out of this material with the skin layer as thin as possible and then coat this membrane with a second material (rubbery polymer) that possessed good permeation properties. The coating material supposedly eliminates any pores and defects that are inherent to the asymmetric membrane. The composite membrane was the latest major innovation, and economically the most successful breakthrough to occur for membranes in gas separations.

1.3 Applications

Today gas separation with membranes is widely accepted in the traditional chemical and petroleum refining industries. The principal applications of these gas separation

membrane systems include recovery of hydrogen from refinery streams for recycling, removal of carbon dioxide and hydrogen sulfide from natural gas, production of nitrogen and enriched air, recovery of methane from mines and landfills, and recovery of certain gases from exhausts [46,12,39].

Removal of hydrogen sulfide and carbon dioxide from natural gas is an ideal application for membranes since both H_2S and CO_2 permeate through the membrane approximately 30 times faster than methane [41]. Natural sour gas is found in very large amounts in the western great plains from Texas to Northern Alberta. The gas found in the southern regions generally contains large amounts of carbon dioxide and methane with small amounts of hydrogen sulfide. In contrast, vast amounts of gas containing 30 mole% of hydrogen sulfide are found in Alberta [39].

Membrane technology can be integrated into existing sour gas processing plants where it would increase the capacity and reduce the energy load of the existing system or eliminate the need for expanding the existing plant when wellhead pressure loss or increased acid gas content occurs [41].

Another application related to sour gas processing is the recovery and reuse of carbon dioxide in enhanced oil recovery (EOR). In EOR production high pressure fluids are injected into the well reservoir to swell and fracture the formation. Next, a slurry of sand is fed into the well to fill the fracture. This forms a highly porous channel for gas and acid to flow to production wells. Carbon dioxide is used as the pressurizing fluid for gas and oil well fracture. A membrane system can be used to recover the CO_2 for reinjection and at the same time used to recover the light hydrocarbons.

Hydrogen recovery from shale, tar sands, and coal conversion processes is another potential application of membranes in the gas industry. These processes often involve high-pressure streams that must be treated in some fashion to recover the valuable H_2.

The separation of nitrogen and oxygen from air is once again of particular interest to the gas industry. Nitrogen is used as an inert purge gas in many processes throughout the chemical industry, and is used for this purpose in substitute natural gas. Nitrogen is also used in EOR applications the same way as carbon dioxide. There are also many uses for a membrane N_2 system in offshore oil production (see [20] for offshore uses). Few industrial plants are without either liquid nitrogen storage or nitrogen production facilities. Membranes must compete with gas cylinders, delivered liquids, on-site pressure swing adsorption, and on-site cryogenic production. In general, for separating nitrogen and oxygen from air membranes are most attractive for the lower volume, lower purity applications [3]. Novel uses for nitrogen gas obtained via membranes are discussed by Bhat et al. [4].

Product streams enriched in oxygen have a major potential market for enhanced combustion. Also a particulate-free stream with a slightly increased oxygen content has many applications in the biomedical field. For example, systems employing silicone rubber membranes produce oxygen-enriched air for home use by asthmatic and others who have lung diseases [2].

One of the newer sources of methane gas comes from landfill as well as digester gas. Both of these gases are approximately 50% CO_2 and 50% CH_4. This high CO_2 concentration and low volume of gas is ideal for membrane processing [37]. Monsanto reports one plant in Alabama which treats 100,000 SCFD and upgrades the gas from 600 Btu/SCF to 960 Btu/SCF [42].

1.4 Business Outlook

Membrane business as a whole is expected to grow at a rate of 10 to 15% per year, with gas separation systems being the main growth area. Du Pont estimates that the present market for gas separation systems is expected to grow to $1.5

billion by 1995. The principal applications are air enrichment for combustion and high-purity nitrogen for blanketing and use as an inert medium. Other major applications would be sweetening pipeline gas and recovering carbon dioxide for reinjection in tertiary oil recovery. The recovery of hydrogen from process streams in refineries and chemical plants is expected to be the largest market for membrane gas separations. The world demand for hydrogen could double by the year 2000, suggested a representative of Du Pont [12].

Predictions such as these have caused industries to react accordingly. The quickest way for developers of advanced technologies to upgrade their in-house engineering skills is through joint ventures. Thus, there have been a number of joint ventures within the gas separation membrane area. For example, Du Pont has recently joined with Air Liquid, the world's largest industrial gas company, to develop, manufacture, and market gas separation systems based on polymeric membrane technology. The first application will be hydrogen recovery systems. Early in May 1988 Air Products & Chemicals and Akzo of Netherlands announced a joint venture to develop membranes for air separation. Also Dow Chemical and U.K.'s BOC recently agreed to develop capabilities in membrane air separation systems. They will manufacture and sell non-cryogenically produced oxygen and nitrogen using BOC's pressure swing absorption technology and Dow's hollow-fibre membrane technology [12].

1.5 Models for Gas Transport

In the literature there can be found several approaches to describe gas transport through a membrane. At one extreme, as in the solution-diffusion model, there is no clear-cut route for transport; while others, like the preferential sorption-capillary flow mechanism, involves definite pores and capillaries [28]. Also there are hundreds

of materials from which membranes can be made, each with its own structural and chemical characteristics. As a result the models describing membrane transport are specific to the particular type of penetrant-membrane material employed.

Models describing gas transport through the so called "homogenous" (non-porous) membranes generally depend on whether the polymer is in its "rubbery" or "glassy" state. The solution-diffusion model and the free volume model have been cited in literature for rubbery polymers whereas the dual sorption model is associated with the glassy state. On the other hand, membranes that have pores (there is a question as to the validity of a membrane having no pores) are described by the surface force-pore flow model.

1.5.1 Membrane Material and Morphology

Membranes may be classified according to their material, morphology, and packaging geometry. The first two factors dictate the permeability and selectivity, while the third is important to the design of practical gas modules.

The material and morphology play an important role in deciding which transport model should be used. There are many types of membrane materials being used in research with the polymeric material being the most popular. The use of glassy or amorphous polymers (cellulose acetates, polyamides, polysulfones, polyimides) and rubbery polymers (silicone rubbers, nitrile rubbers) are the most common polymeric materials.

The natural and synthetic rubbery polymers are the most permeable of the polymeric materials to the permeant gases. Unfortunately as a trade off to their high permeability they have very low selectivities. These polymers, in general, are used as a second coating material or laminant over glassy membranes for the purpose of protecting and/or enhancing separation of the substrate membrane.

Glassy polymers tend to have very high selectivities with permeation rates dependent on the morphology of the membrane. As mentioned before, prior to the 1960's membranes from glassy polymers lacked adequate permeation rates for integration into industry. These membranes were homogenous in structure with thicknesses greater than 25 μm and as a result had very low permeation rates.

With the advent of the asymmetric morphology, membrane technology could finally become industrially competitive. In the Loeb - Sourirajan technique, a solution containing approximately 20% polymer is cast on a glass plate which is then immersed in a water bath. The water rapidly precipitates the top surface of the cast film forming the permselective skin. This skin then slows the entry of water into the underlying polymer solution, which thus precipitates much more slowly, forming a more porous substructure. The rate of gas permeation through the asymmetric membrane will be very high compared to a homogenous membrane since the permeation rate is inversely proportional to the effective membrane (skin) thickness.

A number of studies support the view that the surface of an asymmetric membrane contains pores. More recently even proponents of the solution diffusion model (this model assumes a non-porous membrane) have acknowledged the existence of "voids" on the membrane surface [8]. The terminology used to describe a pore may be different from one researcher to the next (voids, defects, gaps, etc., have been used) but it all boils down to a pore which, in this thesis, is defined as any space between nonbonded material entities that allows mass transport to occur.

Chern et al. [8] (proponents of solution diffusion mechanism) conclude that, "The control of chain backbone rigidity and intersegmental packing density may provide a means of selectively permitting the passage of relatively compact permeant molecules while substantially restricting the nonpermeant". Is not intersegmental packing density referring to the the void spaces in the membrane?

Meares [30] acknowledges that pores (1-5 nm) arise naturally in membranes and

are caused by the irregular packing of the kinked polymer chain molecules. Thus, the presence of some pores in asymmetric membranes is all but impossible to avoid.

Through various studies on reverse osmosis membranes by Sourirajan, Matsuura [33] and colleagues they found that two distinct Gaussian distributions of pore sizes on the membrane surface are required to predict the experimental separation of reference solutes used in RO experiments. The surface of an asymmetric membrane is believed to contain two types of pores. Network pores that are thought to originate from the spaces between polymer segments which form the polymer network within the polymer aggregate. The other pores are called the aggregate pores, since they are thought to originate from the spaces between polymer aggregates [44].

Kesting [16] also supports this view and states that the skins of RO membranes consist of closely packed spherical nodules (aggregates). He notes, in the case of liquid water permeation, the primary pores are found within the interstices between adjacent nodules (aggregate pores). Likewise with gas separation membranes, permeation can occur through such pores. However, he points out, because of the greater fluidity of gases, permeation takes place as well between the chains in the interior of the spherical nodules (network pores).

Figure 1 shows a schematic representation of the polymer aggregate pore and the network pores.

1.5.2 Solution-Diffusion Model

The mechanism of permeation of gases in rubber using the solution-diffusion model was first proposed by Thomas Graham in 1866. This model postulates that permeation occurs through the following steps: (1) sorption of the penetrant gas in the membrane material; (2) diffusion of dissolved gas through the membrane; and (3) desorption at the opposite interface. Accordingly, the rate of permeation is given by the product of diffusivity of the gas dissolved in the membrane and its concentration

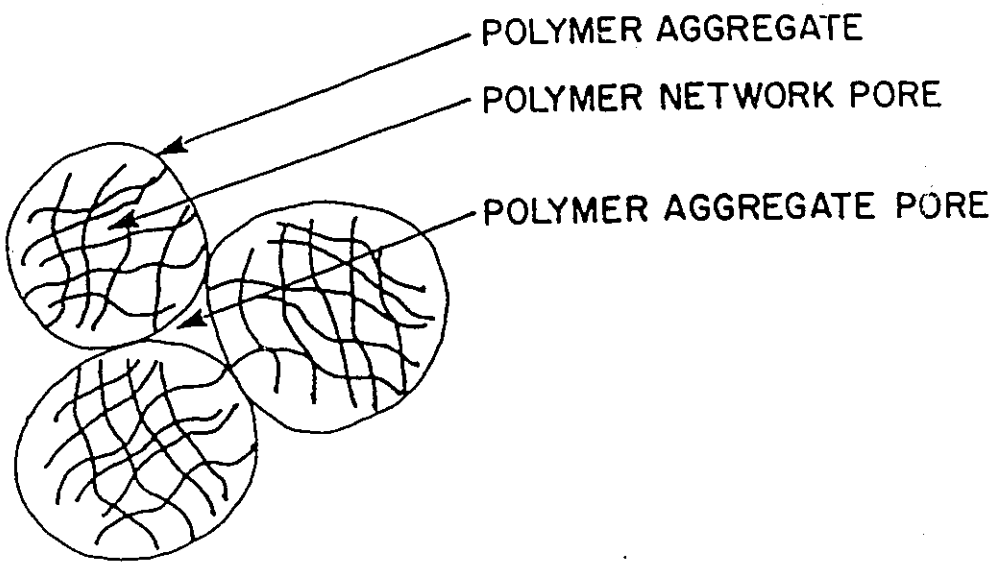

Figure 1: Schematic representation of polymer aggregate pore and network pores.

gradient which in turn is proportional to the gas solubility [26].

Although this model was used originally to describe the permeation through rubber it has been extended to explain the permeation through other polymers with the help of the dual-mode sorption model. It should be noted again that this model assumes that the membrane contains no permanent pores through which gas flow can occur.

1.5.3 Dual-Mode Sorption Model

With the dual sorption model, the solution diffusion mechanism can be used to explain the permeation behavior of gas molecules through glassy polymers. The dual mode theory postulates the existence of two thermodynamically distinct populations of the penetrant gas, namely, molecules dissolved in the polymer by an ordinary dissolution mechanism and molecules residing in a limited number of pre-existing microcavities in the polymer matrix with rapid exchange between the two populations. The ordinary dissolution mechanism obeys Henry's law at equilibrium while the "hole filling" mechanism (molecules residing in microcavities) obeys the non-linear Langmuir-type of isotherm.

There have been numerous studies employing the solution diffusion mechanism with the dual sorption model [38,51,48,56]. A thorough review is given by Vieth et al. [50]. In all of these studies, dense films (homogenous membranes) were employed with the assumption that the membrane is essentially pore free.

1.5.4 Free Volume Model

The free volume approach is based on the theoretical framework proposed by Cohen and Turnball [9]. It was originally developed for the case of self-diffusion in a liquid of hard spheres. It implies that the permeant diffuses by a cooperative movement

of the permeant and the polymer segments, from one "hole" to the other within the polymer, the creation of a "hole" itself caused by fluctuations of local density. Stern and Fang in 1960, using the concept of redistribution of free volume to represent the thermodynamic diffusion coefficient and standard reference state for free volume, interpreted their permeability data for non-porous membranes. Later in 1975, Fang, Stern and Frisch [36] extended the theories to the case of permeation of gas and liquid mixtures.

The usual form of free volume theory [53,54] is based on the premise that the specific volume of a polymer-penetrant mixture is composed of three components, the *occupied volume*, the *interstial free volume*, and the *hole free volume*. The *occupied volume* is defined as the volume of the equilibrium liquid at 0 K, and the remainder of the volume is taken to be the free volume. This free volume is composed of both the *interstial free volume* and the *hole free volume*. The *interstial free volume* is assumed to be distributed uniformly among the molecules of a given species and furthermore the energy for redistribution of this part of the free volume is very large. With the *hole free volume* it is assumed that this quantity can be redistributed without any increase in energy. It is this *hole free volume* that is available for diffusional transport, and hence, it is this volume which forms the basis of the framework which is generally utilized for the analysis of diffusion in non-porous membranes.

1.5.5 Preferential Sorption Capillary Flow Mechanism

The above mechanism is described quantitatively by the surface force-pore flow (SFPF) model. This model assumes that there are pores of the size of a few angstroms on the surface of the membrane. Gaseous components are preferentially adsorbed on the surface of these pores and are transported, due to pressure difference, through the pores to the permeate side. The mechanism of transport

involves simultaneous Knudsen, slip, viscous, and surface flow through the porous membranes. The permeation of a given gas mixture through the membrane is explained by defining an interaction parameter which is evaluated using experimental permeation data. The interaction parameter depends on the mixture components, their partial pressures and membrane material. With the determined interaction parameter the preferential sorption capillary flow model describes the performance of the membrane.

There have been a number of studies employing the surface force pore flow model to asymmetric membranes for permeation of both pure and mixed gases [36,29,10,31]. In general, the pore model leads to a useful working transport analysis for interpreting gas permeation data and forms a framework for a predictive procedure for both pure and mixed gases.

To recap this brief summary of the above models, it seems that the solution-diffusion, dual mode sorption, and free volume model are used by people who believe that the "ideal" membrane is a homogeneous (pore free) membrane. Whereas people who use the SFPF model acknowledge the existence of definite pores where transport occurs.

The existence or non-existence of pores in gas separating membranes undoubtedly separates the membrane community into two, and only a brief review was possible in this present discussion. However, I would like to quote a few researchers on the topic of morphology and transport models.

Mazid from his review of transport models in RO membranes concludes, "The solution-diffusion model, and others like it, try to seek an alternative in the so-called homogeneous or perfect membrane which don't exist in practice [28]."

Kesting in his book on Synthetic Polymeric Membranes [17] states, "that it is time to restrict the solution-diffusion model to some specially prepared defect-free dense films which are unrelated to any functional membrane".

Koros et al. [19], proponents of the solution diffusion mechanism wrote that the majority of membranes presently used for the separation of gas mixtures are composed of organic polymers and usually are asymmetric or composite in structure.

It becomes clear that the surface force pore flow model is a transport model that can be used to help understand and model the permeation of gases through industrially applicable membranes (asymmetric membranes).

Gas separation by membranes proves to be an exciting and new technology where further research both on the fundamental level and the more applied level will be welcomed by both the membrane scientist as well as the engineer.

Chapter 2

The Pore Flow and Resistance Model

2.1 Surface Force-Pore Flow Model

For the development of the transport equations it is assumed that the pores on an asymmetric porous membrane are composed of a bundle of cylindrically shaped capillary tubes situated at right angles to the skin layer. The gaseous flow through these tubes is considered to consist of four main flow mechanisms, namely, Knudsen, slip, viscous and surface flows. The first three mechanisms are classed as pore flow and they depend on the pore size involved whereas the fourth mechanism, surface flow, depends on the interaction forces between the gas and the membrane material. The concept of the "pore" used in this work is defined as any space between non bonded material entities in the membrane matrix, through which mass transfer can take place. The equivalent diameter of such a pore is expressed by some distance (however small) greater than zero [45].

Note that all the following symbols are defined in the nomenclature. It has been found that, depending on the relative magnitude of of pore radius, R, and the

mean free path, λ, of the gas, gas molecules pass through a capillary by any one of the pore flow mechanisms stated above. It was reported by Liepmann [21] that Knudsen flow occurs in the pores of radii from 0 to 0.05λ. According to Stahl [47] slip flow occurs in the pores of radii 0.05λ to 50λ, and viscous flow occurs in the pores of radii $> 50\lambda$. Surface flow applies to pores of all sizes. The mean free path, λ is represented by the following equation:

$$\lambda = \frac{\mathbf{R}T}{2^{1/2}\pi d^2 N \overline{P}} \tag{1}$$

A distribution of pore sizes is assumed to occur on the surface of an asymmetric porous membrane, and is usually represented by the normal distribution shown in equation 2. However, other distributions have been used such as the log-normal distribution law adopted in reference [10].

$$N(R) = \frac{N_t}{(2\pi)^{1/2}\sigma} exp\left[-1/2\left(\frac{R-\overline{R}}{\sigma}\right)^2\right] \tag{2}$$

Unless the pore size is very small, the effect of pore blocking by different permeating gases is negligible. Thus, for a given membrane, the standard deviation, σ, is assumed to be constant regardless of the permeating gas. The mean pore radius, $\overline{R}$, on the other hand, is assumed to vary depending on the nature of the gas and the mobility of the adsorbed molecules through the membrane pore.

For a single capillary, the following equations for Knudsen, slip and viscous flow can be used.

Knudsen flow, q_K, occurs when the pore radius is between 0 to 0.05λ

$$q_K = \frac{2\pi R^3}{3}\left(\frac{8\mathbf{R}T}{\pi \mathbf{M}}\right)^{1/2}\left(\frac{\Delta P}{\delta \mathbf{R}T}\right) = \left(\frac{32\pi}{9\mathbf{M}\mathbf{R}T}\right)^{1/2}\frac{R^3\Delta P}{\delta} \tag{3}$$

viscous flow, q_v, occurs when the pore radius is 50λ and larger

$$q_v = \frac{\pi R^4 \overline{P}\Delta P}{8\eta \mathbf{R}T\delta} \tag{4}$$

slip flow, q_{sl}, occurs when the pore radius is between 0.05λ to 50λ

$$q_{sl} = \frac{\pi R^3 \Delta P}{\mathbf{M}\bar{c}\delta} \tag{5}$$

where $\Delta P = (P_2 - P_3)$ is the pressure differential across the membrane and $\bar{c}$ is the mean speed of gas molecules and is given by:

$$\bar{c} = (8\mathbf{R}T/\mathbf{M})^{1/2} \tag{6}$$

The total quantity of gas permeation occurring from the transport of molecules in the gas-phase, Q_g, is simply the sum of q_K, q_{sl} and q_v.

$$\begin{aligned} Q_g &= Q_K + Q_{sl} + Q_v & (7)\\ &= \sum_{R=0}^{R=0.05\lambda} N(R)q_K + \sum_{R=0.05\lambda}^{R=50\lambda} N(R)q_{sl} + \sum_{R=50\lambda}^{R=R_{max}} N(R)q_v & (8) \end{aligned}$$

It is to be noted that the upper limit of each integration is altered by the relative values of R_{max} (arbitrarily set at 100×10^{-10}m) and the upper limit.

Using a pore size distribution as given in equation 2 the summations in equation 8 can be replaced by integrations to give the following expression.

$$Q_g = \frac{N_t}{\delta}\{G_1 I_1 + G_2 I_2 + G_3 I_3\}\Delta P \tag{9}$$

where:

$$G_1 = \left(\frac{32\pi}{9\mathbf{MR}T}\right)^{1/2}; G_2 = \frac{\pi}{\mathbf{M}\bar{c}}; G_3 = \frac{\pi \overline{P}}{8\eta \mathbf{R}T} \tag{10}$$

$$I_1 = \frac{1}{(2\pi)^{1/2}\sigma}\int_{R=0}^{0.05\lambda} R^3 exp\{-1/2\left(\frac{R-\overline{R}}{\sigma}\right)^2\}dR \tag{11}$$

$$I_2 = \frac{1}{(2\pi)^{1/2}\sigma}\int_{R=0.05\lambda}^{50\lambda} R^3 exp\{-1/2\left(\frac{R-\overline{R}}{\sigma}\right)^2\}dR \tag{12}$$

and

$$I_3 = \frac{1}{(2\pi)^{1/2}\sigma}\int_{R=50\lambda}^{R_{max}} R^4 exp\{-1/2\left(\frac{R-\overline{R}}{\sigma}\right)^2\}dR \tag{13}$$

The total gas flow, Q_t is given by the sum of the gas phase flow, Q_g, and the surface flow, Q_s. As mentioned previously the surface flow is the transport of gas molecules under the influence of gas-polymer interactions. Detailed derivations of the surface flow can be found in references [45] and [7].

Following the work done in reference [45] where Henry's gas adsorption isotherm is used in the derivation of the surface flow contribution, equation 14 is obtained.

$$Q_s = \frac{\mathbf{R}T\rho_{app}}{2000\tau C_R \delta^2} k_H^2 \frac{I_4}{I_5} \overline{P} \Delta P \tag{14}$$

where

$$I_4 = \pi \int_{R=0}^{R_{max}} N(R) R^2 dR \tag{15}$$

and

$$I_5 = 2\pi\delta \int_{R=0}^{R_{max}} N(R) R dR \tag{16}$$

It is desirable to define a gas permeability, A_G, as the amount of gas permeating per second per unit area per unit pressure. Combining equations 9 and 14 and denoting the membrane area as S, we obtain

$$A_G = \frac{Q_t}{S\Delta P} = A_1\{G_1 I_1 + G_2 I_2 + G_3 I_3\} + A_2 \frac{I_4}{I_5} \overline{P} \tag{17}$$

The $G's$ are physicochemical constants and the $I's$ are defined integrals dependent on the porous structure of the membrane. Furthermore:

$$\overline{P} = \frac{P_2 + P_3}{2} \tag{18}$$

A_1 is expressed as:

$$A_1 = \frac{N_t}{S\delta} \tag{19}$$

which is related to the total number of pores and the thickness of a given membrane.

A_2 is expressed, for the case of a Henry's adsorption isotherm, as

$$A_2 = \frac{\mathbf{R}T\rho_{app} {k_H}^2}{2000\tau C_R \delta^2 S} \tag{20}$$

The quantity A_2 is related to the adsorption equilibrium, the mobility of the adsorbed gas and the porous structure of the entire membrane.

2.1.1 The Characterization of Membranes

It has been shown by Rangarajan et al.[36] that the transport of a gas through a membrane can be fully characterized by the four parameters $(A_1)_i$, $(A_2)_i$, $\overline{R}_i$ and σ_i. In order to obtain these four unknowns one must employ the surface force pore flow model in conjunction with the experimental gas permeability coefficient, $A_{G,exptl}$ versus pressure (P_2 or $\overline{P}$) data for gas i.

As noted before the gas permeability coefficient, A_G is given by

$$A_G = A_1\{G_1 I_1 + G_2 I_2 + G_3 I_3\} + A_2 \frac{I_4}{I_5}\overline{P} \tag{21}$$

where the first three terms refer to the pore flow mechanisms of Knudsen, slip, and viscous flow. The last term refers to the surface flow mechanism. The quantities G_1, G_2, and G_3 can be calculated from the physical properties of the feed gas and the operating conditions. The quantities I_1, I_2, I_3, I_4, and I_5 can be calculated when the pore size and pore size distribution are given. The quantity $\overline{P}$ is the mean pressure across the membrane. From equation 21 two unknowns exist A_1 and A_2 along with the pore size, $\overline{R}$, and pore size variance, σ, for a particular gas i.

To obtain these unknowns, values of $\overline{R}$ and σ are assumed and then the optimum set of A_1 and A_2 that best represent the experimental data of A_G versus pressure is chosen. The combination of $(A_1)_i$, $(A_2)_i$, $\overline{R}_i$ and σ_i that yields the smallest sum of the squared residuals (SS_R) according to the equation

$$SS_R = \sum_{i=1}^{n}(A_{G,exptl} - A_{G,calcd})^2 \tag{22}$$

is chosen.

Values of $\overline{R}$ and σ are changed on a two dimensional grid so as to obtain every possible combination for $\overline{R}$ between 1 to 200×10^{-10}m and σ between 1 to 30×10^{-10}m in increments of 0.1×10^{10}m. For each combination of $\overline{R}$ and σ the optimum set of A_1 and A_2 are obtained by the steepest descent method. The corresponding SS_R

is calculated and the set of $(A_1)_i$, $(A_2)_i$, $\overline{R}_i$ and σ_i. that yield the smallest SS_R is designated the characterization set.

2.1.2 Prediction Using SFPF Model

By applying the SFPF model, a membrane can be characterized using four quantities $(A_1)_i$, $(A_2)_i$, $\overline{R}_i$ and σ_i. Rangarajan et al. [36] notes in order to predict the permeation of a gas given the permeation of a reference gas two new parameters need to be defined.

The ratio of A_2 for one gas to that of a reference gas is considered independent of the porous structure of the membrane thus the following relation can be made:

$$(A_2)_i = (A_2)_{ref}\Phi_i \tag{23}$$

where Φ_i is called the relative surface transport coefficient. Furthermore for any gas i, the mean pore radius, $\overline{R}_i$ is

$$\overline{R}_i = R_{ref} + \Delta_i \tag{24}$$

where Δ_i is called the radius correction factor. Values of Φ_i and Δ_i for various gases and membrane materials can be easily generated from the characterization parameters obtained by employing the SFPF model on the experimental data of A_G versus pressure.

Note that the quantity A_1 is assumed to remain constant for a given membrane irrespective of the penetrating gas since $A_1 = N_t/S\delta$.

The steps below illustrate how equation 17 could be used to calculate A_G for any gas through the membrane characterized by a reference gas (helium) at any operating pressure:

1. Determine $(A_1)_{ref}$, $(A_2)_{ref}$, $(\sigma)_{ref}$, and R_{ref} from the experimental pressure versus flux data.

2. For any gas i calculate $\overline{R}_i$ by using equation 24.

3. For the given membrane and the given gas i calculate $(A_2)_i$ using equation 23.

4. Calculate λ, 0.05λ, and 50λ for the mean pressure, $\overline{P}$ using equation 1.

5. Evaluate all the integrals, I_1, I_2, I_3, I_4, and I_5 given by equations 11, 12, 13, 15, 16.

6. From the physicochemical properties of the gas evaluate G_1, G_2, and G_3 using equation 10.

7. Substitute the values obtained from steps 1 thru 6 into equation 17 for the given gas at the given pressure.

The development of transport equations describing the permeation of mixed gases through RO membranes follows the same approach as used to develop the equation describing permeation of pure gases. For a detailed derivation of the SFPF model for pure and mixed gases see reference [45]. Excellent articles that summarize the development of the surface force-pore flow model are references [29] and [36].

The SFPF model is still undergoing slight modification as new insight into the mechanism of transport is discovered. A recent investigation by Chen et al. [7], contributed to the understanding of the surface flow contribution to gas transport. Their work attempted to describe the nature of the adsorbed layer of gas molecules on the polymer surface and the concentration gradient at the gas-polymer interface more clearly. An attempt is also made in this paper to describe the movement of the adsorbed layer on the wall of the pore.

2.2 Resistance Model

In the past, composite membranes have been made by supporting a thin separating membrane on a porous substrate to achieve high fluxes. In these membranes, the coating serves as the separating barrier, and the substrate serves only as a physical support. Henis et al. [15] decided to use the concept of making a membrane with two different materials in a slightly different approach. Their membrane was composite of a porous asymmetric membrane coated on top with a rubbery polymer. According to Henis and Tripodi the asymmetric membrane or substrate polymer should exhibit good separation properties; whereas the coating polymer should have good permeation properties. The porous substrate when appropriately coated serves as the effective separating barrier as well as the physical support of the system and the coating serves to cover any pinholes or defects that occur on the substrate.

To describe the behavior with respect to gas permeation and separation of their new composite membrane, Henis and Tripodi developed the resistance model [13,14]. In the resistance model an analogy is made between gas permeation and electrical flow and the various portions of the composite membrane are described in terms of their resistance to gas permeation.

The permeation rate or flux is given by:

$$Q_i = \frac{P_i A \Delta p_i}{l} \tag{25}$$

where Q_i is the permeation rate of component i, P_i is the intrinsic permeability of the polymer material to component i, A is the cross sectional surface area of the membrane available for permeation, l is the thickness of the membranes through which the component permeates, and Δp_i is the partial pressure difference of component i across the membrane.

The above relation describing the permeation of a gas i through a membrane is

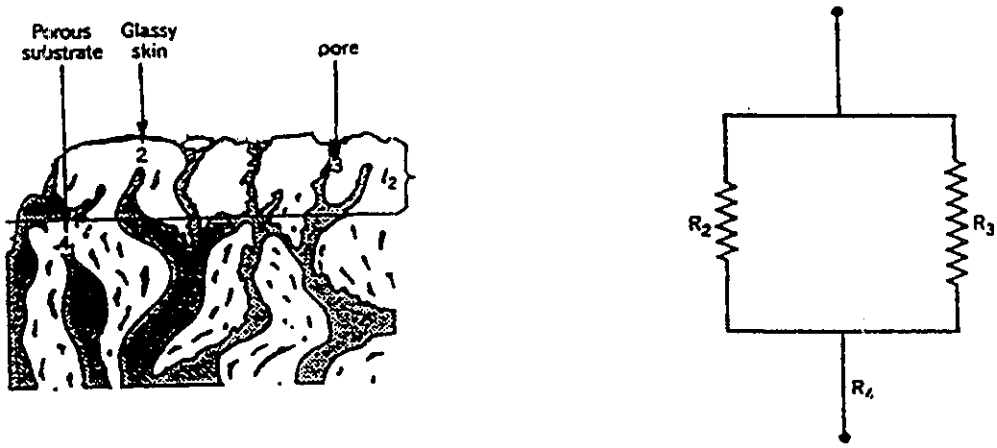

Figure 2: Asymmetric membrane and electric circuit analog.

equivalent to Ohm's law which describes the current flow through a resistor:

$$I = E/R \tag{26}$$

The permeation rate, Q_i is equated to the current I. The partial pressure difference across the membrane, Δp_i, is analogous to the driving force for current flow, E. It is then possible to define a resistance to permeate flow, R_i, which is equivalent to the electrical resistance R :

$$R_i = l/P_i A \tag{27}$$

thus

$$Q_i = \Delta p_i / R_i \tag{28}$$

Figure 2 shows a schematic representation of the cross section of an asymmetric membrane and it's electrical circuit analog. Three regions are defined in this substrate membrane: the skin or surface region, of thickness l_2 is denoted as 2; the pores (aggregate pores) or any defects on the skin is denoted as 3; and the very porous region below the skin layer is denoted as 4.

The total resistance to permeate flow, $(R_t)_i$ of the porous asymmetric membrane is composed of three elements, $(R_2)_i$, the resistance of the polymer matrix

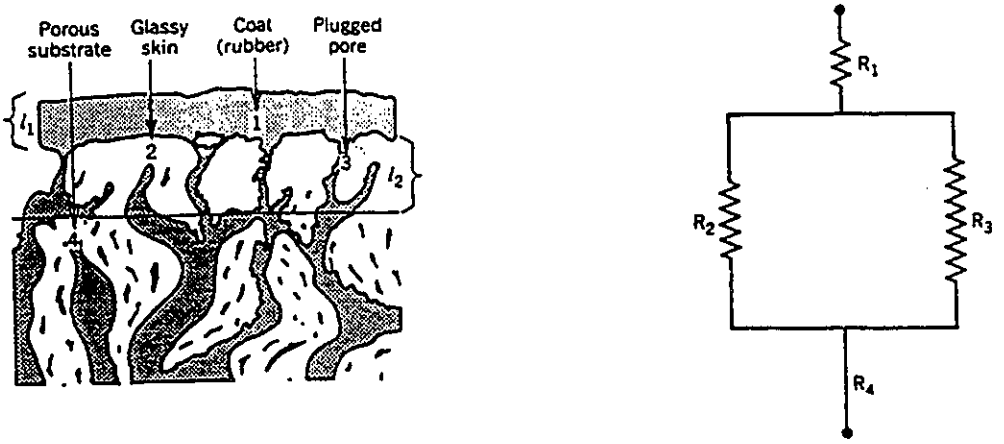

Figure 3: Coated membrane and electric circuit analog.

(network pores) or "dense" portion of the membrane; $(R_3)_i$, the resistance of the pores (aggregate pores) in the surface of the membrane; and $(R_4)_i$, the resistance of the highly porous region below the surface of the membrane. Note the terms that are in parentheses correspond with the terminology used in this thesis, these were not used by Henis and Tripodi.

Using Ohm's law for resistors in parallel and series the following equation can be derived.

$$(R_t)_i = \frac{(R_2)_i(R_3)_i}{(R_2)_i + (R_3)_i} + (R_4)_i \tag{29}$$

Figure 3 shows a schematic representation of the cross section of a composite membrane and it's electrical circuit analog. According to Henis and Tripodi the permeation behavior of their composite membrane is related to the resistance to gas flow of four elements: the porous substrate material (network pores), $(R_2)_i$; the pores (aggregate pores) in the skin layer, $(R_3)_i$; the open internal structure, $(R_4)_i$; and the coating material, $(R_1)_i$. Again, using Ohm's law for resistors in parallel and series, the following equation can be derived for the total resistance of gas

permeation through a composite membrane.

$$(R_t^L)_i = (R_1)_i + \frac{(R_2)_i(R_3)_i}{(R_2)_i + (R_3)_i} + (R_4)_i \tag{30}$$

Henis and Tripodi note that for high flux and good separating properties of the substrate membrane it is desirable to have very open internal structures, and therefore $(R_4)_i$ should be negligible compared to $(R_1)_i$, $(R_2)_i$ and $(R_3)_i$. Thus equations 29 and 30 simplify to

$$(R_t)_i = \frac{(R_2)_i(R_3)_i}{(R_2)_i + (R_3)_i} \tag{31}$$

$$(R_t^L)_i = (R_1)_i + \frac{(R_2)_i(R_3)_i}{(R_2)_i + (R_3)_i} \tag{32}$$

Although this model describes the composite membrane when the top layer is coated onto the porous substrate it fails to describe the situation when the top layer is laminated to the porous substrate. In the next section a model based on the resistance approach will be applied to the case where the porous substrate is laminated with a second polymeric membrane.

2.3 Modified Resistance Model

2.3.1 Development of Modified Resistance Model

The modified resistance model was developed by Matsuura et al. [27] at the National Research Council of Canada. As in the Henis's resistance model an analogy is made between the resistance of gas flow and electrical flow. Whereas Henis's model is used exclusively when the substrate is coated with a polymer, the modified resistance model presented in this section can be used when the substrate membrane is either coated or laminated with a second polymer on top. As a result of this difference two new elements of resistance to gas flow arise, namely $(R_{1'})_i$ and possibly $(R_x)_i$. These two new terms will be explained later.

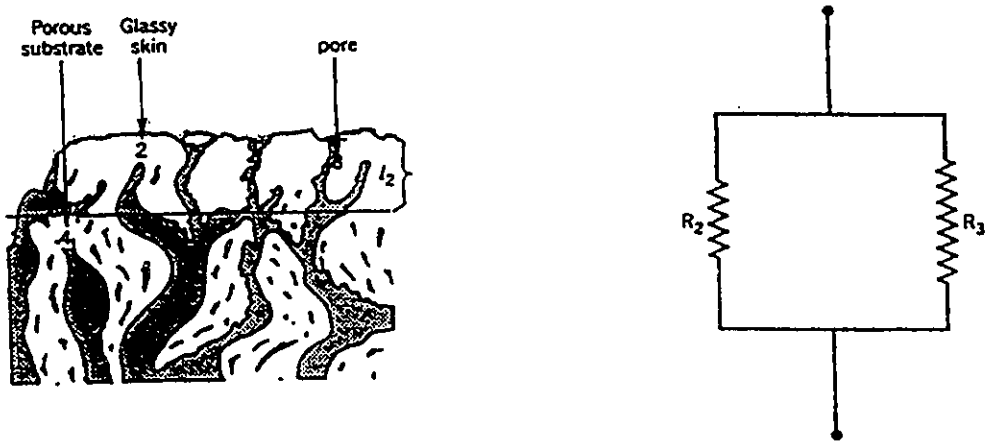

Figure 4: Asymmetric membrane and electric circuit analog.

As before the total resistance to permeate flow of the porous asymmetric membrane, $(R_t)_i$, is composed mainly of two elements: $(R_2)_i$ the resistance of gas flow through the polymer matrix or network pores of the membrane; and $(R_3)_i$ the resistance of gas flow through the aggregate pores on the surface of the membrane. The resistance of the open porous structure beneath the skin layer is assumed to be negligible compared to the other two resistances. Figure 4 shows the membrane and the electrical analog. By using Ohm's law for resistors in parallel the total resistance to permeate flow, $(R_t)_i$ can be derived as follows:

$$1/(R_t)_i = 1/(R_2)_i + 1/(R_3)_i \tag{33}$$

$$1/(R_t)_i = \frac{(R_2)_i + (R_3)_i}{(R_2)_i(R_3)_i} \tag{34}$$

$$(R_t)_i = \frac{(R_2)_i(R_3)_i}{(R_2)_i + (R_3)_i} \tag{35}$$

Consider now a composite membrane where the porous asymmetric membrane from Figure 4 is laminated on top with a rubbery membrane. The resulting membrane and electrical analog are shown in Figure 5. As before $(R_t^L)_i$ is defined as the total resistance to the permeation of gas i in the laminated membrane. The terms $(R_2)_i$ and $(R_3)_i$ are defined as previously mentioned. The term $(R_1)_i$ is the

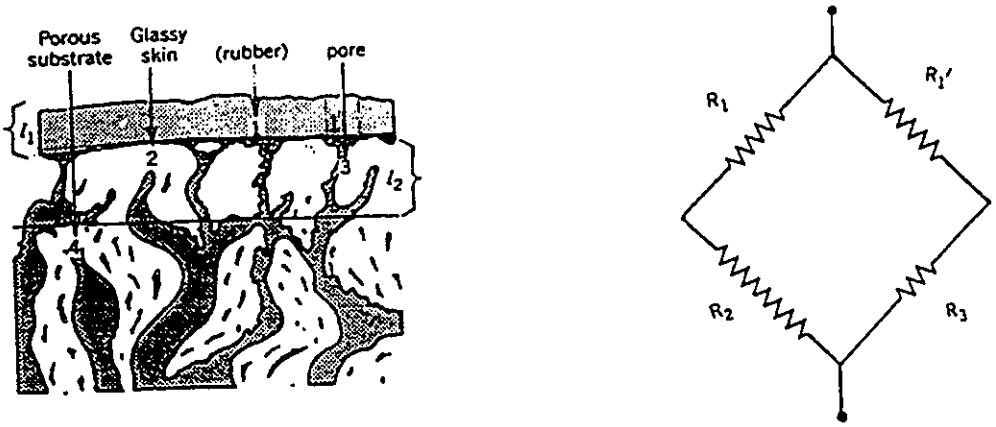

Figure 5: Laminated membrane and electric circuit analog.

resistance of gas flow for the laminated polymer that is over the dense region of the substrate polymer. The term $(R_{1'})_i$ is described as the resistance of gas flow for region 1' where layer 1 is over the aggregate pores of layer 2. The term $(R_x)_i$ is the resistance of cross flow of gas i from region 1 to 1' or from between region 1 and 2 to 3. This cross flow resistance can be assumed to be infinite or, in other words, the amount of cross flow can be assumed negligible in comparison to the flows through the pores and dense regions. Once again using Ohm's law for resistors in series and parallel we can obtain the following equation for the total resistance of a porous membrane with lamination.

$$(R_t^L)_i = \frac{[(R_1)_i + (R_2)_i][(R_{1'})_i + (R_3)_i]}{[(R_1)_i + (R_2)_i + (R_{1'})_i + (R_3)_i]} \tag{36}$$

The individual resistances of equations 35 and 36 can be determined from equation 27 where:

$$(R_3)_i = \frac{l_3}{P_{3,i}A_3} \tag{37}$$

$$(R_2)_i = \frac{l_2}{P_{2,i}A_2} \tag{38}$$

$$(R_1)_i = \frac{l_1}{P_{1,i}A_1} \tag{39}$$

$$(R_{1'})_i = \frac{l_{1'}}{P_{1',i}A_{1'}} \tag{40}$$

and the total resistances are defined as below:

$$(R_t)_i = \frac{\Delta P_{t,i}}{Q_{t,i}} \tag{41}$$

$$(R_t^L)_i = \frac{\Delta P_{t,i}^L}{Q_{t,i}^L} \tag{42}$$

2.3.2 Method of Analysis Using Resistance Approach

It is convenient to define a quantity called the pure gas permeation rate ratio designated hereafter as PGPR. The PGPR is simply the permeation rate of one pure gas divided by the permeation rate of another pure gas through the membrane. For the resistance analysis in this thesis the PGPR's are all with respect to hydrogen gas permeation where α_L and α denote the ratio of the gas i permeation to hydrogen gas permeation for laminated and non-laminated membranes respectively. The PGPR's are given by:

$$\alpha_L = \frac{(R_t^L)_i}{(R_t^L)_{H_2}} = \frac{Q_{t,H_2}^L}{Q_{t,i}^L} \tag{43}$$

$$\alpha = \frac{(R_t)_i}{(R_t)_{H_2}} = \frac{Q_{t,H_2}}{Q_{t,i}} \tag{44}$$

Further it is convenient to define the term α_j, as the resistance of gas i flux over the resistance of hydrogen gas flux for region j of the composite membrane.

$$\alpha_1 = \frac{(R_1)_i}{(R_1)_{H_2}} = \frac{P_{1,H_2}}{P_{1,i}} \tag{45}$$

$$\alpha_{1'} = \frac{(R_{1'})_i}{(R_{1'})_{H_2}} = \frac{P_{1',H_2}}{P_{1',i}} \tag{46}$$

$$\alpha_2 = \frac{(R_2)_i}{(R_2)_{H_2}} = \frac{P_{2,H_2}}{P_{2,i}} \tag{47}$$

$$\alpha_3 = \frac{(R_3)_i}{(R_3)_{H_2}} = \frac{P_{3,H_2}}{P_{3,i}} \tag{48}$$

Note that the intrinsic permeability of the top layer $P_{1,i}$ and $P_{1',i}$ are identical and only represent different regions of the same polymer matrix. Thus $\alpha_1 = \alpha_{1'}$.

For the purpose of analysis it is necessary to use α_j, α_L, and α with the equations for total resistance of laminated and non-laminated membranes altogether to obtain the unknowns. The equations are:

$$(R_t)_{H_2} = \frac{(R_2)_{H_2}(R_3)_{H_2}}{(R_2)_{H_2} + (R_3)_{H_2}} \tag{49}$$

$$\alpha(R_t)_{H_2} = \frac{\alpha_2(R_2)_{H_2}\alpha_3(R_3)_{H_2}}{\alpha_2(R_2)_{H_2} + \alpha_3(R_3)_{H_2}} \tag{50}$$

$$(R_t^L)_{H_2} = \frac{[(R_1)_{H_2} + (R_2)_{H_2}][(R_{1'})_{H_2} + (R_3)_{H_2}]}{[(R_1)_{H_2} + (R_2)_{H_2} + (R_{1'})_{H_2} + (R_3)_{H_2}]} \tag{51}$$

$$\alpha_L(R_t^L)_{H_2} = \frac{[\alpha_1(R_1)_{H_2} + \alpha_2(R_2)_{H_2}][\alpha_1(R_{1'})_{H_2} + \alpha_3(R_3)_{H_2}]}{[\alpha_1(R_1)_{H_2} + \alpha_2(R_2)_{H_2} + \alpha_1(R_{1'})_{H_2} + \alpha_3(R_3)_{H_2}]} \tag{52}$$

From the experimental data all the above quantities are known except for $(R_3)_{H_2}, (R_2)_{H_2}, (R_{1'})_{H_2}$ and α_3. The total resistances, $(R_t)_i$ and $(R_t^L)_i$ are easily obtained from the experimental flux versus pressure data for a given gas i through an asymmetric and laminated asymmetric membrane respectively. Likewise the PGPR's, α and α_L, are simply the ratio of the total resistances of gas i permeation over H_2 gas permeation for asymmetric and laminated membranes respectively.

A few simplifying assumptions are made in order to facilitate the calculations of the individual resistances. First the area of the matrix region of the substrate membrane, A_2, is made equivalent to the total area available for permeation, A_t. The area of the aggregate pore, A_3, is extremely small and can be considered negligible in comparison to either the total area or the area of the membrane matrix. The above reasoning also applies for A_1 where $A_1 = A_t$ and $A_{1'}$ is very small in comparison.

In this thesis the top layer of the composite membrane is a homogenous silicone rubber membrane of known thickness, l_1. This membrane is well documented in literature and comes from the manufacturer with experimental intrinsic permeability

data for various gases. As a result $(R_1)_i$ along with α_1 are easily calculated for a given membrane area A_1.

The ratio of intrinsic permeabilities of H_2 gas over gas i for the substrate matrix, α_2, is required for the successful completion of the calculations. A polyamide polymer is used in this thesis as the substrate membrane material and unlike the silicone rubber membrane the intrinsic permeability is not documented in the literature. As a result an approximation was used for the α_2 term.

The intrinsic permeability of a gas is the permeation rate solely through the network pores (membrane matrix) of a given membrane material. As a consequence of this, it follows that the value of α_2 should be a limiting value; the maximum obtainable value for a membrane composed from a given polymeric solution.

It was assumed that this α_2 value could be best represented by the laminated membrane that exhibited the highest PGPR, since the actual effect of laminating with silicone rubber is to block any aggregate pores (large pores) on the substrate membrane and as a result restrict flow through only the network pores (small pores).

As mentioned previously equations 49 to 52 must be employed to solve for the four unknowns, $(R_3)_{H_2}, (R_2)_{H_2}, (R_{1'})_{H_2}$ and α_3. The procedure used to solve these unknowns is as follows:

Step I Solve equations 51 and 52 for $(R_{1'})_{H_2}$ and $(R_2)_{H_2}$ assuming $\alpha_3(R_3)_{H_2}$ approaches zero.

Step II Solve equations 49 and 50 for α_3 and $(R_3)_{H_2}$.

Step III Once again solve equations 51 and 52 but now with the revised $(R_3)_{H_2}$ and α_3 values.

Step IV Again solve equations 49 and 50 for α_3 and $(R_3)_{H_2}$ with the new value of $(R_2)_{H_2}$ calculated in step 3.

Step V Repeat steps 3 and 4 until the $(R_3)_{H_2}$ value for both steps are the same.

Upon obtaining the unknowns one may proceed to calculate the total area of the aggregate pores in the substrate layer (the porous asymmetric membrane), A_3, for various gas combinations as follows:

$$(R_{1'})_i = \frac{l_{1'}}{P_{1',i} A_{1'}} \tag{53}$$

Noting that $A_3 = A_{1'}$ and $l_{1'} = l_1$ and assuming $P_{1',i} = P_{1,i}$ we obtain from equation 53:

$$A_3 = A_{1'} = \frac{l_1}{P_{1,i}(R_{1'})_i} \tag{54}$$

Chapter 3

Experimental

3.1 Preparation of Membranes

Aromatic polyamide membranes were cast using a filtered solution of the following composition (wt.%): polyamide polymer 16.0, dimethyl acetamide solvent 77.5, and lithium nitrate 6.5.

The specific polyamide polymer used is called poly-m-phenylene-iso(70)-co-tere(30)-phthalamide (abbreviated as PA hereafter) and is shown in Figure 6. The PA average molecular weight is approximately 31,100 g/gmol and the intrinsic viscosity of the PA solution is 1.616 dl/g at 30 °C [34]. Before casting, the polymer solution was

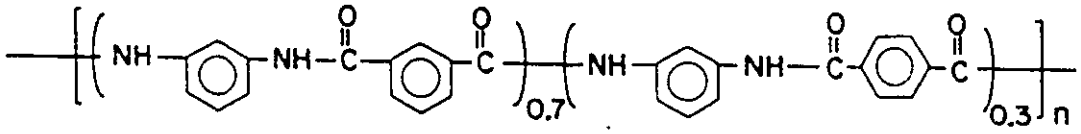

Figure 6: The structure of the repeat unit of poly-m-phenylene-iso(70)-co-tere(30)-phthalamide polymer.

filtered using a 3 micron filter obtained from the Millipore Corporation. All membranes were cast by pouring the PA solution onto a 7.25 by 11 inch glass plate and then drawing the solution across the plate with a metal bar (doctor's blade). All the membranes were cast to equal nominal thickness of 254 μm. The temperature of the casting solution and the casting atmosphere were both kept constant at 23 °C. The relative humidity of the atmosphere was measured to be 80 %. Upon casting, the membranes were immediately placed in an oven kept at a constant temperature of 95 °C.

Generally, different porosity membranes can be produced by varying the evaporation (drying) time in the oven. It is known that increasing the evaporation time prior to immersion in the gelation bath causes a decrease in porosity and hence, a decrease in permeability. Permselectivity on the other hand first increases and then decreases as the drying time is increased [17]. Oven evaporation times of 9, 11, 13, 15, 17 and 19 minutes were used in this study.

The membranes were then gelled in ice cold water at a temperature between 3 to 5 °C. Membranes produced in this manner form an asymmetric structure with a thin dense skin layer and a relatively thick porous substrate. The membranes were kept in this gelation bath for approximately one hour after which time the sheets were either stored in distilled water or immediately cut into circular coupons of diameter three inches. The coupons were cut so as to avoid any pinholes or irregularity on the membrane sheet. The water wet membranes were then heat treated in a water bath at a temperature of 80 °C for half an hour, after which the solvent exchange method could be employed to dry the membranes. By not employing a heat treating step the membranes were found to exhibit extreme curling and shrinking upon placement into a 25 volume % of isopropyl alcohol solution (the first step in solvent exchange). It was noted that the degree of curling and shrinking increased with increase of the evaporation period in the oven. This is a good indication that the morphology of

Table 1: Intrinsic permeabilities of various gases through poly dimethyl siloxane rubber membrane.

Gas	CO_2	CH_4	H_2	O_2	He	N_2
mol.m/m^2.s.Pa	8.28E-11	2.45E-11	1.69E-11	1.53E-11	9.20E-12	7.67E-12

the membrane differs with different evaporation times.

In the solvent exchange technique the water in the membrane is first replaced by a water miscible solvent (called the "first solvent") which is a non-solvent for the membrane material. The replacement of water in the membrane by the first solvent is done by a succession of progressively concentrated aqueous solutions. Then the first solvent is replaced by a second solvent which is volatile. The second solvent is subsequently air evaporated to obtain the dry membrane [31].

In this work the first solvent used was isopropyl alcohol and the second solvent was hexane. The membranes were contacted with 25, 50, 75 and 100 volume % aqueous solution of isopropyl alcohol. In each succession the membranes were contacted with the aqueous isopropyl alcohol solution for a period of twenty-four hours. The membranes were then contacted with 100 % hexane for a period of twenty four hours after which time they were removed from the solvent and placed in a desiccator under hexane vapor. All the solvent exchanges were done at room temperature.

Some of the PA membranes produced were also laminated with a 25.4 μm thickness of poly dimethyl siloxane rubber (silicone rubber) obtained from the General Electric Company. The intrinsic permeabilities of various gases through this silicone membrane, as observed by the manufacturer, is shown in Table 1. Note that the silicone membrane, unlike the PA membrane, has a homogenous morphology.

3.2 Preparing for Permeation Experiments

A schematic diagram of the experimental apparatus along with an expanded drawing of a single permeation cell are shown in Figure 7. Before placing the coupon into the permeation cell both the O-rings and surfaces that come into contact with the membrane were cleaned using ethanol. The coupon was placed on top of a filter paper and both were attached with four small pieces of tape to the bottom flange of the cell. The membrane skin is left exposed to the gas feed, which enters from the top of the cell. The O-rings were coated with a small amount of silicone grease and put into place. The bottom flange was then fastened to the rest of the cell with six bolts. This procedure was performed for all three cells. Helium gas was then passed through the apparatus at 100 psi and all fittings were checked for leaks using a solution of soap water. Flow rates were checked to ensure that none of the coupons were broken. A broken coupon exhibits very high permeation rates that were not measurable with the bubble meters. If a broken coupon was found it was immediately replaced following the procedure above. Once no leaks were detected at 100 psi the pressure was increased to 300 psi and again the system was checked for leaks and broken coupons. The membranes were then pressure treated at a pressure 20% greater than the normal operating pressure for a period of three to four hours. After which time the pressure was released and the membrane left to relax overnight before the permeation experiments. The membrane structure is stabilized after such a pressure treatment and as a result the experimental flux data becomes more consistent.

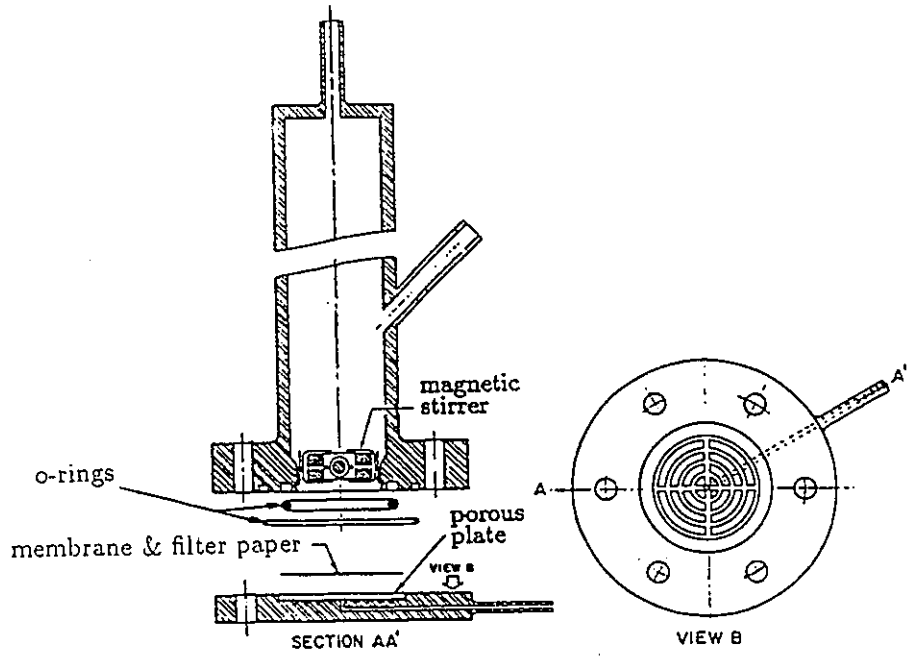

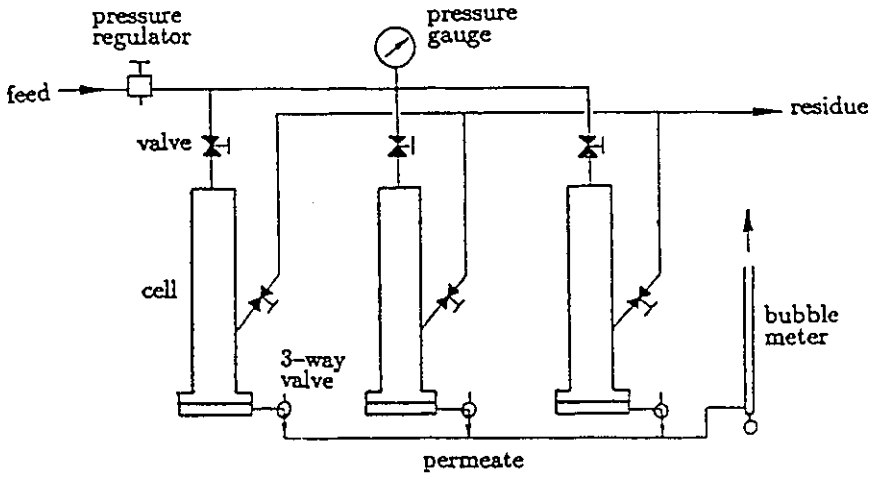

Figure 7: Permeation cell and schematic diagram of experimental apparatus.

3.3 Permeation Experiments

The steady-state permeation rates at different operating pressures (recorded as psig, but converted to kPag) were measured at room temperature and pressure with a bubble flow meter. All gases were supplied by Air Products with a purity of 99.9% or better.

The experimental data collected as volume flow rate for different gases at different pressure gradients is first corrected to standard temperature and pressure, and then converted to permeability coefficient, A_G (kmol/m^2.s.Pa). The effective area of the membrane used for the permeation studies was 9.62×10^{-4} m^2. A_G is the amount of gas per unit time, per unit area, per unit pressure differential across the membrane.

All membranes were tested with the gases in the following order: He, H_2, O_2, N_2, CH_4 and then CO_2. After this sequence was completed the membrane was retested with He gas to ensure that membrane performance did not change significantly during the sequence. If a change was noticed the entire sequence was repeated and the He gas permeation tested again. If there still was a significant difference the membrane was discarded.

It should be noted that the feed gas pressure was first decreased from 2068 to 345 kPag in increments of 345 kPag and the volume flow rate of permeate gas measured at each pressure. Then the feed gas pressure was increased from 345 to 2068 kPag and again the volume flow rate of permeate gas was measured at each increment for each membrane (with and without lamination).

Once the decreasing and increasing pressure experiments were completed for one gas the membranes were left to relax for a period of 24 hours, after which time another gas would be employed. The entire apparatus was flushed several times with this new gas and the pressure decreasing and pressure increasing experiments

performed once again.

Atmospheric temperature and pressure were recorded daily while the experiment was in operation.

3.4 X-Ray Diffraction

Wide angle x-ray diffraction (WAXD) was performed by the NRC's chemistry department on the dried polyamide membranes used in this study. Polyamide membranes of various oven evaporation times were tested. Also PA membranes dried by using solvents other than isopropyl alcohol and hexane were tested as well.

WAXD in conjunction with Bragg's equation, $n\lambda = 2d\sin\theta$, can be used to determine the intersegmental distance of polymeric molecules [5]. This distance corresponds to the network pore described in Chapter 1, the voids found between polymeric chains. The term n is the order of diffraction; the term λ is the wave length of the x-ray; the term d called the d-spacing is the average intersegmental distance of polymer chains; and the term 2θ is the scattering angle of the x-ray.

Wide angle x-ray diffraction measurements were made using a Stoe powder diffractometer with Cu radiation, of average $\lambda = 1.5418$ Å. The generator was set to 45 kV and 32 mA. All experiments were carried out in the transmission geometry. Specimens for x-ray scattering measurements were prepared by cutting the polyamide membranes into 15 mm diameter circles and then orienting the film so that the skin layer is exposed to the x-ray. A thorough explanation about the principals of WAXD can be found in references [5] and [43].

Chapter 4

Results & Discussion

4.1 Experimental Data

As mentioned previously, this thesis deals with pure gas permeation through polyamide asymmetric membranes and through laminated polyamide asymmetric membranes. The experimental variables in this thesis were:

1. Membranes were made using six different oven evaporation times of 9, 11, 13, 15, 17, and 19 minutes.

2. Six pure gases were used, helium, hydrogen, carbon dioxide, oxygen, nitrogen and methane.

3. Six different pressures were used with each gas, 345, 689, 1034, 1379, 1724, and 2068 kPag (50, 100, 150, 200, 250, 300 psig). Both increasing and decreasing pressure runs were performed.

The data collected for the six gases for all the membranes were in terms of volume flow rate versus pressure. This volume flow rate was corrected to STP and then converted to the permeability coefficient, A_G. The permeability coefficient versus

pressure for each membrane for the six different gases are shown in Tables 13 to 22 in Appendix A. As noted previously all the experiments were conducted at room temperature (23 °C) with the permeate side being at atmospheric pressure. For all subsequent calculations the average permeation rate was used from the pressure decreasing and pressure increasing experiments for each pressure.

One of the first problems encountered with the permeation experiments was the constantly changing flux occurring with certain gases as the membrane was being tested. It was found that for oxygen, nitrogen, and methane gases, the pressure increasing and decreasing experiments yielded the same curve; whereas, for helium, hydrogen and occasionally carbon dioxide, the pressure increasing and decreasing experiments did not yield the same curve. Figure 8 shows the variable permeation rate of helium gas for the decreasing and increasing pressure experiments.

The procedure in obtaining the volumetric flow rate consisted of setting the feed gas pressure to the proper increment and then waiting a 1/2 hour before taking the first flow rate measurement. A second flow rate measurement was taken 15 minutes later and compared with the first. If a significant difference arose a third flow rate measurement would be taken in another 15 minutes and again compared. This was repeated every 15 minutes until the flow rates were the same. This procedure worked well for O_2, N_2 and CH_4 because the flow rates of these gases remained constant after 1/2 hour or less at any given pressure. However this procedure did not work well for He, H_2 and CO_2 because it was discovered that 2 to 80 hours were needed for a constant flow rate to be established. This change in flux was not detectable in the 15 minute intervals initially used but was very noticeable for flux measurement taken on the hour.

Flux versus time for helium gas at a constant pressure of 300 psig is shown in Figure 9. As can be seen in the figure, He gas takes between 50 to 80 hours to reach steady state permeation for the two membranes shown. This was found to

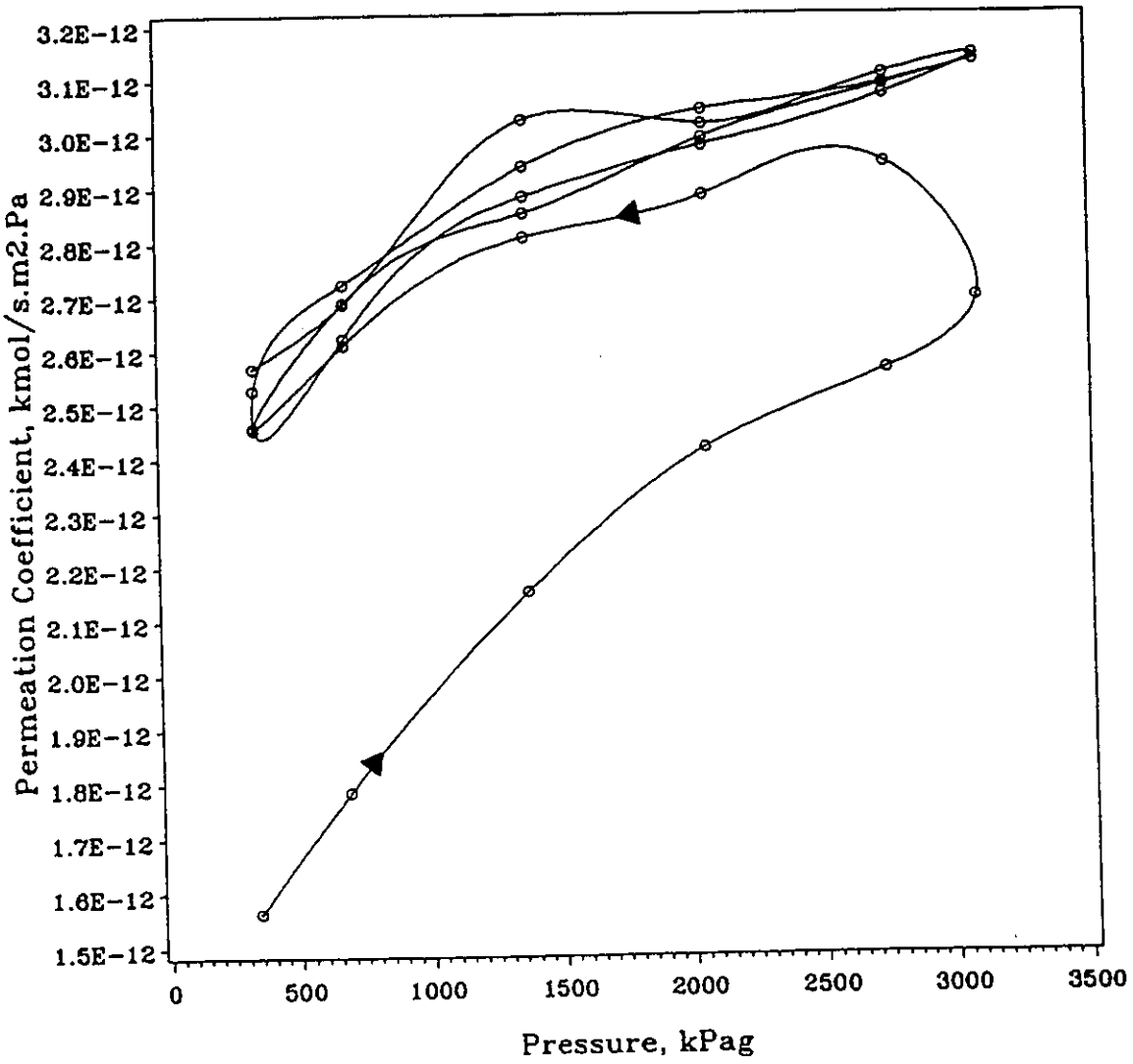

Figure 8: Permeation coefficient of He gas versus pressure for membrane PA-13.

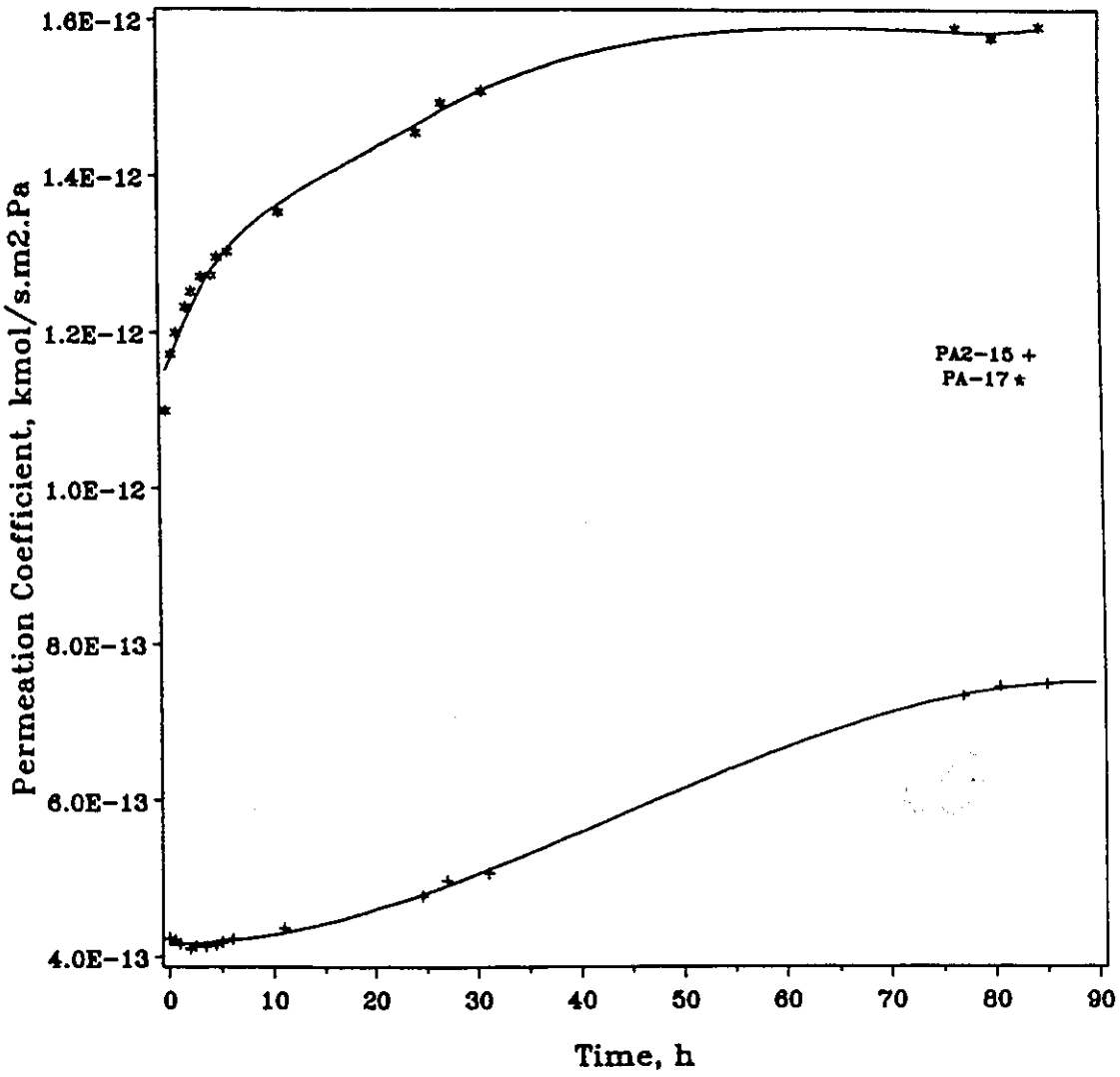

Figure 9: Permeation coefficient of He gas versus time at a pressure of 300 psig.

be the case for all the membranes used in this study. Furthermore, it was observed that CO_2 and H_2 take between 2 and 24 hours to reach steady state values. Why it takes longer for these gases to reach steady state as opposed to O_2, N_2, and CH_4 is not clear at this moment. But it is interesting to note that He and H_2 are the two lightest gases used in this study and that CO_2 has been known to plasticize [56] polymers (soften the membrane) whereupon increased permeability occurs. Discussion or acknowledgement of this phenomenon could not be found in the literature.

The permeability coefficient versus pressure of the six gases for membrane PA-9 is shown in Figure 10. This figure is typical of how all the PA membranes performed. Helium gas had the largest permeation rate followed by H_2, CO_2, and then O_2, N_2, and CH_4. The order of O_2, N_2, and CH_4 varied between the membranes but generally the permeation rate was the greatest for O_2, followed by CH_4 then N_2. This order was more evident with the lamination of silicone rubber on top of the PA membranes as will be discussed later. Figures 21 through 30 in Appendix B contain the graphs of A_G versus pressure for all the membranes used in this study.

No trend could be established between the oven evaporation time and the flux nor between the oven evaporation time and the pure gas permeation rate ratio (PGPR) of the membranes. As noted before, the PGPR is simply the permeation rate of one gas divided by the permeation rate of another gas. This value does not necessarily reflect the separation factor for a mixture of the two gases rather it gives an indication of how the various membranes compare with each other and the direction of separation. The PGPR for various combinations of gases for each membrane is shown in Table 2. The pure gas permeation rate ratios are the average values over the pressure range used in this work. It was observed that the pure gas permeation rate ratios involving hydrogen slightly increased with increase of pressure. This is easily explained by referring to the permeation rate versus pressure

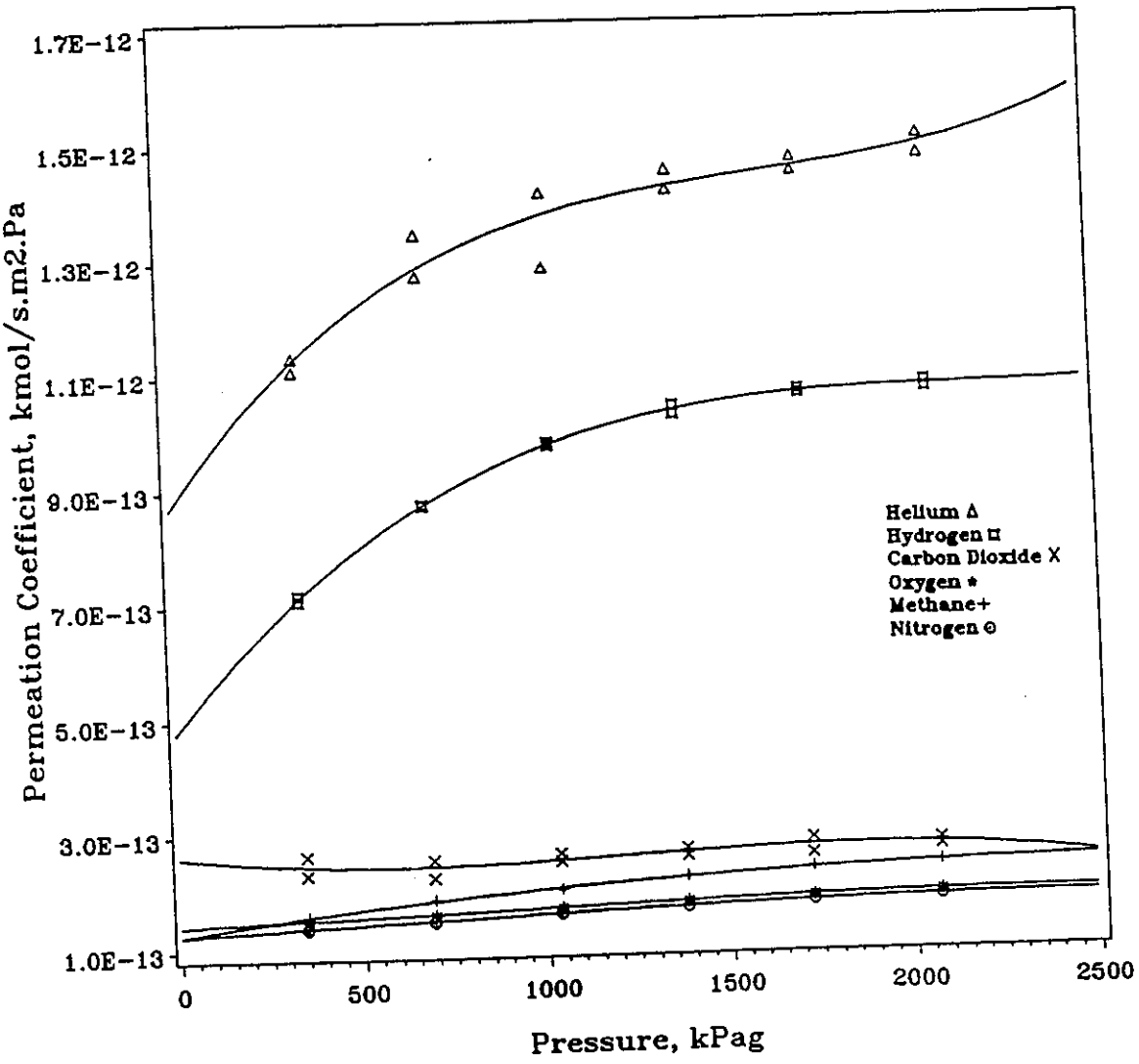

Figure 10: Permeation coefficient of pure gases versus pressure for membrane PA-9.

Table 2: Average pure gas permeation rate ratio (PGPR) at a pressure range of 345 to 2068 kPa for various polyamide membranes.

Gas ratio	PA-9	PA-11	PA-13	PA-15	PA2-15	PA-17	PA-19
H_2/CO_2	3.74	1.63	3.78	4.10	3.01	2.72	2.53
H_2/O_2	5.63	2.77	8.11	5.86	3.35	3.32	3.84
H_2/N_2	5.99	3.47	8.61	4.32	2.97	3.37	17.0
H_2/CH_4	4.71	3.17	7.11	4.28	2.34	2.75	6.57
He/H_2	1.43	2.04	1.89	0.79	1.08	1.34	2.69
CO_2/CH_4	1.27	2.02	1.92	1.04	0.79	1.04	2.82

plots for any of the polyamide membranes. The hydrogen permeation rate increases more than any other gas (with the exception of He) with increase in pressure and as a result the difference in permeation rates between H_2 and another gas would get larger.

4.2 Pore Flow Analysis

The experimental data obtained from the permeation experiments of PA membranes were predominantly analyzed using the pore flow model. Three objectives were to be met: first to characterize the membranes; second to describe the permeation behavior of a gas using the pore flow model; and third to predict the permeation of any pure gas given the permeation of a reference gas for a given membrane.

4.2.1 Characterization of Membranes

It appears that many researchers characterize membranes based solely on the properties of the membrane material. For example, proponents of the solution diffusion and dual sorption model utilize parameters such as the solubility and diffusivity properties of a polymer film. It is increasingly clear that such attempts even

though valid for polymeric characterization are not valid for the characterization of an asymmetric membrane.

The figures in Appendix B illustrate the diversity possible for the flux versus pressure data for the same polyamide material. It is evident from these figures that attempting to characterize membranes solely on the material properties will not account for the differences in permeation behavior for these membranes. The morphology must also be taken into consideration when dealing with asymmetric membranes.

It has been shown by Rangarajan et al. [36] that the transport of a gas i through a membrane can be fully characterized by using the four parameters $\overline{R}$ and σ_i, the average pore size and pore size distribution, $(A_1)_i$, which represent the morphological structure, and A_2, which represents the polymeric properties.

The procedure to obtain the above four parameters from the transport equations of the pore flow model was described previously. In brief, values of $\overline{R}_i$ and σ_i are assumed and then an optimum set of $(A_1)_i$ and $(A_2)_i$ is obtained using the steepest descent method. The combination of $\overline{R}_i$, σ_i and the fitted parameters $(A_1)_i$ and $(A_2)_i$ that yield the least amount of deviation when compared to the experimental data is chosen. The smallest sum of the squared residuals (SS_R) as given by

$$SS_R = \sum_{i=1}^{n} (A_{G,exptl} - A_{G,calcd})^2 \tag{55}$$

is the measure of deviation between experimental and calculated permeability coefficients.

Using the above approach, values of $\overline{R}_i$, σ_i, $(A_1)_i$ and $(A_2)_i$ were obtained for each gas (He, H_2, CO_2, O_2, N_2, CH_4) in all of the membranes used in this thesis. These values are shown in Tables 23 through 29 in Appendix C. Table 3 is typical of the values obtained for the characterization parameters. There is a definite trend of decreasing pore size with increasing molecular size or increasing adsorption between

Table 3: SFPF parameters for membrane PA-11 (11 min. oven evap. time).

Gas	*Kinetic dia. 10^{10}m	$\overline{R} \times 10^{10}$ m	$\sigma \times 10^{10}$ m	A_1 m^{-3}	A_2 $kmol/m^3.s.Pa^2$
He	2.6	9.2	1.6	0.17673E+18	0.35615E-09
H_2	2.89	4.9	1.1	0.94488E+18	0.39792E-09
CO_2	3.3	3.2	1.4	0.94393E+19	0.24073E-09
O_2	3.46	2.8	1.4	0.58710E+19	0.17100E-09
N_2	3.64	2.4	1.2	0.89111E+19	0.18001E-09
CH_4	3.8	2.7	1.2	0.37585E+19	0.28157E-09

*based on sorption in zeolites [6]

the gas molecule and membrane material. Unfortunately, no data could be found in the literature pertaining to the adsorption of gases onto the polyamide polymer used in this study. For purposes of comparisons, results from Long et al. [23] show that Henry's adsorption constant decreases in the following order

$$CO_2 > CH_4 > O_2 > N_2 > H_2 \tag{56}$$

for materials such as cellulose acetate, cellulose triacetate, and polyethersulfone [23]. On average this order parallels the trend found with the pore size as given by the surface force pore flow model.

4.2.2 Prediction of Permeation

Two methods of prediction are attempted using the surface force pore flow model. In the first, an attempt is made to predict the permeation rate of any gas given the permeation rate of a reference gas following the method employed by Rangarajan et al. [36]. In the second method the membrane is characterized by the A_G versus $\overline{P}$ data for the pressure range of 0 to 1034 kPag and then the model is used to predict the permeation rate for pressures between 1034 and 2068 kPag. The results of both methods are described below.

Table 4: Radius correction factors, Δ_i and relative surface transport coefficients, Φ_i for different gases in polyamide (membrane PA2-15).

Gas i	Δ_i $\times 10^{10}$ m	Φ_i
hydrogen	-3.0	1.95
carbon dioxide	-7.5	0.94
oxygen	-7.4	0.76
nitrogen	-7.1	0.94
methane	-6.7	1.55

Following the work of Rangarajan et al. [36], we attempted to predict the permeation of any gas given the permeation data of one reference gas by employing the pore flow model. In this study helium gas was chosen as the reference gas due to it's inertness compared to the other gases. For purposes of prediction it is necessary to obtain data of Δ_i and Φ_i for a given combination of membrane material and gas. As noted previously Φ_i, the relative surface transport coefficient, is defined as the ratio of A_2 for gas i to that of a reference gas (Helium). Also Δ_i, the radius correction factor, is defined as the difference between the mean pore radius of gas i and that of the reference gas.

From the helium characterization, values of the gas permeability coefficient, A_G, for different gases at several operating pressures were calculated for PA membranes using the procedure described in section 2.1.2. Prediction calculations were done for the membranes whose experimental data of A_G versus pressure were not used in the generation of Δ_i and Φ_i. Table 4 shows the Δ_i and Φ_i values obtained from membrane PA2-15.

The comparison between experimental and predicted values of A_G at different pressures for hydrogen, oxygen, carbon dioxide, methane, and nitrogen in PA membranes are shown in Table 5. The agreement between the predicted and experimental A_G values in many cases are unsatisfactory.

Table 5: Average permeation rate of increasing and decreasing experiments and predicted permeation rate from SFPF model for membranes PA-17 & PA-11.

Pressure kPag	Menbrane PA-17		Membrane PA-11	
	Experimental kmol/s.m^2.Pa	Predicted kmol/s.m^2.Pa	Experimental kmol/s.m^2.Pa	Predicted kmol/s.m^2.Pa
	Hydrogen Gas			
345	6.26E-13	6.2 E-13	2.28E-13	3.3 E-13
689	7.93E-13	8.5 E-13	2.57E-13	4.1 E-13
1034	9.58E-13	1.07E-12	2.92E-13	4.9 E-13
1379	1.09E-12	1.27E-12	3.23E-13	5.9 E-13
1723	1.23E-12	1.45E-12	3.55E-13	6.8 E-13
2068	1.27E-12	1.64E-12	3.70E-13	7.8 E-13
	Oxygen Gas			
345	2.68E-13	3.41E-14	9.33E-14	1.96E-14
689	2.79E-13	5.50E-14	1.06E-13	3.12E-14
1034	2.90E-13	7.59E-14	1.10E-13	4.29E-14
1379	3.04E-13	9.68E-14	1.12E-13	5.45E-14
1723	3.12E-13	1.18E-13	1.15E-13	6.61E-14
2068	3.24E-13	1.39E-13	1.19E-13	7.77E-14
	Methane Gas			
345	2.74E-13	1.06E-13	6.53E-14	5.64E-14
689	3.12E-13	1.70E-13	8.49E-14	8.90E-14
1034	3.51E-13	2.34E-13	9.37E-14	1.22E-13
1379	3.74E-13	2.98E-13	1.04E-13	1.55E-13
1723	4.05E-13	3.62E-13	1.11E-13	1.87E-13
2068	4.21E-13	4.25E-13	1.19E-13	2.20E-13
	Nitrogen Gas			
345	2.56E-13	1.05E-13	6.93E-14	5.54E-14
689	2.70E-13	1.69E-13	7.69E-14	8.83E-14
1034	2.86E-13	2.33E-13	8.58E-14	1.21E-13
1379	2.99E-13	2.97E-13	9.20E-14	1.54E-13
1723	3.12E-13	3.61E-13	9.90E-14	1.87E-13
2068	3.29E-13	4.25E-13	1.01E-13	2.20E-13
	Carbon Dioxide Gas			
345	3.64E-13	3.89E-14	1.93E-13	2.25E-14
689	3.40E-13	6.30E-14	1.82E-13	3.61E-14
1034	3.57E-13	8.71E-14	1.79E-13	4.96E-14
1379	3.62E-13	1.11E-13	1.80E-13	6.32E-14
1723	3.81E-13	1.35E-13	1.76E-13	7.68E-14
2068	3.79E-13	1.59E-13	2.14E-13	9.04E-14

There are several possible reasons why this method of prediction did not perform up to expectations. The assumption that pore blocking is negligible may not be valid in this study. It is entirely possible that a large molecule like methane will see a different pore size and different amount of pores compared to a small molecule like helium. As a result keeping A_1 $(= N_t/S\delta)$ and σ, the pore size distribution, constant regardless of permeating gas may not adequately describe the PA membrane. The lack of success with predicting the permeation of one gas given the permeation of another gas could also stem from the method of characterizing the membrane in terms of $\overline{R}_i$, σ_i, $(A_1)_i$ and $(A_2)_i$. The four parameters, $\overline{R}_i$, σ_i, $(A_1)_i$ and $(A_2)_i$ chosen by the computer program to represent the gas permeation through the membrane is based solely on the combination that yields the smallest sum of the squared residuals(SS_R). In fact, there are several combinations with similar SS_R and these combinations could equally be assumed the best solution. Various combinations of the characterization parameters and their corresponding SS_R are shown in Table 6. These values were generated for membrane PA-19 using helium gas permeation. Combination number 730 would be chosen since it has the smallest SS_R, but as illustrated in the table many other combinations have very close SS_R values.

Thus, it appears that for a given pressure versus flux data it is not always possible to obtain a unique set of characterization parameters; whereas, if given the values of $\overline{R}$, σ, A_1, and A_2 one can obtain, for a given pressure, a unique value for the flux. To obtain a truly unique set of characterization parameters from the pressure versus flux data one may have to employ some additional data such as adsorption properties of the polymeric material and incorporate this into the transport equations of the surface force pore flow model.

Another form of prediction using the SFPF model involves generating the characterization parameters $\overline{R}_i$, σ_i, $(A_1)_i$ and $(A_2)_i$ for each individual gas between the pressures of 0 and 1034 kPag. Predictions of permeation rates are then made for

Table 6: Various SFPF parameters with similar SS_R for membrane PA-19 (19 min. oven evap. time).

Combination number	$R \times 10^{10}$ m	$\sigma \times 10^{10}$ m	A_1 m^{-3}	A_2 $kmol/m^3sPa^2$	SS_R *
254	2.6	2.3	0.79931E+18	0.36992E-09	0.95131E-08
373	3.4	2.2	0.49241E+18	0.32341E-09	0.93420E-08
432	3.8	2.1	0.46621E+18	0.32756E-09	0.89604E-08
462	4.0	2.1	0.40486E+18	0.31147E-09	0.88690E-08
492	4.2	2.1	0.35425E+18	0.29655E-09	0.92869E-08
551	4.6	2.0	0.35291E+18	0.30582E-09	0.86652E-08
581	4.8	2.0	0.31399E+18	0.29312E-09	0.85239E-08
611	5.0	2.0	0.28085E+18	0.28120E-09	0.88702E-08
670	5.4	1.9	0.28903E+18	0.29327E-09	0.89459E-08
700	5.6	1.9	0.26154E+18	0.28288E-09	0.83635E-08
730	5.8	1.9	0.23760E+18	0.27304E-09	0.82946E-08
849	6.6	1.8	0.21019E+18	0.26950E-09	0.87312E-08
879	6.8	1.8	0.19371E+18	0.26156E-09	0.83192E-08
909	7.0	1.8	0.17900E+18	0.25396E-09	0.84028E-08
939	7.2	1.8	0.16584E+18	0.24668E-09	0.89454E-08
1118	8.4	1.7	0.13562E+18	0.23700E-09	0.94511E-08

* $SS_R = \sum_{i=1}^{n}(A_{G,expt} - A_{G,calcd})^2$

the individual gases between the pressures of 1034 and 2068 kPag.

These predicted values are compared to the experimental values in Figure 11 for membranes PA-11, PA2-15, and PA-17. Predicted permeation values for the above membranes are shown for all six gases (He, H_2, CO_2, O_2, N_2 and CH_4) at feed pressures of 1379, 1723, and 2068 kPa. As is evident from the figure the predictions are fairly good with only a few deviations from the 45° line. The points that stray the furthest from the 45° line (for each membrane) correspond to hydrogen and helium gas permeation. This deviation is easily understood when one looks at the permeation rate versus pressure graphs in Appendix B. Generally the hydrogen and helium permeation rates increase linearly for pressures under 1034 kPa, and above this pressure the permeation rates start to dip below a projection of the earlier linear permeation line. As a result when the SFPF model is applied to the first three pressures points for these two gases it usually estimates larger permeation rate at the higher pressures than is observed. Nevertheless, as noted before, this form of prediction performs very well with only a few minor exceptions.

4.3 Laminated PA Membranes

Three polyamide asymmetric membranes with varying PGPR ratios were chosen to be laminated with 25.4 μm (1 mil) thickness of poly dimethyl siloxane rubber (silicone rubber). Membranes PA-9, PA-15, and PA-19 were chosen to be laminated.

Using the same experimental procedure as before, He, H_2, CO_2, O_2, N_2 and CH_4, gas feed pressures were varied between 2068 and 345 kPag. The feed gas pressure was first decreased and then increased in increments of 345 kPag and the volume flow rate of permeate gas measured for each increment.

The results of before and after lamination with respect to flow rate is shown in Table 7 for the three membranes. With lamination the permeation rate for the

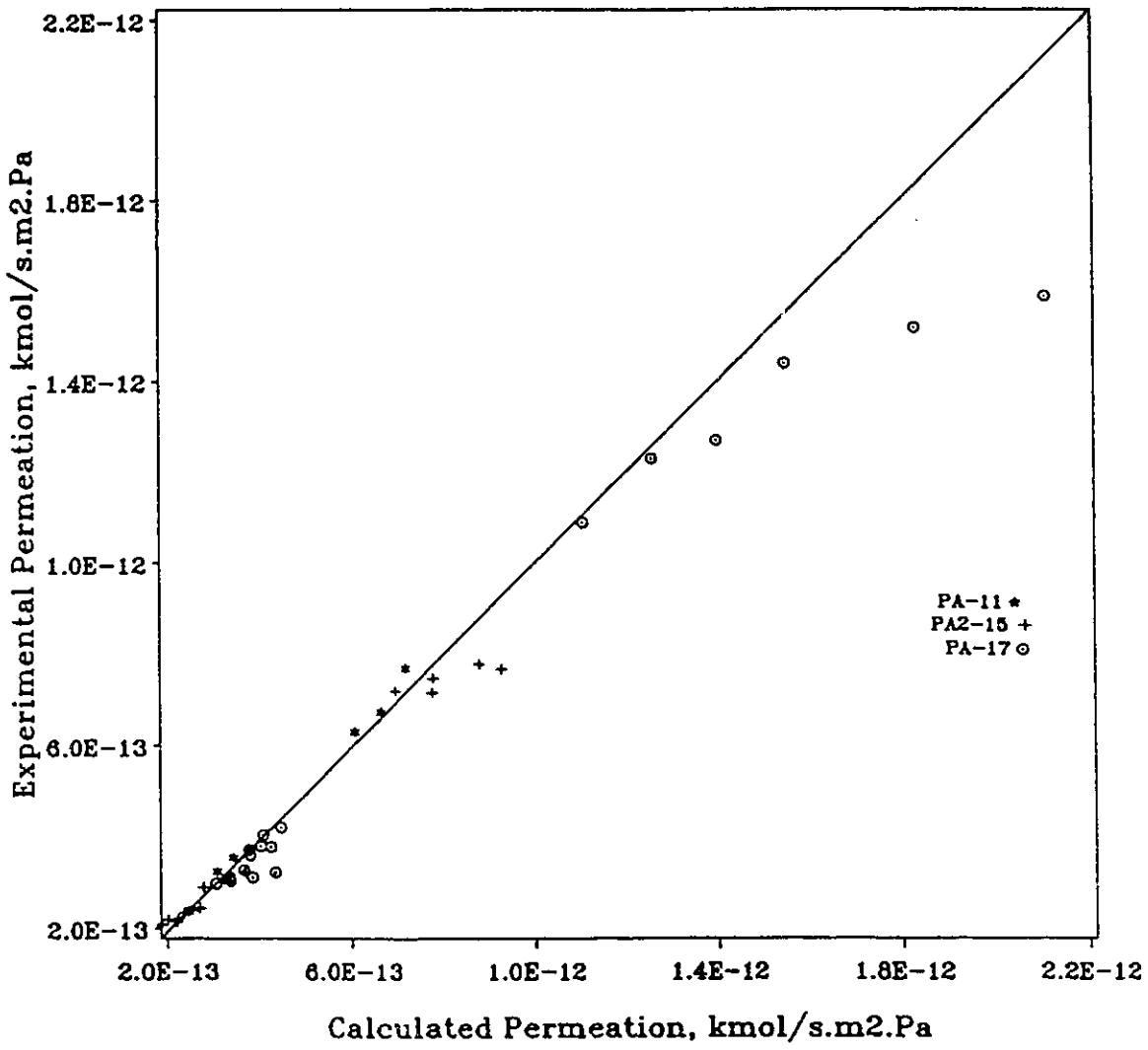

Figure 11: Experimental permeation rate versus calculated permeation

Table 7: Pure gas permeation rate in kmol/s.m^2.Pa at 2068 kPag for membranes with and without lamination.

Gas	PA-9	laminated PA-9	PA-15	laminated PA-15	PA-19	laminated PA-19
He	1.49E-12	2.56E-13	4.09E-12	6.53E-13	5.28E-13	2.84E-13
H_2	1.07E-12	1.07E-13	5.26E-12	3.51E-13	1.84E-13	1.19E-13
CO_2	2.68E-13	4.41E-14	1.21E-12	4.29E-14	5.94E-13	2.52E-14
O_2	1.84E-13	3.09E-15	8.61E-13	6.10E-15	4.45E-14	3.47E-15
CH_4	2.34E-13	3.19E-16	1.22E-12	3.62E-16	3.14E-14	1.08E-15
N_2	1.75E-13	3.36E-16	1.09E-12	8.58E-16	1.15E-14	3.23E-15

Table 8: Kinetic (sieving) diameters of penetrants.

Gas	He	H_2	CO_2	O_2	N_2	CH_4
*Kinetic dia. (10^{10}m)	2.6	2.89	3.3	3.46	3.64	3.8
	decreasing permeation $\longrightarrow$					

*based on sorption in zeolites [6]

smaller molecules (He, H_2) decreased slightly (by a factor of 10); whereas, for the larger molecules (O_2, N_2, CH_4) the permeation rate decreased greatly (by a factor > 25).

The order of decreasing gas permeation for all the laminated asymmetric membranes parallels the order of increasing molecular size of the gas molecules (see Table 8).

The pure gas permeation rate ratio before and after lamination is shown in Table 9. As can be seen the PGPR increased significantly upon lamination. Membrane PA-15 before lamination had a PGPR for H_2/CH_4 of only 4.3 and after lamination this increased to an average of 734.

Table 9: Average pure gas permeation rate ratio over a pressure range of 345 to 2068 kPag for membranes with and without lamination.

Gas pair	PA-9	laminated PA-9	PA-15	laminated PA-15	PA-19	laminated PA-19
H_2/CO_2	3.74	2.10	4.10	7.91	2.53	3.74
H_2/O_2	5.63	38.0	5.86	58.4	3.84	26.2
H_2/N_2	5.99	285	4.32	522	17.0	57.8
H_2/CH_4	4.71	335	4.28	734	6.57	84.3
He/H_2	1.43	2.46	0.79	1.86	2.69	2.55

4.3.1 Resistance Model Analysis

All laminated membranes were analyzed using the modified resistance model. As noted previously it was necessary to approximate α_2, the ratio of the intrinsic permeability of gas i over H_2 gas permeation for the polyamide substrate. Laminated membrane PA-15 which had the largest pure gas permeation rate ratios out of all the membranes tested was considered to best represent the α_2 values. In other words, the assumption is made that α_L (PGPR) approaches the value of α_2 for membrane PA-15. This is a reasonable assumption since membrane PA-15 shows a PGPR extraordinarily high compared to the other laminated membranes.

By using both the laminated and non-laminated experimental data for membranes PA-9 and PA-19 with the estimated α_2 values from laminated membrane PA-15 we are able to utilize the resistance model. The analysis was done for five gas pairs (H_2/O_2, H_2/N_2, H_2/CO_2, H_2/CH_4, and H_2/He) at 2068 kPag. The first half of the computer program in Appendix D was utilized to calculate all the parameters used in the resistance model.

An interesting variable that is obtained with the resistance analysis is the calculated pore area on the polyamide surface, A_3, for different gas pairs. This pore area actually corresponds to the total aggregate pore area on the membrane surface. As illustrated in Table 10 the larger the gas molecule that is paired with the hydrogen

Table 10: Molecular diameters versus the calculated pore area for different gas pairs.

Gas	H_2/He	H_2/CO_2	H_2/O_2	H_2/N_2	H_2/CH_4
*Kinetic dia. ($\times 10^{10}$m)	2.6	3.3	3.46	3.64	3.8
PA-9 A_3 (m^2)	1.98E-6	1.07E-6	1.98E-7	2.29E-8	2.24E-8
PA-19 A_3 (m^2)	2.84E-6	4.18E-7	2.32E-7	1.28E-6	9.83E-8
	decreasing pore area $\longrightarrow$				

*based on sorption in zeolites [6]

Table 11: Resistances for membrane PA-19 in units of Pa.s/mol for P=2068 kPag.

Resistance Pa.s/mol	Helium	Hydrogen	Carbon Dioxide	Oxygen	Nitrogen	Methane
R_1	2.87E+11	1.56E+11	3.19E+10	1.72E+11	3.44E+11	1.08E+11
$R_{1'}$	9.73E+13	1.18E+14	7.33E+13	7.13E+14	2.59E+14	1.05E+15
R_2	3.48E+12	9.24E+12	7.24E+13	5.03E+14	3.78E+15	8.41E+15
R_3	4.53E+12	1.44E+13	2.31E+13	2.45E+13	9.28E+13	3.33E+13
R_t	1.97E+12	5.63E+12	1.75E+13	2.34E+13	9.05E+13	3.31E+13
R_t^L	3.64E+12	8.77E+12	4.13E+13	2.99E+14	3.22E+14	9.61E+14

note : $\alpha_j = (R_j)_i/(R_j)_{H_2}$ where j =1, 1', 2, 3, t and i =He, CO_2, O_2, N_2, CH_4

atom, the smaller the available pore area on the surface of the polyamide membrane for permeation.

The resistance to permeate flow of the various sections of the composite membrane are shown in Tables 11 and 12 for membranes PA-19 and PA-9 respectively.

A closer inspection of these tables reveals the path taken by the permeating gas through the PA membrane. The difference between the permeate resistance through the membrane matrix (network pores), R_2, and the permeate resistance through the pore (aggregate pore), R_3, becomes greater as the molecular size increases. Table 11 shows for membrane PA-19 the relation between R_2 and R_3 to be as follows:

Table 12: Resistances for membrane PA-9 in units of Pa.s/mol for P=2068 kPag.

Resistance Pa.s/mol	Helium	Hydrogen	Carbon Dioxide	Oxygen	Nitrogen	Methane
R_1	2.87E+11	1.56E+11	3.19E+10	1.72E+11	3.44E+11	1.08E+11
$R_{1'}$	1.40E+14	6.59E+15	2.86E+13	8.35E+14	1.45E+16	4.62E+15
R_2	3.85E+12	9.60E+12	8.45E+13	5.59E+14	3.93E+15	9.32E+15
R_3	8.63E+11	1.08E+12	4.08E+12	5.72E+12	5.94E+12	4.45E+12
R_t	7.05E+11	9.72E+11	3.89E+12	5.66E+12	5.94E+12	4.44E+12
R_t^L	4.01E+12	9.74E+12	2.36E+13	3.36E+14	3.09E+15	3.09E+15

note : $\alpha_j = (R_j)_i/(R_j)_{H_2}$ where j =1, 1', 2, 3, t and i =He, CO_2, O_2, N_2, CH_4

He	$R_2 < R_3$
H_2	$R_2 < R_3$
CO_2	$R_2 > R_3$
O_2	$R_2 >> R_3$
N_2	$R_2 >>> R_3$
CH_4	$R_2 >>>> R_3$

With membrane PA-19, hydrogen and helium experience a slightly greater resistance through the aggregate pore than through the network pore. Whereas for N_2, CO_2, O_2, and CH_4 the resistance through the network pore is much greater than the resistance through the aggregate pore. Table 12 for membrane PA-9 shows a similar relationship.

He	$R_2 > R_3$
H_2	$R_2 >> R_3$
CO_2	$R_2 >>> R_3$
O_2	$R_2 >>>> R_3$
N_2	$R_2 >>>>> R_3$
CH_4	$R_2 >>>>>> R_3$

These cases indicates that sieving does occur, especially on the membrane matrix (network pore) for both PA-9 and PA-19.

With the modified resistance model it was possible to do some computer simulations using the experimental data as a basis. The pore area of the polyamide, A_3, was varied as well as the thickness of silicone rubber laminate, l_1. The resulting PGPR along with the flux was calculated from the resistance model. The calculations employed in predicting the performance of a composite membrane were done using the computer program in Appendix D.

Figures 12 through 15 illustrate the effect of the surface porosity of the polyamide substrate and the lamination thickness of the silicone rubber, on the PGPR of H_2/O_2, H_2/N_2, H_2/CO_2, H_2/CH_4 gas pairs. Figures 12 - 15 show slightly different surface patterns depending on which gas pair is employed. In general, as the polyamide surface porosity decreases the separation or PGPR increases to a maximum level; note this maximum level is actually the α_2 value for the substrate membrane material. If this maximum level (α_2 value) is reached, with sufficiently low surface porosity, any addition of silicone rubber actually deters from the PGPR factor. On the other hand, if this maximum level (α_2 value) is not reached addition of silicone rubber enhances the PGPR. As shown in the figures, the continued addition of silicone rubber also obtains a maximum PGPR value, whereupon any further increase in the thickness will deter from the pure gas permeation rate ratio. These graphs also indicate that the optimum lamination thickness and substrate porosity for the separation of one gas pair is not necessarily the optimum values for another gas pair.

Henis and Tripodi [13] illustrate the effect of surface porosity on the permeation properties of a polysulfone membrane coated (not laminated) with silicone rubber for a hydrogen/carbon monoxide gas mixture; they calculate this effect using their resistance model described in Section 2.2 of this thesis. Their analysis shows that the surface porosity of the polysulfone membrane has a greater effect on the permeation properties of an uncoated membrane than for a coated membrane. Separation

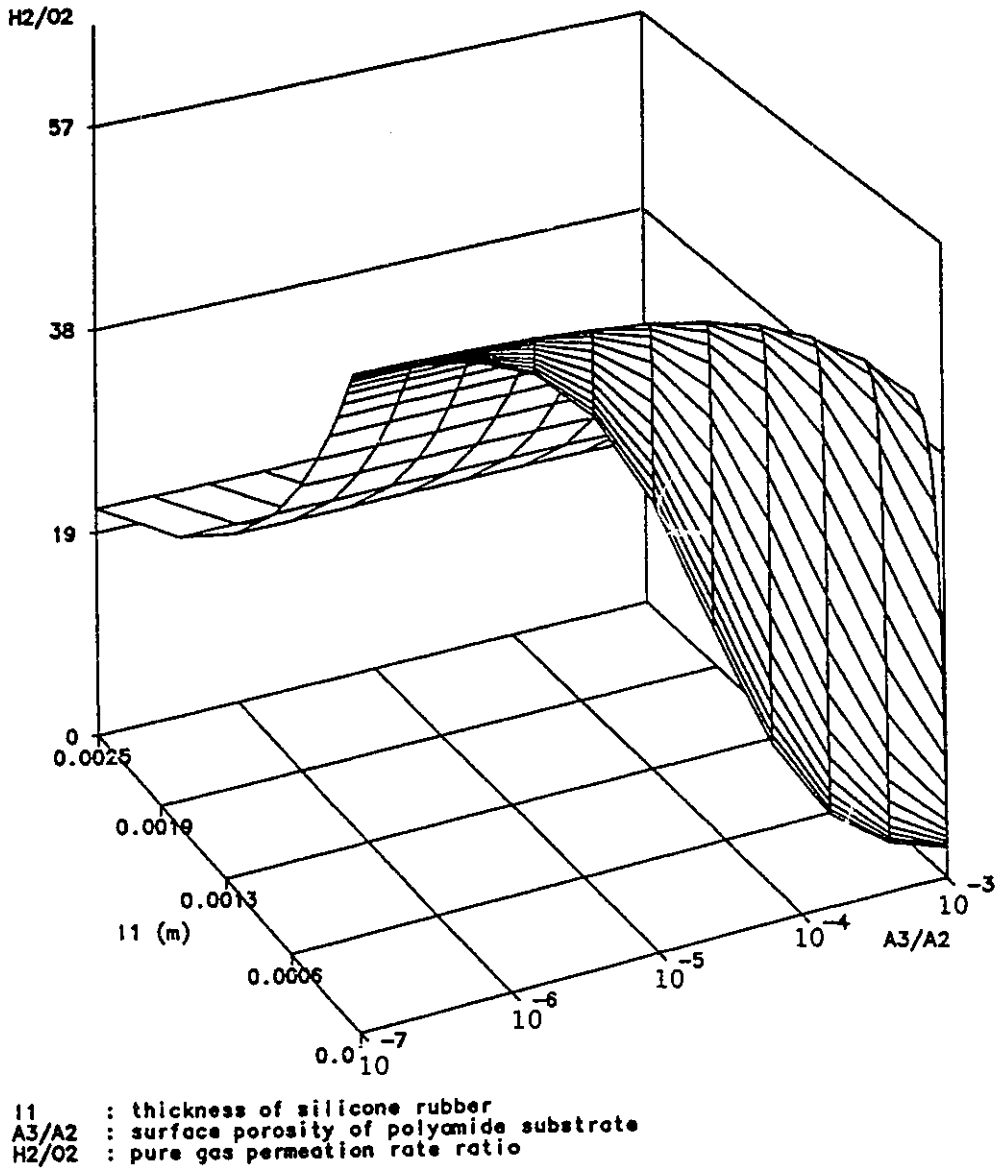

Figure 12: Ideal separation versus silicone rubber thickness and substrate polyamide porosity for P=2068 kPag.

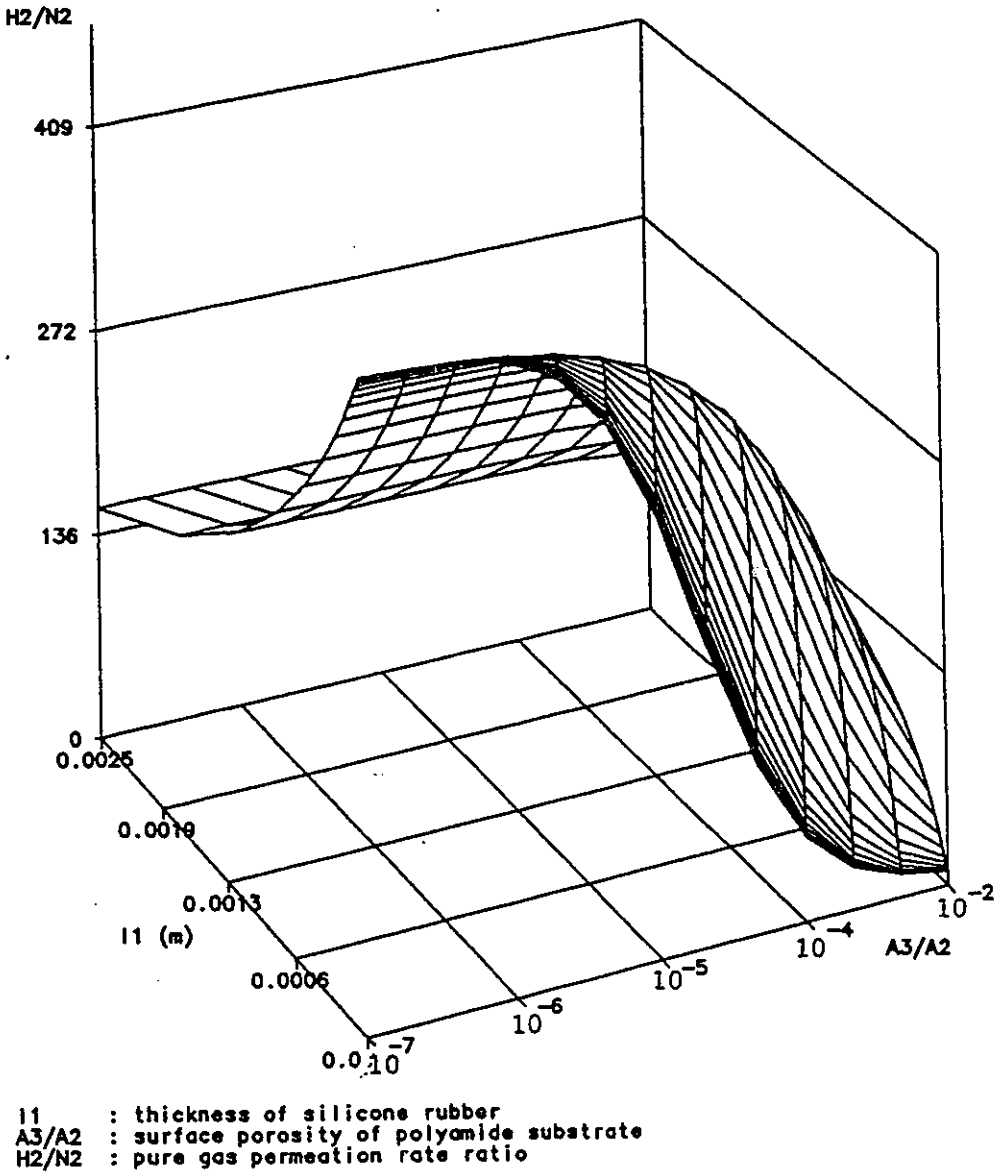

Figure 13: Ideal separation versus silicone rubber thickness and substrate polyamide porosity for P=2068 kPag.

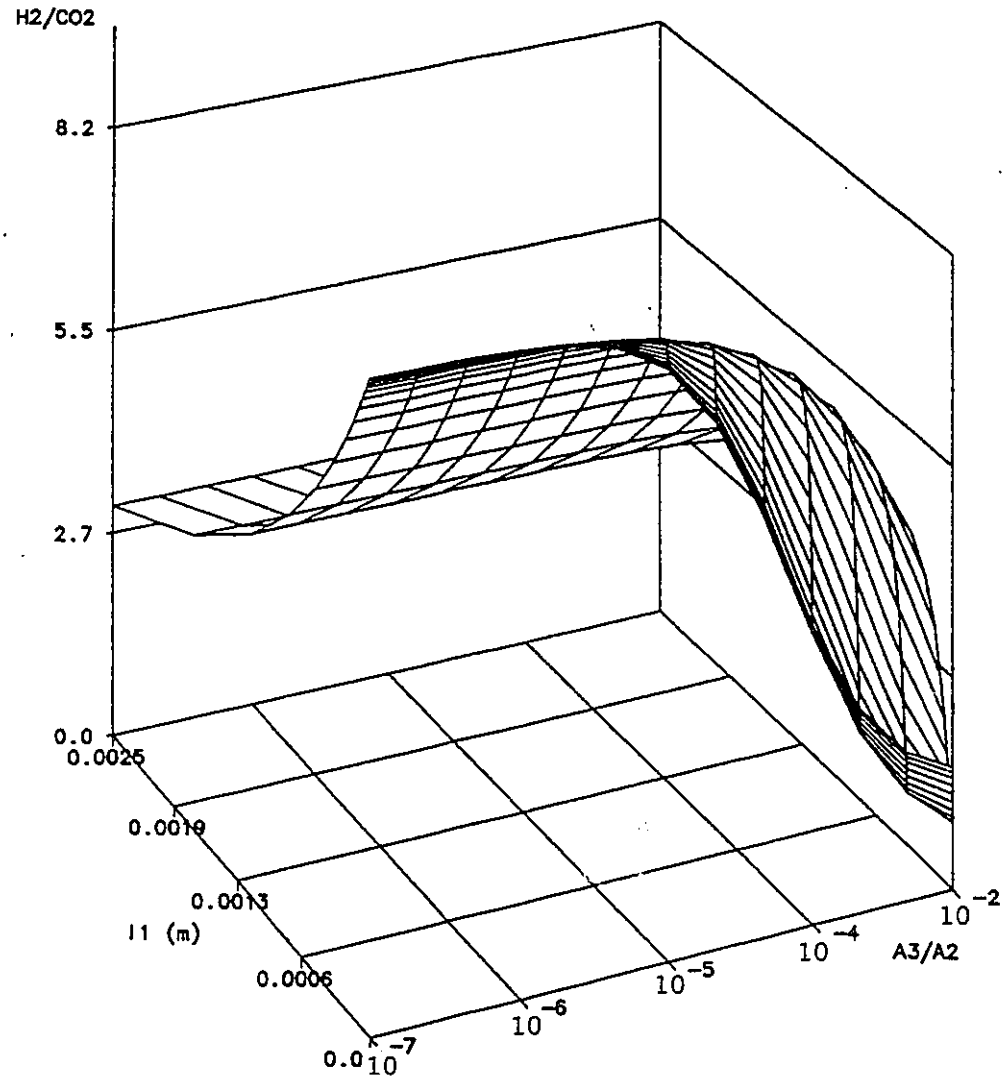

Figure 14: Ideal separation versus silicone rubber thickness and substrate polyamide porosity for P=2068 kPag.

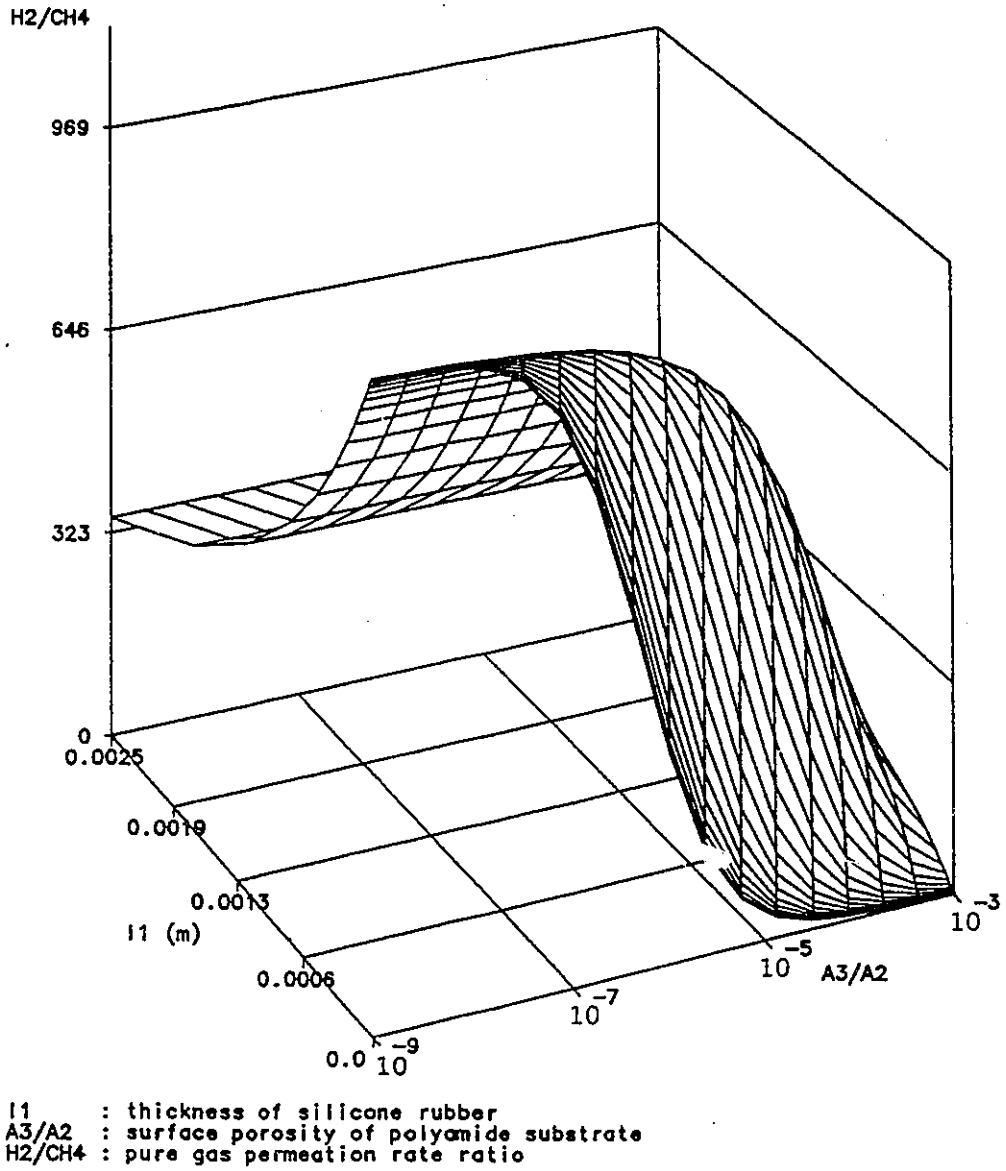

Figure 15: Ideal separation versus silicone rubber thickness and substrate polyamide porosity for P=2068 kPag.

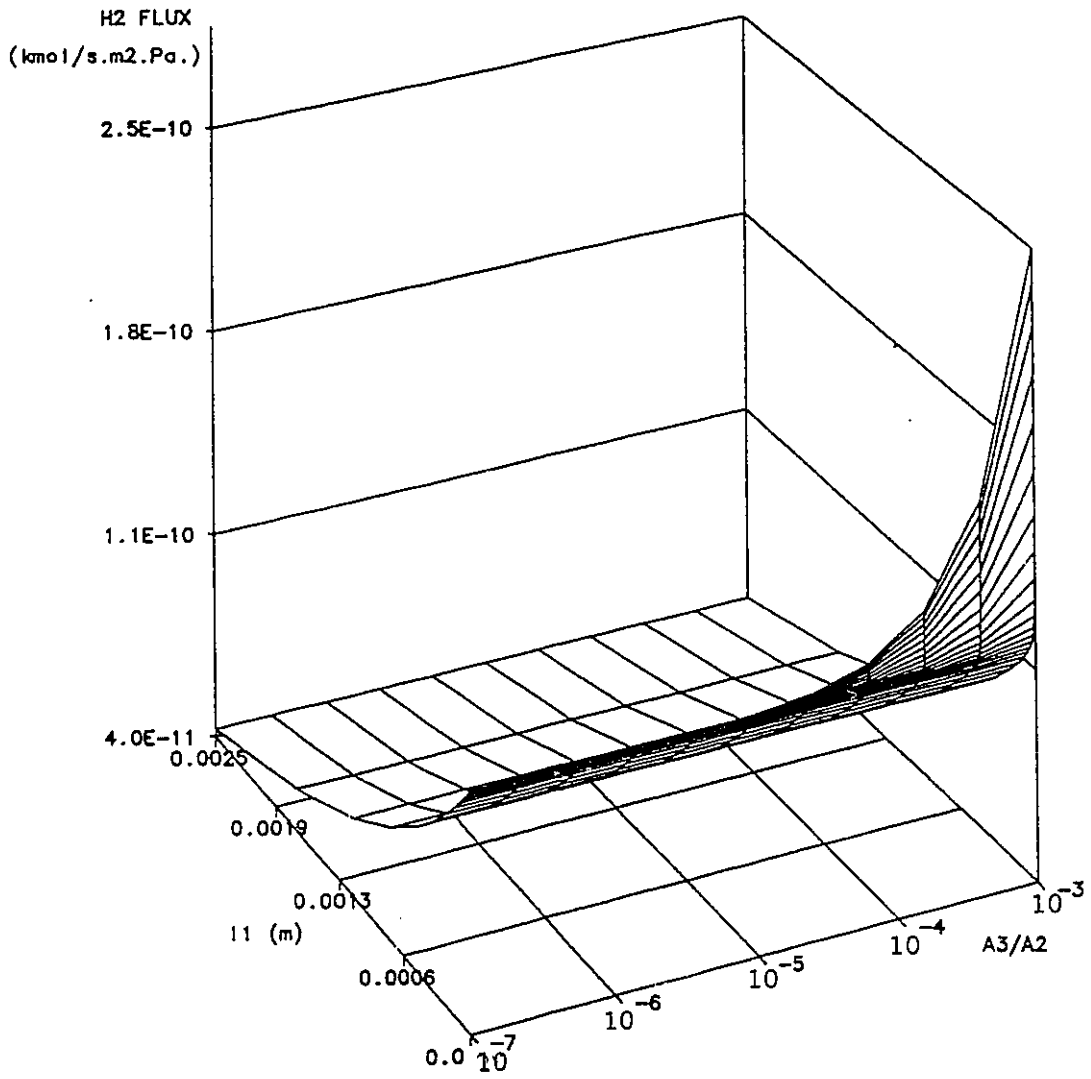

Figure 16: Hydrogen flux versus silicone rubber thickness and substrate polyamide porosity for P=2068 kPag.

factors of a coated membrane can be maintained even though the surface porosity of the substrate is increased; whereas, separation factors of an uncoated membrane will decrease drastically with an increase in surface porosity. The above observations are confirmed for the polyamide membrane used in this thesis. Their analysis showed for increasing silicone rubber thicknesses a continued decrease of separation occurred. This too is illustrated in the Figures 12 to 15 for surface porosities below approximately 10^{-7}.

Figure 16 shows the corresponding hydrogen flux versus silicone thickness and porosity of polyamide membrane. As expected the flux increases with an increase in surface porosity and decreases with an increase with silicone rubber thickness.

For industrial applications, the silicone rubber thickness is anywhere between 0 and 6.5×10^{-5} m. Focusing on the H_2/CH_4 simulation, the region of silicone rubber thickness between 0 and 6.5×10^{-5} m was enlarged as shown in Figure 17. Contour plots of flux and separation versus the polyamide surface porosity and silicone rubber thickness is shown on the next page (Figures 18 and 19). These contours show that for pure gas permeation rate ratios higher than 50 the hydrogen flux will not change appreciably; in other, words only the flux of the slow permeating gas is affected. As a result it is preferable to produce a composite membrane with as high as possible PGPR since there will be no appreciable loss in the hydrogen flux.

All of the above simulations deal solely with pure gas permeation and undoubtedly if mixed gases were used the actual separation factors would be lower. This effect, dubbed the "mixed gas effect", has been well documented in literature by several investigators [32,35,1]. More precisely, it is the reduction in the permeability of the fast gas in the presence of a slow gas and the increase in the permeability of a slow gas in the presence of the fast gas. Taking into consideration the "mixed gas effect" it is apparent that these simulations would lead to lower separations than

actually predicted. Nevertheless, they still provide a means of designing a optimum composite membrane for a particular gas pair.

It should be recognized that the maximum PGPR factor obtainable for the polyamide membrane is the α_2 value or intrinsic permeability ratio for a given gas pair. It should be noted that in these simulations the effective thickness of the polyamide membranes is kept constant to that of membrane PA-19. In practice it may be very difficult to produce membranes of this low surface porosity without increasing the effective thickness of the polyamide membrane and thereby affecting the flux of the permeating gas.

4.4 X-Ray Diffraction

Wide angle x-ray diffraction measurements were made on PA membranes of 13, 17 and 19 minute oven evaporation times using isopropyl alcohol and hexane as the drying solvents for solvent exchange technique. Also a PA membrane with a oven evaporation time of 13 minutes dried by various other solvent combinations was tested. The solvent pairs used for drying this membrane were as follows: isopropyl alcohol and toluene, methanol and toluene, methanol and hexane, and finally methnol and pentane.

All of the above membranes produced identical diffraction patterns as shown in Figure 20. This is understandable since WAXD measures a property of the polymeric film that is considered to be intrinsic in nature for a given polymeric material. The pattern produced is similar in shape to those reported by researchers Boehme et al. [5] and Kim et al. [18] for a polyimide membrane material.

The broad peak at $2\theta = 22.7^{o}$ in Figure 20 is attributed to the intersegmental interference. By applying Bragg's equation, $n\lambda = 2d\sin\theta$, the intersegmental distance of the polymeric molecules can be determined. This distance corresponds to

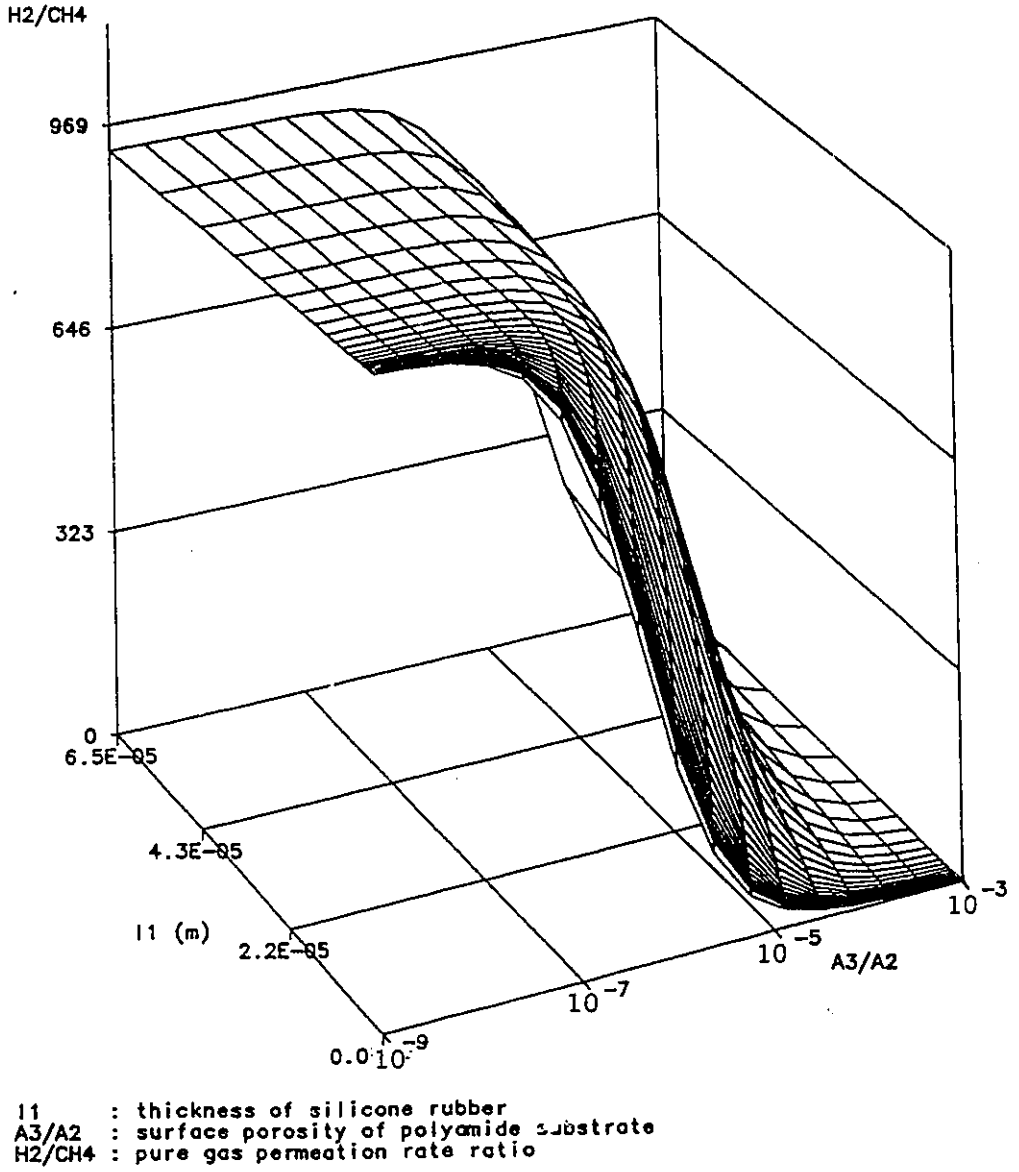

Figure 17: A closer look at H_2/CH_4 separation versus silicone rubber thickness and substrate polyamide porosity for P=2068 kPag.

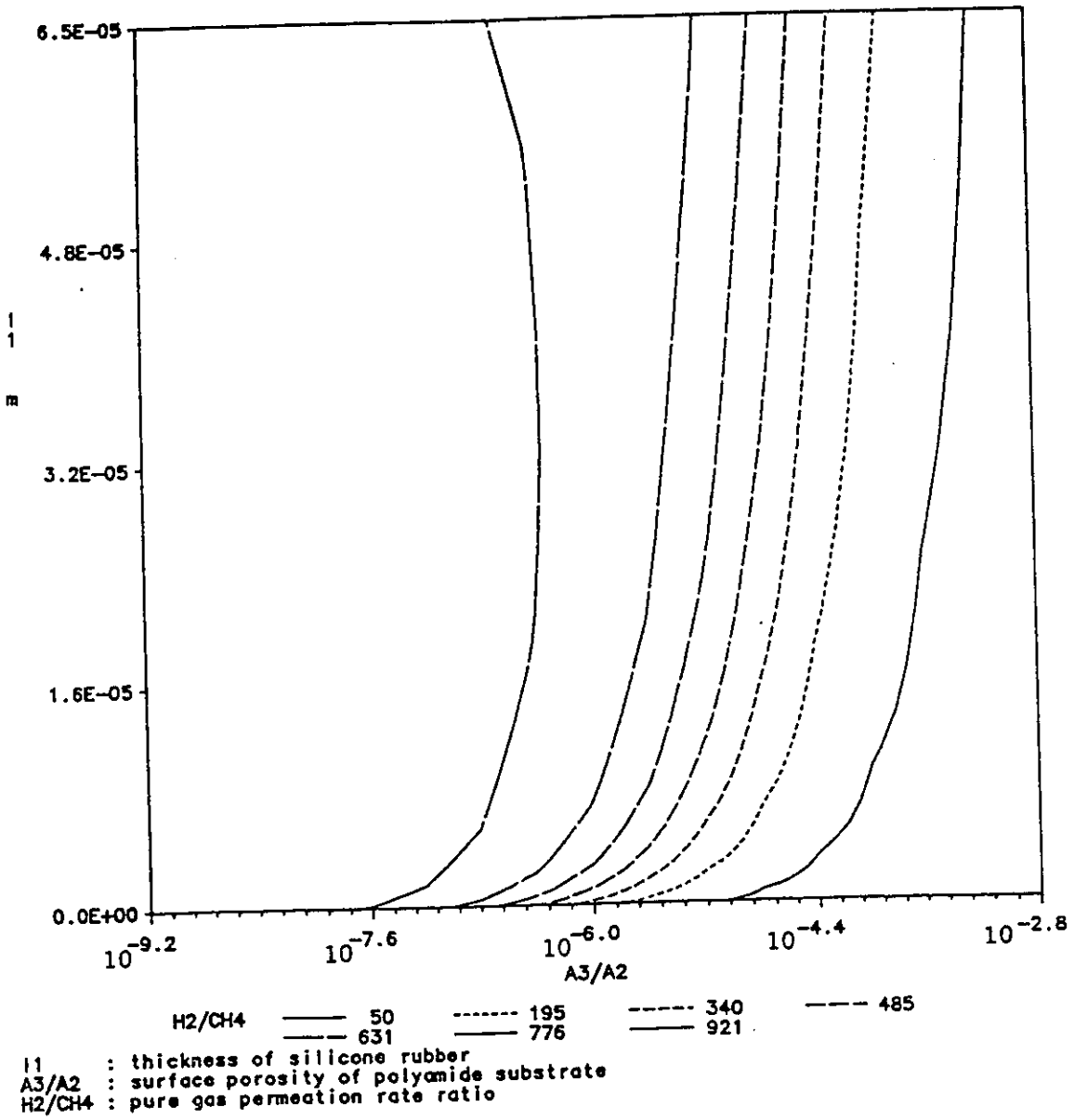

Figure 18: A contour plot of of H_2/CH_4 separation for silicone rubber thickness versus substrate polyamide porosity at P=2068 kPag.

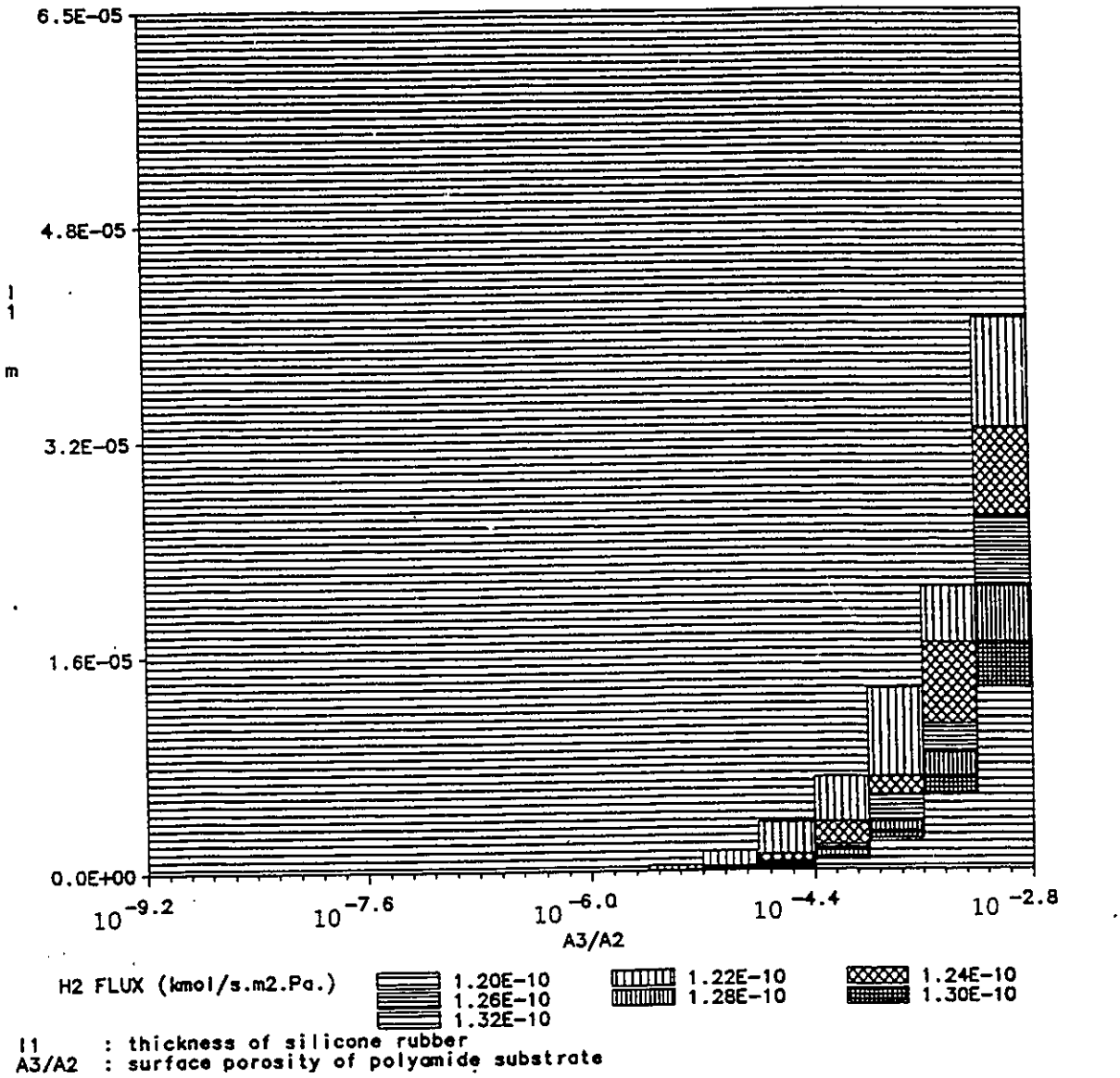

Figure 19: A contour plot of hydrogen flux for silicone rubber thickness versus substrate polyamide porosity at P=2068 kPag.

the network pore described in Chapter 1, which are the voids found between polymeric chains. With the order of diffraction, n, set equal to 1 and the wave length of the x-ray, λ, equal to 1.54 Åthe average intersegmental distances of polymer chains, d, is calculated to be 3.92 Å.

This distance is very close to the diameters of the large gas molecules used in this work. This measurement by WAXD further supports the conclusion from the resistance model that a sieving effect is occurring through the membrane matrix (aggregate pores).

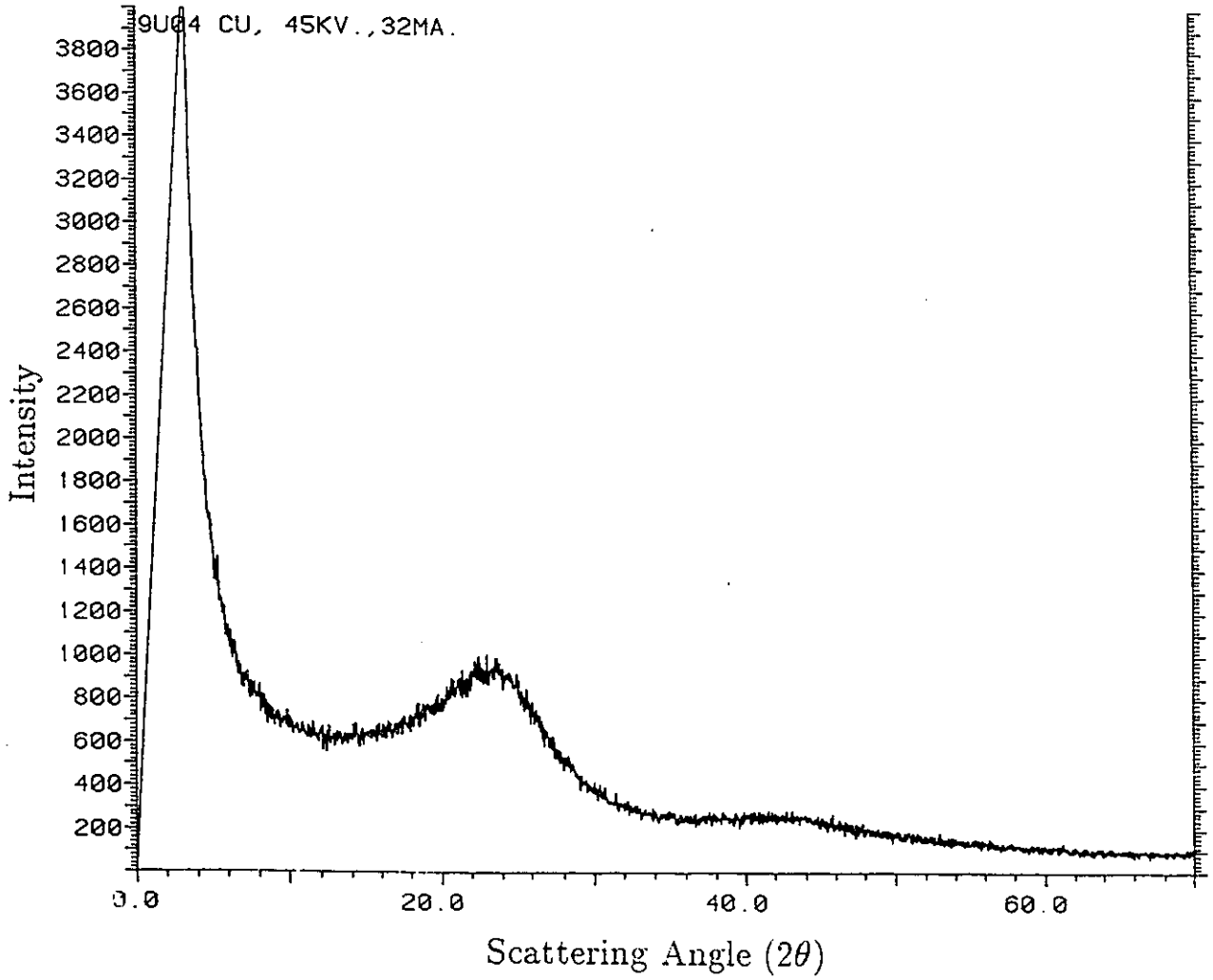

Figure 20: X-ray scattering of PA membrane using Cu radiation of λ=1.54 Å.

Chapter 5

Conclusions

5.1 Polyamide Membranes

1. Permeation of He, H_2 and CO_2 take between 2-80 hours to reach steady state. The reasons for this are unclear at the moment. However, it is interesting to note that He and H_2 are the two lightest molecules used in this study; whereas, CO_2 is known to plasticize polymers whereupon increased permeation occurs.

2. Pore sizes of the polyamide membrane as given by the surface force pore flow program decrease with an increase in molecule size and/or an increase in adsorption power.

3. Employing the SFPF model to characterize the membrane using the experimental permeation data from first three pressure points (345, 689, 1034 kPag), it was possible to predict the permeation rate for the next three pressure points (1379, 1723, 2068 kPag).

4. Characterization of the membrane by $\overline{R}$, σ, A_1, and A_2 values using the computer program does not necessarily give unique values. However, the range of values are generally close together.

5. Predicting the permeation rate of any gas given the permeation rate of a reference gas does not work with the polyamide membranes used in this study. A probable reason is that the pore size variance, σ, and A_1 $(= N_t/\delta S)$ for polyamide membranes is not constant for different gases as is assumed in this method of prediction. In other words, the effect of pore blocking cannot be considered negligible.

5.2 Laminated Polyamide Membranes

1. Lamination increases the pure gas permeation rate ratio greatly while the hydrogen or helium flux is only affected by a factor less than 10.

2. The permeation rate increases with a decrease in the gas molecule diameter.

3. The modified resistance model indicates that a sieving effect is occurring for the permeation of larger molecules through the network pores (membrane matrix). Helium and hydrogen gas show a preference to permeate through the network pore; whereas, the other larger molecules show a preference to permeate through the aggregate pore.

4. The modified resistance model could be used to design membranes of specific permeation and separations properties through computer simulations.

5. Wide angle x-ray diffraction indicates an average intersegmental distance of 3.92 Å. This further supports the conclusion regarding the sieving effect taking place through the membrane matrix.

Chapter 6

Recommendations

Care must be taken when trying to characterize the membrane given only the pressure versus permeation rate experimental data. It may not be possible to obtain a unique characterization for a given membrane using the surface force pore flow program. A unique characterization in terms of $\overline{R}$, σ, A_1, and A_2 may be achieved if one is able to incorporate along with the pressure versus flux data some type of high pressure adsorption data. Another solution could be to incorporate two pore size distributions thus enabling both the network pores and aggregate pores to be represented by their own distribution.

Bibliography

Bibliography

[1] C.R. Antonson, R.U. Gardner, C.F. King, and D.Y. Ko. Analysis of gas separation by permeation in hollow fibers. *Ind. Eng. Chem. Proc. Des. Dev.*, 16:463, (1977).

[2] R.W. Baker and I. Blume. Permselective membranes separate gases. *CHEMTECH*, 222, April (1986).

[3] E.R. Beaver, P.V. Bhat, and D.S. Sarcia. Integaration of membranes with other air separations technologies. In *New Membrane Materials and Processes for Separation*, page 113, (1988). AICHE Symposium Series.

[4] P.V. Bhat and E.R. Beaver. Innovations in nitrogen inerting using membrane systems. In *New Membrane Materials and Processes for Separation*, page 124, (1988). AICHE Symposium Series.

[5] R.F. Boehme and G.S. Cargill III. X-ray scattering measurements demostrating in-plane anisotropy in Kapton polyimide films. In K.L. Mittal, editor, *Polyimides*, Plenum Press, New York, (1984).

[6] D.W. Breck. *Zeolite Molecular Sieves.* John Wiley & Sons, Inc., (1974). p. 636.

[7] Y. Chen, A.E. Fouda, and T. Matsuura. A study on dry cellulose acetate membranes for the separation of carbon dioxide/methane gas mixtures. In

Symposium on Advances in Reverse Osmosis and Ultrafiltration, page 259, National Research Council of Canada, (1989). The Third Chemical Congress of North America Continent.

[8] R.T. Chern, W.J. Koros, H.B. Hopfenberg, and V.T. Stannett. Material selection for membrane-based gas separations. *Mat. Sci. Syn. Membr.*, 0:25, (1985).

[9] M.H. Cohen and D. Turnbull. Molecular transport in liquids and glasses. *J. Chem. Phys.*, 31:1164, (1959).

[10] A.E. Fouda, T.K. Matsuura, and A. Lui. Permeation of gas mixtures in cellulose acetate membranes - practical approach to predict the permeation rate of CO_2/CH_4 mixture. *Sep. Sci. Tech.*, 23(12&13):2175, (1988).

[11] P.K. Gantzel and U. Mertan. Gas separations with high - flux cellulose acetate membranes. *I&EC Proc. Des. Dev.*, 9:331, (1970).

[12] J. Haggin. New generation of membranes developed for industrial separation. *C & EN Chicago*, 7, June (1988).

[13] J.M.S. Henis and M.K. Tripodi. Composite hollow fiber membranes for gas separation: the resistance model approach. *J. Membrane Sci.*, 8:233, (1981).

[14] J.M.S. Henis and M.K. Tripodi. The developing technology of gas separating membranes. *Science*, 220(4592):11, April (1983).

[15] J.M.S. Henis and M.K. Tripodi. A novel approach to gas separations using composite hollow fiber membranes. *Sep. Sci. Technol.*, 15(4):1059, (1980).

[16] R.E. Kesting. The nature of pores in integrally-skinned phase inversion membranes. In *Symposium on Advances in Reverse Osmosis and Ultrafiltration*, National Research Council of Canada, (1989). The Third Chemical Congress of North America Continent.

[17] R.E. Kesting. *Synthetic Polymeric Membranes A Structural Perspective.* John Wiley & Sons, (1985).

[18] T.H. Kim, W.J. Koros, and G.R. Husk. Relationship between gas separation properties and chemical structure in a series of aromatic polyimides. *J. Membrane Sci.*, 37:45, (1988).

[19] W.J. Koros and R.T. Chern. *Handbook of Separation Process Technology.* Wiley Interscience, New York, (1987).

[20] B.W. Laverty and J.G. O'Hair. Applications of membrane technology in the gas industry. In *Membranes Gas Separation and Enrichment : The Proceedings of the Fourth BOC Priestley Conference*, September (1986).

[21] H.W. Liepmann. J. fluid mech. 10:85, (1961).

[22] S. Loeb and S. Sourirajan. *Sea Water Dimineralization by Means of a Semipermeable Membrane.* Dept. Eng. Repts. 60-60, University of California, Los Angeles, (1961).

[23] V.T. Long, B.S. Minhas, T. Matsuura, and S. Sourirajan. Gas chromatographic method for the measurement of gas sorption on polymeric materials. *J. Colloid Interface Sci.*, 125(2):478, October (1988).

[24] Manos. *Gas Separation Membrane Drying with Water Replacement Liquid.* Technical Report 4080744, U.S. Patent, March (1978).

[25] Manos. *Membrane Drying Process.* Technical Report 4080743, U.S. Patent, March (1978).

[26] L. Matson, J. Lopez, and J.A. Quinn. Separation of gases with synthetic membranes. *Chem. Eng. Sci.*, 38(4):503, (1983).

[27] T. Matsuura, Y. Chen, and T. Okeda. Science of membrane transport and membrane design. In *North American Membrane Society, Inc. 3rd Annual Meeting*, May (1989).

[28] M.A. Mazid. Review : Mechanisms of transport through reverse osmosis membranes. *Sep. Sci. Tech.*, 19(6&7):357, (1984).

[29] M.A. Mazid, R. Rangarajan, T. Matsuura, and S. Sourirajan. Separation of hydrogen-methane gas mixtures by permeation under pressure through porous cellulose acetate membranes. *I & EC Process Design and Development*, 24:907, (1985).

[30] P. Mears. *Membrane Separation Processes.* Elsevier Scientific, Amsterdam, (1976).

[31] B.S. Minhas, T. Matsuura, and S. Sourirajan. Solvent-exchange drying of cellulose acetate membranes for the separation of hydrogen-methane gas mixtures. In *Reverse Osmosis and Ultrafiltration*, ACS Symposium Series No. 281, (1985).

[32] B.S. Minhas, S.P. Wang, and M.B. Sherwin. Effect of process variables on cellulose acetate membranes performance for separation of carbon dioxide-methane mixtures. In *Proceedings of the International Membrane Conference on the 25th Anniversary of Membrane Research in Canada*, page 213, (1986).

[33] T.D. Nguyen and T. Matsuura. Design of aromatic polyamide membrane for reverse osmosis. In *Proc. Int. Membrane Conf.*, (1986). NRC Ottawa.

[34] T.D. Nguyen, T. Matsuura, and S. Sourirajan. Effect of nonsolvent additives on the pore size and the pore size distribution of aromatic polyamide RO membranes. *Chem. Eng. Comm.*, 54:17, (1987).

[35] D.G. Pye, H.H. Hoehn, and M. Panar. Measurement of gas permeability of polymers. i. Permeabilities in constant volume/variable pressure aparatus. *J. Appl. Polym. Sci.*, 20:1921, (1976).

[36] R. Rangarajan, M.A. Mazid, T. Matsuura, and S. Sourirajan. Permeation of pure gases under pressure through asymmetric porous membranes. membrane characterization and prediction of performance. *Ind. Eng. Chem. Proc. Des. Dev.*, 23(1):79, (1984).

[37] A. Ruf and S. Egli. Application of gas separation shown through the purification of landfill gas. *Gas Separation & Purification*, 2:90, June (1988).

[38] E. Sada, H. Kumazawa, P. Xu, and M. Nishigaki. Mechanism of gas permeation through glassy polymer films. *J. Membrane Sci.*, 37:165, (1988).

[39] C.W. Saltonstall. Gas membranes. In *The 1984 2nd Annual Membrane Technology/Planning Conference*, October (1984).

[40] W.J. Schell. Separation of coal hydrogasification of gases by permselective membranes. *ACS Div. Fuel Chem. Reprints*, 20:253, (1975).

[41] W.J. Schell and C.D. Houston. Membrane gas separations for chemical processes and energy applications. In *Industrial Gas Separations*, page 125, American Chemical Society, (1983). ACS Symposium series 223.

[42] R.L. Schendel. Separation of acid gas and hydrocarbons. In *Membranes Gas Separation and Enrichment : The Proceedings of the Fourth BOC Priestley Conference*, September (1986).

[43] L.H. Schwartz and J.B. Cohen. *Diffraction from Materials*, chapter 3. Academic Press, New York, (1977).

[44] S. Sourirajan. *Lectures on Reverse Osmosis.* National Research Concil of Canada, Ottawa, (1983). Lecture 4.

[45] S. Sourirajan and T. Matsuura. *Reverse Osmosis / Ultrafiltration Process Principles.* National Research Concil of Canada, Ottawa, (1985). section 11.

[46] R.W. Spillman. An overview of gas separation membranes. In *The 1988 6th Annual Membrane Technology/Planning Conference Proceedings*, November (1988).

[47] D.E. Stahl. *Ph.D. Thesis.* PhD thesis, Chemical Engineering Department, The University of Iowa, Iowa City, IA, (1971).

[48] S.A. Stern and V. Saxena. Concentration-dependent transport of gases and vapors in glassy polymers. *J. Membrane Sci.*, 7:47, (1980).

[49] S.A. Stern, S.K. Sen, and A.K. Rao. The permeation of gases through symmetric and asymmetric (Loeb-type) cellulose acetate membranes. *J. Macromol. Sci. Phys.*, 10:507, (1974).

[50] W.R. Vieth, J.M. Howell, and J.H. Hsieh. Review paper : Dual Sorption Theory. *J. Membrane Sci.*, 1:177, (1976).

[51] W.R. Vieth and Y. Jiang. Counterdiffusion of carbon dioxide and methane in a glassy polymer. *J. Membrane Sci.*, 38:1, (1988).

[52] K.D. Vos and F.O. Burris Jr. Drying cellulose acetate reverse osmosis membranes. *Ind. Eng. Chem. Proc Des. Dev.*, 8:84, (1969).

[53] J.S. Vrentas, J.L. Duda, and H.-C. Ling. Free-volume theories for self-diffusion in polymer- solvent systems.I. Conceptual differences in theories. *J. Polym. Sci., Polym. Phys. Ed.*, 23:275, (1985).

[54] J.S. Vrentas, J.L. Duda, H.-C. Ling, and A.-C. Hou. Free-volume theories for self-diffusion in polymer- solvent systems.II. Predictive capabilities. *J. Polym. Sci., Polym. Phys. Ed.*, 23:289, (1985).

[55] U. Werner. Some technical and economical aspects of gas separation by means of membranes. In *Membranes Gas Separation and Enrichment : The Proceedings of the Fourth BOC Priestley Conference*, September (1986).

[56] A.G. Wonders and D.R. Paul. Effect of CO_2 exposure history on sorption and transport in polycarbonate. *J. Membrane Sci.*, 5:63, (1979).

Appendix A

Experimental Data

Table 13: Permeation coefficients for membrane PA-9 with pure gases in kmol/s.m^2.Pa (9 min. oven evap. time).

Pressure kPag	Nitrogen	Methane	Oxygen	Carbon Dioxide	Hydrogen	Helium
2068	1.75E-13	2.34E-13	1.84E-13	2.73E-13	1.07E-12	1.51E-12
1723	1.71E-13	2.28E-13	1.80E-13	2.79E-13	1.06E-12	1.47E-12
1379	1.64E-13	2.17E-13	1.75E-13	2.66E-13	1.04E-12	1.45E-12
1034	1.58E-13	1.98E-13	1.67E-13	2.60E-13	9.73E-13	1.42E-12
689	1.46E-13	1.84E-13	1.59E-13	2.53E-13	8.74E-13	1.35E-12
345	1.38E-13	1.56E-13	1.52E-13	2.62E-13	7.17E-13	1.13E-12
345	1.37E-13	1.57E-13	1.50E-13	2.29E-13	7.07E-13	1.11E-12
689	1.48E-13	1.84E-13	1.58E-13	2.22E-13	8.72E-13	1.27E-12
1034	1.56E-13	1.98E-13	1.67E-13	2.47E-13	9.78E-13	1.29E-12
1379	1.64E-13	2.16E-13	1.73E-13	2.53E-13	1.02E-12	1.42E-12
1723	1.71E-13	2.27E-13	1.79E-13	2.52E-13	1.06E-12	1.45E-12
2068	1.75E-13	2.33E-13	1.83E-13	2.62E-13	1.06E-12	1.47E-12

Table 14: Permeation coefficients for membrane PA-11 with pure gases in kmol/s.m^2.Pa (11 min. oven evap. time).

Pressure kPag	Nitrogen	Methane	Oxygen	Carbon Dioxide	Hydrogen	Helium
2068	1.01E-13	1.19E-13	1.20E-13	1.85E-13	3.71E-13	7.73E-13
1723	9.87E-14	1.13E-13	1.15E-13	1.76E-13	3.48E-13	6.81E-13
1379	9.47E-14	1.05E-13	1.12E-13	1.82E-13	3.17E-13	6.33E-13
1034	8.61E-14	9.47E-14	1.10E-13	1.82E-13	2.89E-13	5.82E-13
689	7.70E-14	8.46E-14	1.06E-13	1.83E-13	2.56E-13	5.34E-13
345	6.97E-14	6.47E-14	9.39E-14	1.94E-13	2.29E-13	5.10E-13
345	6.90E-14	6.56E-14	9.26E-14	1.93E-13	2.26E-13	5.09E-13
689	7.72E-14	8.49E-14	1.06E-13	1.81E-13	2.59E-13	5.40E-13
1034	8.62E-14	9.24E-14	1.09E-13	1.76E-13	2.96E-13	5.85E-13
1379	8.99E-14	1.03E-13	1.13E-13	1.77E-13	3.31E-13	6.28E-13
1723	.	1.09E-13	1.16E-13	1.76E-13	3.62E-13	6.68E-13
2068	.	1.19E-13	1.18E-13	1.80E-13	3.66E-13	7.63E-13

Table 15: Permeation coefficients for membrane PA-13 with pure gases in kmol/s.m^2.Pa (13 min. oven evap. time).

Pressure kPag	Nitrogen	Methane	Oxygen	Carbon Dioxide	Hydrogen	Helium
345	1.24E-13	1.30E-13	1.43E-13	3.28E-13	1.09E-12	2.46E-12
689	1.56E-13	1.85E-13	1.66E-13	3.72E-13	1.33E-12	2.62E-12
1379	1.93E-13	2.51E-13	2.00E-13	4.07E-13	1.64E-12	2.88E-12
2068	2.21E-13	2.97E-13	2.22E-13	4.48E-13	1.82E-12	2.98E-12
2758	2.41E-13	3.27E-13	2.45E-13	4.62E-13	1.97E-12	3.07E-12
3103	2.52E-13	3.42E-13	2.52E-13	4.81E-13	2.05E-12	3.14E-12
2758	2.41E-13	3.29E-13	2.46E-13	4.64E-13	2.00E-12	3.11E-12
2068	2.21E-13	2.93E-13	2.23E-13	4.49E-13	1.87E-12	3.02E-12
1379	1.94E-13	2.49E-13	2.00E-13	4.17E-13	1.71E-12	3.03E-12
689	1.57E-13	1.83E-13	1.68E-13	3.80E-13	1.39E-12	2.69E-12
345	1.31E-13	1.37E-13	1.43E-13	3.31E-13	1.12E-12	2.57E-12

Table 16: Permeation coefficients for membrane PA-15 with pure gases in kmol/s.m^2.Pa (15 min. oven evap. time).

Pressure kPag	Nitrogen	Methane	Oxygen	Carbon Dioxide	Hydrogen	Helium
2068	1.09E-12	1.20E-12	.	1.19E-12	5.28E-12	4.11E-12
1723	1.08E-12	1.18E-12	.	1.17E-12	5.12E-12	3.97E-12
1379	1.06E-12	1.17E-12	.	1.13E-12	4.92E-12	3.77E-12
1034	1.03E-12	1.12E-12	.	1.07E-12	4.53E-12	3.50E-12
689	9.93E-13	1.04E-12	.	9.81E-13	3.96E-12	3.15E-12
345	8.94E-13	9.24E-13	.	8.85E-13	3.20E-12	2.66E-12
345	9.02E-13	9.28E-13	6.46E-13	8.86E-13	3.16E-12	2.64E-12
689	9.82E-13	1.05E-12	6.92E-13	9.71E-13	3.88E-12	3.14E-12
1034	1.04E-12	1.12E-12	7.38E-13	1.09E-12	4.40E-12	3.46E-12
1379	1.08E-12	1.17E-12	7.84E-13	1.14E-12	4.71E-12	3.72E-12
1723	.	1.19E-12	8.03E-13	1.20E-12	4.94E-12	3.91E-12
2068	.	1.23E-12	8.61E-13	1.23E-12	5.24E-12	4.07E-12

Table 17: Permeation coefficients for membrane PA2-15 with pure gases in kmol/s.m^2.Pa (15 min. oven evap. time).

Pressure kPag	Nitrogen	Methane	Oxygen	Carbon Dioxide	Hydrogen	Helium
2068	2.44E-13	3.20E-13	2.15E-13	2.37E-13	7.98E-13	7.84E-13
1723	2.36E-13	3.07E-13	2.07E-13	2.36E-13	7.66E-13	7.47E-13
1379	2.21E-13	2.88E-13	1.95E-13	2.16E-13	7.15E-13	7.20E-13
1034	2.07E-13	2.63E-13	1.83E-13	2.07E-13	6.26E-13	6.85E-13
689	1.90E-13	2.37E-13	1.68E-13	1.92E-13	5.25E-13	6.11E-13
345	1.67E-13	1.93E-13	1.51E-13	1.83E-13	3.78E-13	4.92E-13
345	1.66E-13	1.91E-13	1.52E-13	1.67E-13	3.69E-13	4.92E-13
689	1.90E-13	2.36E-13	1.71E-13	1.82E-13	5.26E-13	5.84E-13
1034	2.09E-13	2.63E-13	1.73E-13	2.01E-13	6.23E-13	6.37E-13
1379	2.21E-13	2.91E-13	1.99E-13	2.13E-13	7.14E-13	7.14E-13
1723	2.36E-13	3.07E-13	2.10E-13	2.35E-13	7.65E-13	7.43E-13
2068	2.45E-13	3.21E-13	2.20E-13	2.45E-13	8.29E-13	7.77E-13

Table 18: Permeation coefficients for membrane PA-17 with pure gases in kmol/s.m^2.Pa (17 min. oven evap. time).

Pressure kPag	Nitrogen	Methane	Oxygen	Carbon Dioxide	Hydrogen	Helium
2068	3.29E-13	4.21E-13	3.23E-13	3.93E-13	1.27E-12	1.58E-12
1723	3.13E-13	4.05E-13	3.14E-13	3.94E-13	1.23E-12	1.53E-12
1379	2.99E-13	3.75E-13	3.05E-13	3.64E-13	1.12E-12	1.48E-12
1034	2.85E-13	3.51E-13	2.88E-13	3.57E-13	9.80E-13	1.39E-12
689	2.68E-13	3.19E-13	2.79E-13	3.47E-13	8.12E-13	1.25E-12
345	2.56E-13	2.72E-13	2.66E-13	3.80E-13	6.36E-13	9.13E-13
345	2.57E-13	2.77E-13	2.71E-13	3.47E-13	6.14E-13	9.09E-13
689	2.73E-13	3.18E-13	2.79E-13	3.34E-13	7.73E-13	1.09E-12
1034	2.86E-13	3.50E-13	2.92E-13	3.60E-13	9.36E-13	1.18E-12
1379	2.98E-13	3.73E-13	3.03E-13	3.62E-13	1.07E-12	1.39E-12
1723	3.12E-13	4.06E-13	3.11E-13	3.73E-13	1.23E-12	1.51E-12
2068	3.29E-13	4.21E-13	3.25E-13	3.74E-13	1.27E-12	1.56E-12

Table 19: Permeation coefficients for membrane PA-19 with pure gases in kmol/s.m^2.Pa (19 min. oven evap. time).

Pressure kPag	Nitrogen	Methane	Oxygen	Carbon Dioxide	Hydrogen	Helium
2068	1.15E-14	3.17E-14	4.69E-14	5.90E-14	1.85E-13	5.29E-13
1723	1.10E-14	2.99E-14	4.44E-14	5.76E-14	1.78E-13	4.79E-13
1379	9.11E-15	2.95E-14	4.49E-14	6.29E-14	1.71E-13	4.44E-13
1034	1.05E-14	2.64E-14	4.41E-14	6.82E-14	1.58E-13	4.14E-13
689	7.39E-15	2.48E-14	4.32E-14	6.64E-14	1.40E-13	3.84E-13
345	.	1.35E-14	4.11E-14	7.59E-14	1.35E-13	3.65E-13
345	.	1.34E-14	3.80E-14	7.61E-14	1.35E-13	3.64E-13
689	8.47E-15	2.47E-14	4.03E-14	6.63E-14	1.38E-13	3.85E-13
1034	1.03E-14	2.64E-14	3.85E-14	6.64E-14	1.60E-13	4.20E-13
1379	9.36E-15	2.94E-14	4.10E-14	6.35E-14	1.78E-13	4.43E-13
1723	1.10E-14	2.91E-14	4.08E-14	5.95E-14	1.94E-13	4.73E-13
2068	1.15E-14	3.11E-14	4.20E-14	5.98E-14	1.84E-13	5.2 7E-13

Table 20: Permeation coefficients for laminated membrane PA-9 with pure gases in kmol/s.m^2.Pa (9 min. oven evap. time).

Pressure kPag	Nitrogen	Methane	Oxygen	Carbon Dioxide	Hydrogen	Helium
2068	3.36E-16	3.19E-16	3.09E-15	4.34E-14	1.06E-13	2.59E-13
1723	2.44E-16	.	2.89E-15	4.71E-14	1.02E-13	2.52E-13
1379	.	.	3.11E-15	4.46E-14	9.45E-14	2.35E-13
1034	.	.	1.76E-15	5.20E-14	9.07E-14	2.28E-13
689	.	.	.	5.12E-14	8.82E-14	2.17E-13
345	.	.	.	5.43E-14	8.47E-14	2.13E-13
345	.	.	.	5.37E-14	9.12E-14	2.15E-13
689	.	.	.	4.54E-14	8.79E-14	2.24E-13
1034	.	.	.	3.89E-14	9.33E-14	2.41E-13
1379	.	.	.	4.07E-14	9.35E-14	2.50E-13
1723	.	.	.	3.86E-14	9.91E-14	2.68E-13
2068	.	.	.	4.48E-14	1.07E-13	2.52E-13

Table 21: Permeation coefficients for laminated membrane PA-15 with pure gases in kmol/s.m^2.Pa (15 min. oven evap. time).

Pressure kPag	Nitrogen	Methane	Oxygen	Carbon Dioxide	Hydrogen	Helium
2068	8.58E-16	3.62E-16	6.10E-15	4.00E-14	3.48E-13	6.55E-13
1723	7.81E-16	4.27E-16	4.98E-15	3.97E-14	3.41E-13	6.46E-13
1379	7.56E-16	3.32E-16	5.27E-15	4.59E-14	3.45E-13	6.45E-13
1034	5.97E-16	6.49E-16	6.19E-15	4.96E-14	3.45E-13	6.17E-13
689	5.04E-16	1.01E-15	7.40E-15	4.88E-14	3.29E-13	6.05E-13
345	.	.	.	3.38E-14	2.85E-13	5.64E-13
345	.	.	.	3.25E-14	2.79E-13	5.67E-13
689	.	.	.	4.48E-14	3.22E-13	5.99E-13
1034	.	.	.	4.29E-14	3.46E-13	6.02E-13
1379	.	.	.	4.29E-14	3.43E-13	6.26E-13
1723	.	.	.	4.26E-14	3.48E-13	6.35E-13
2068	.	.	.	4.58E-14	3.54E-13	6.50E-13

Table 22: Permeation coefficients for laminated membrane PA-19 with pure gases in kmol/s.m^2.Pa (19 min. oven evap. time).

Pressure kPag	Nitrogen	Methane	Oxygen	Carbon Dioxide	Hydrogen	Helium
2068	3.23E-15	1.08E-15	3.47E-15	2.58E-14	1.17E-13	2.86E-13
1723	1.51E-15	1.20E-15	3.98E-15	2.75E-14	1.11E-13	2.85E-13
1379	1.48E-15	1.19E-15	3.73E-15	3.00E-14	1.01E-13	2.71E-13
1034	1.68E-15	1.29E-15	3.79E-15	3.47E-14	9.64E-14	2.54E-13
689	1.27E-15	1.43E-15	5.20E-15	3.41E-14	8.47E-14	2.33E-13
345	2.00E-15	.	.	2.72E-14	8.66E-14	2.03E-13
345	.	.	.	2.69E-14	8.83E-14	2.03E-13
689	.	.	.	2.32E-14	8.52E-14	2.32E-13
1034	.	.	.	2.75E-14	9.89E-14	2.49E-13
1379	.	.	.	2.53E-14	1.00E-13	2.67E-13
1723	.	.	.	2.21E-14	1.11E-13	2.79E-13
2068	.	.	.	2.45E-14	1.20E-13	2.82E-13

Appendix B

Figures

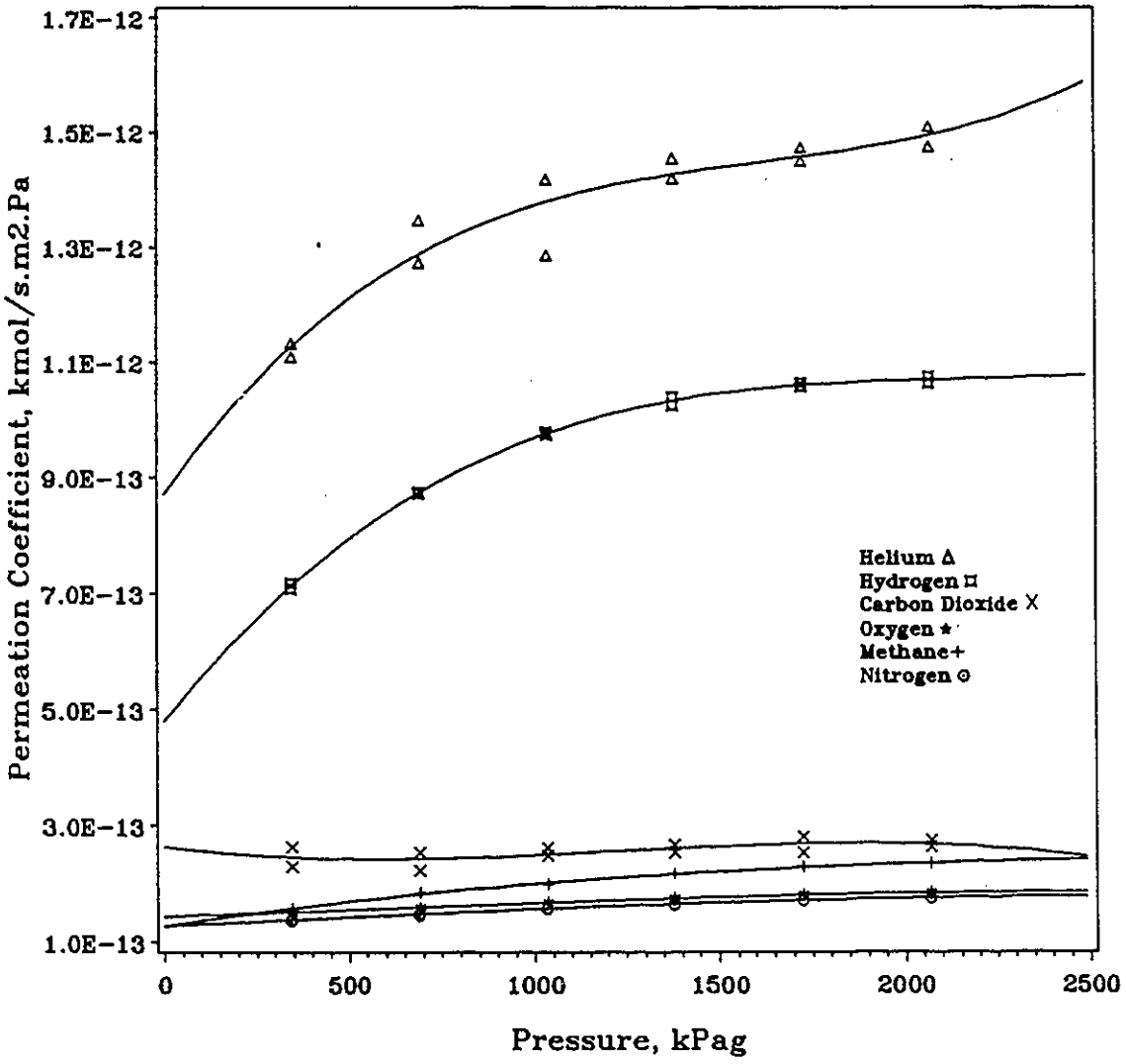

Figure 21: Permeation coefficient of pure gases versus pressure for membrane PA-9.

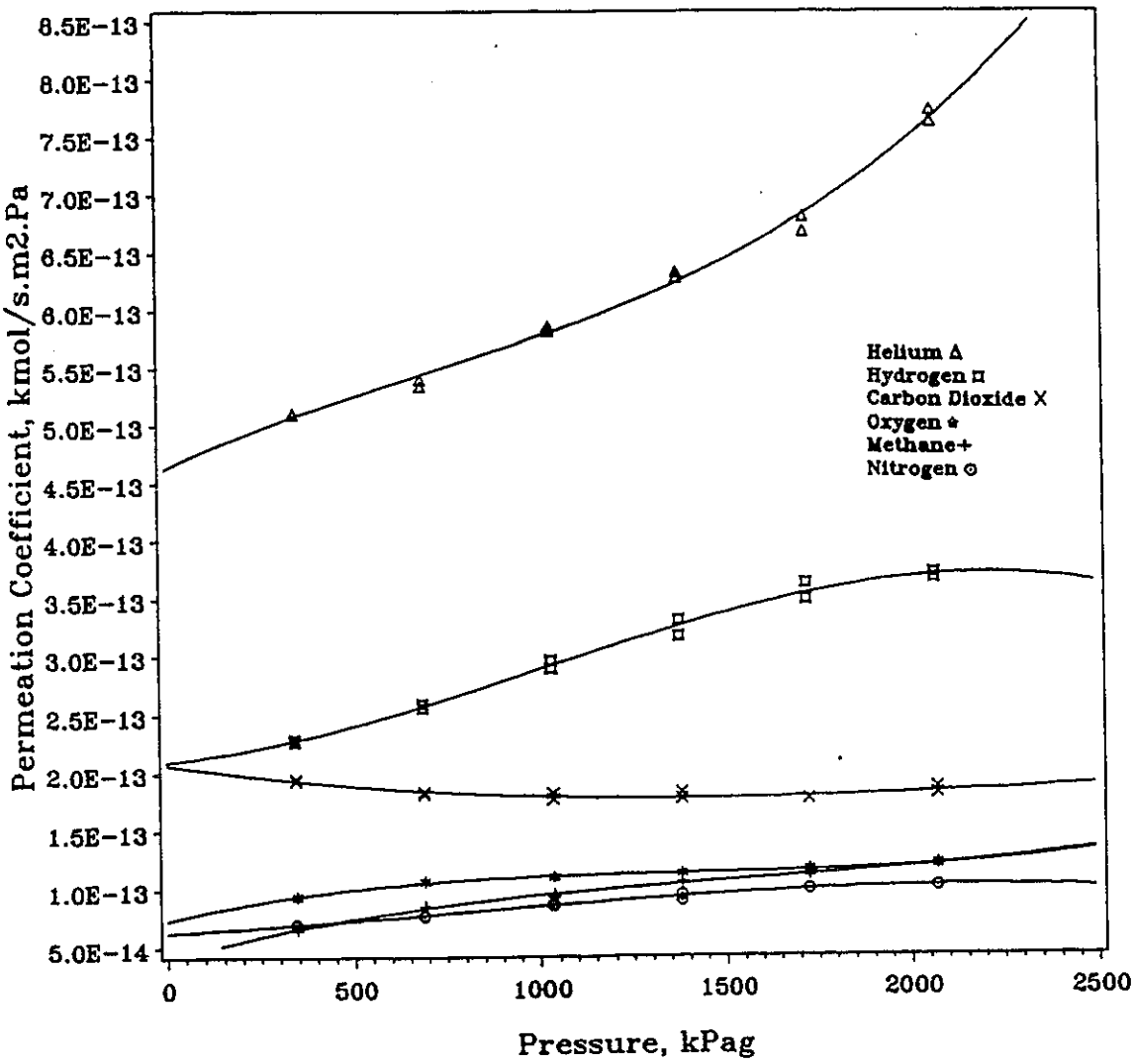

Figure 22: Permeation coefficient of pure gases versus pressure for membrane PA-11.

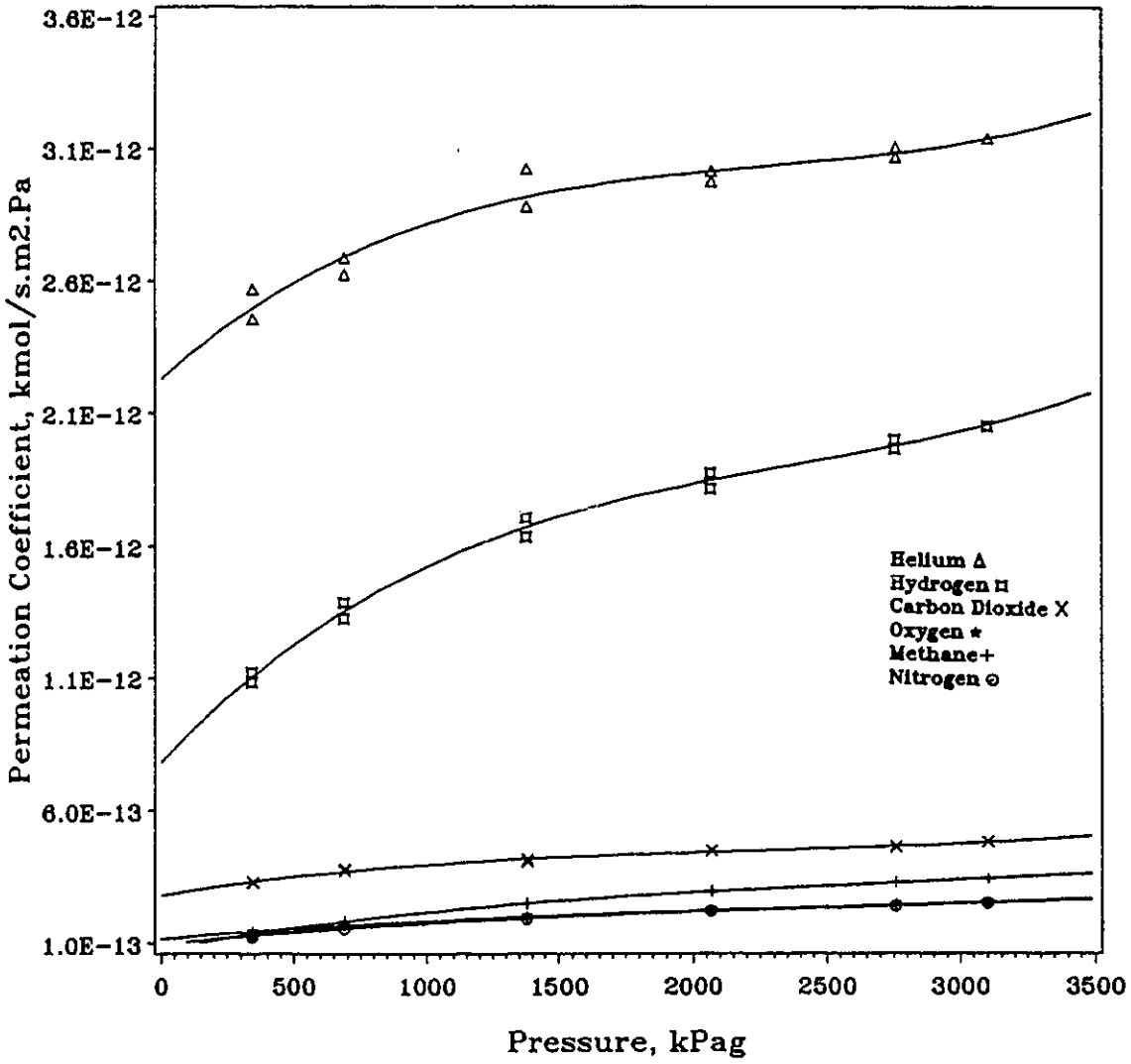

Figure 23: Permeation coefficient of pure gases versus pressure for membrane PA-13.

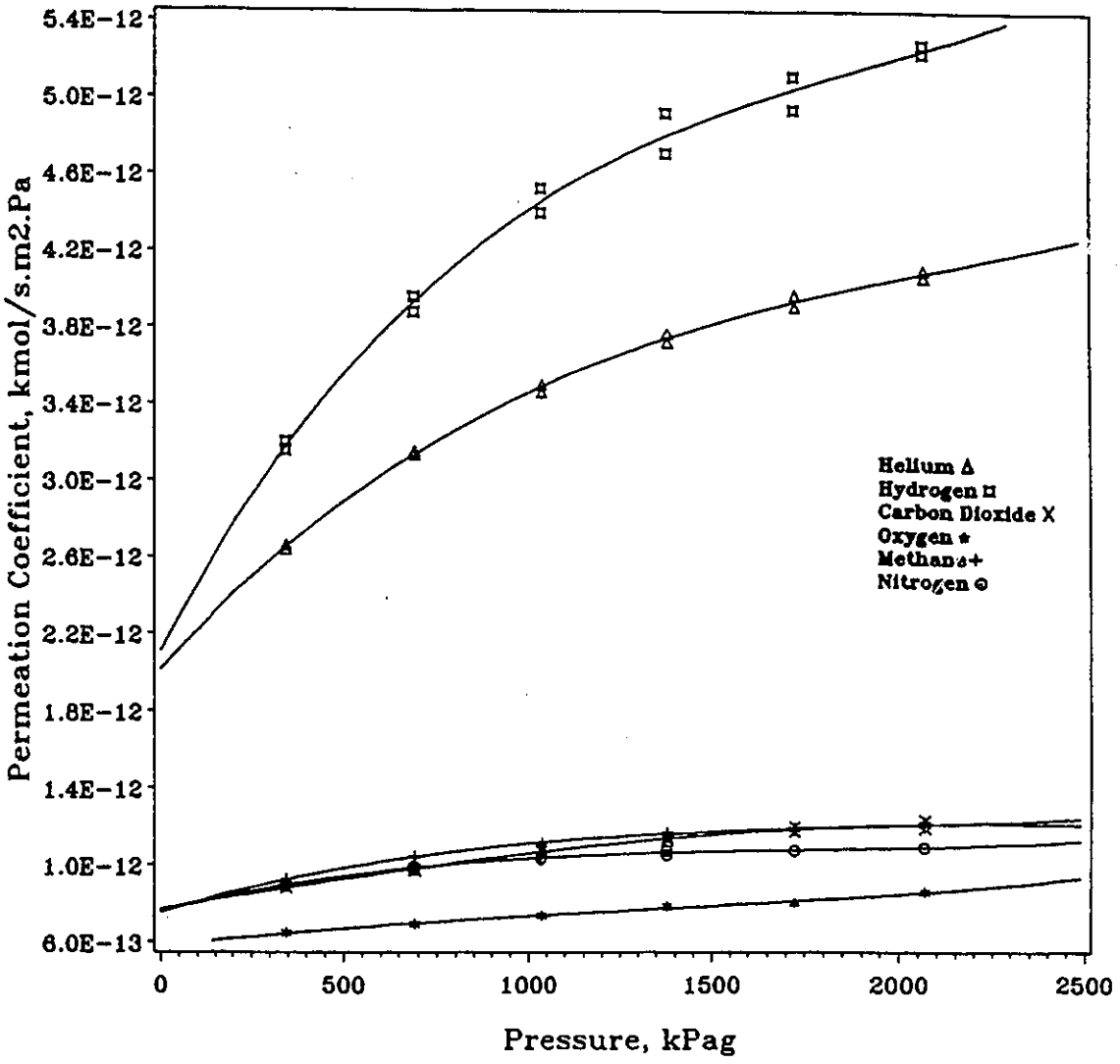

Figure 24: Permeation coefficient of pure gases versus pressure for membrane PA-15.

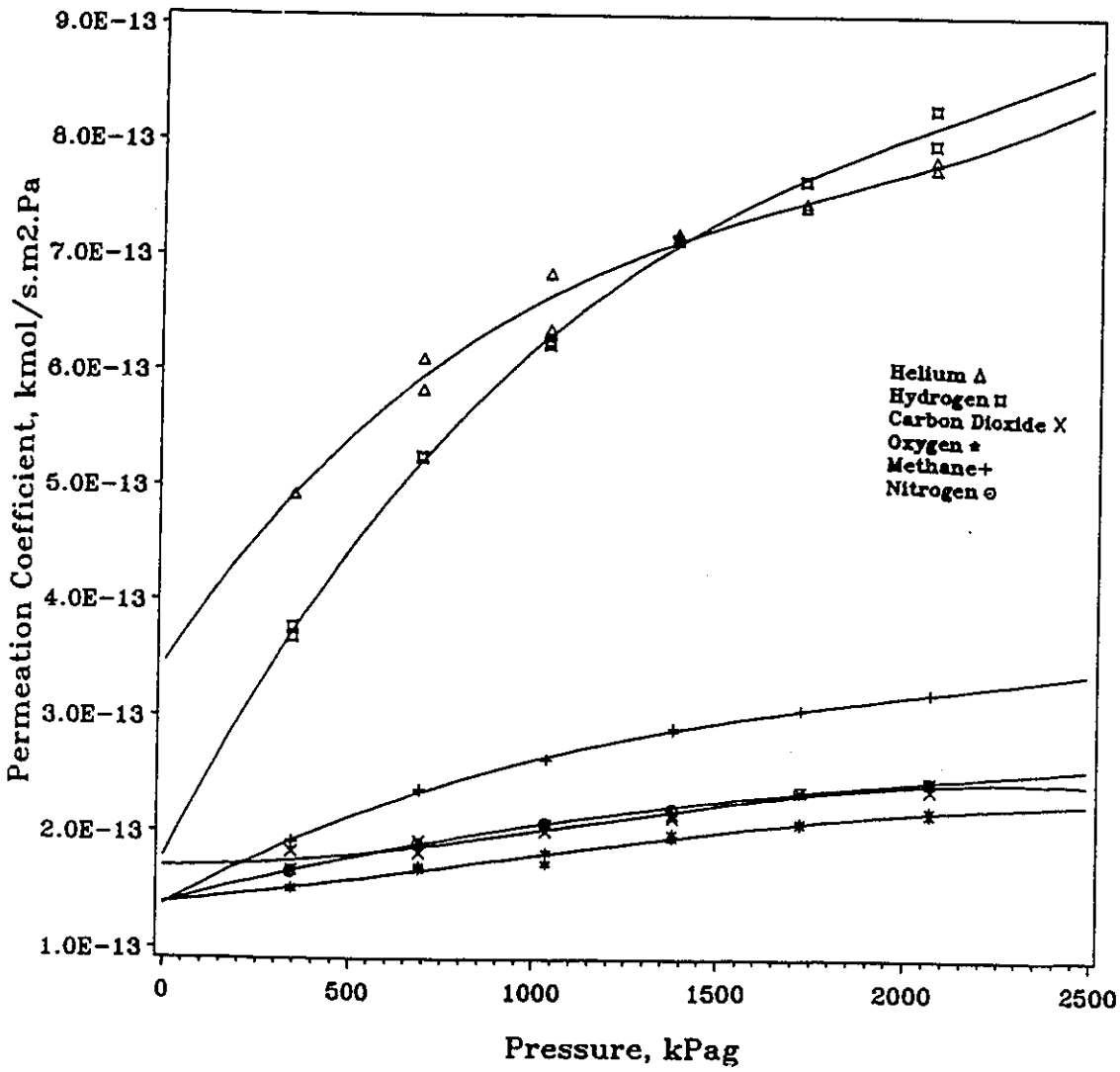

Figure 25: Permeation coefficient of pure gases versus pressure for membrane PA2-15.

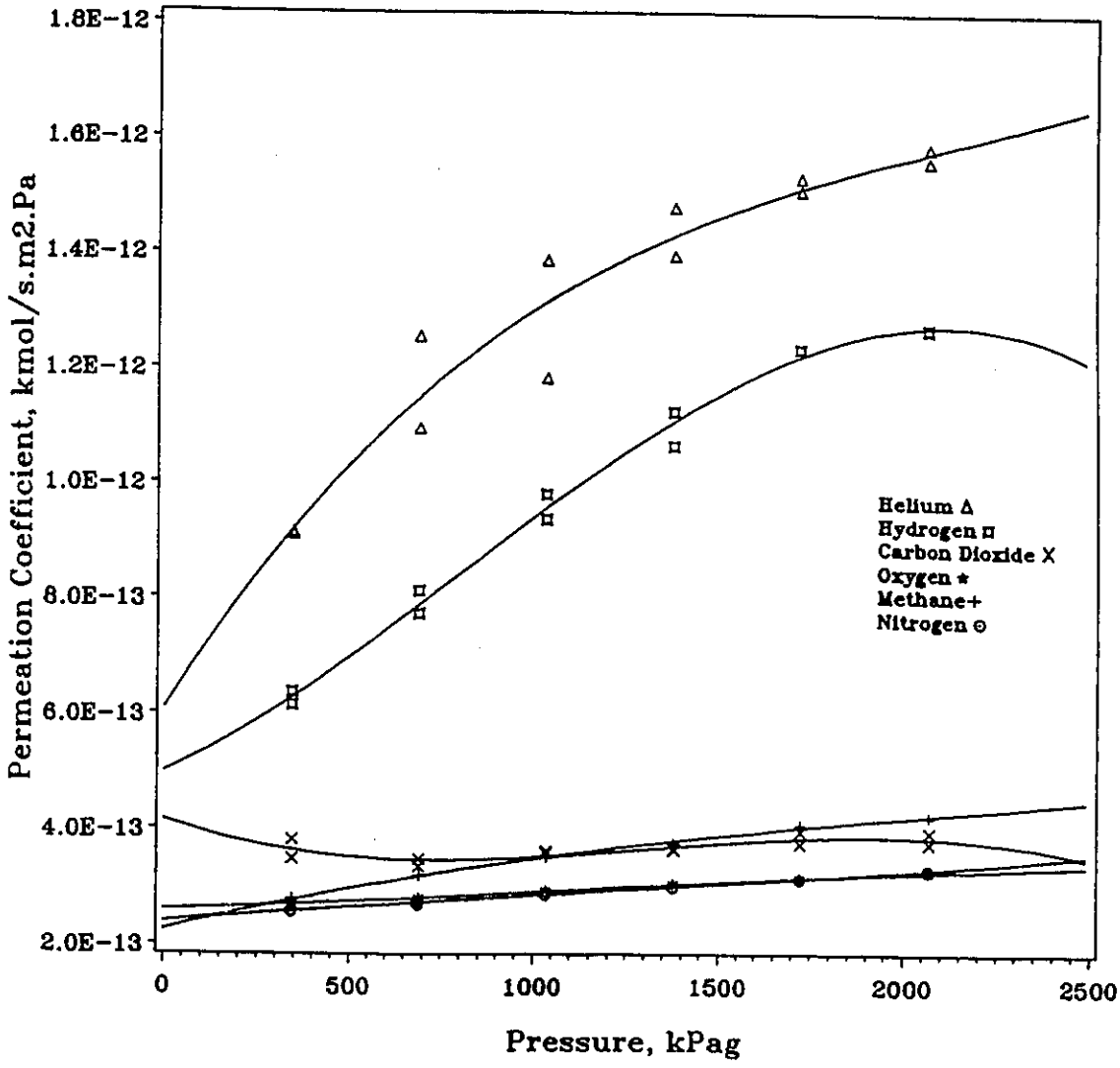

Figure 26: Permeation coefficient of pure gases versus pressure for membrane PA-17.

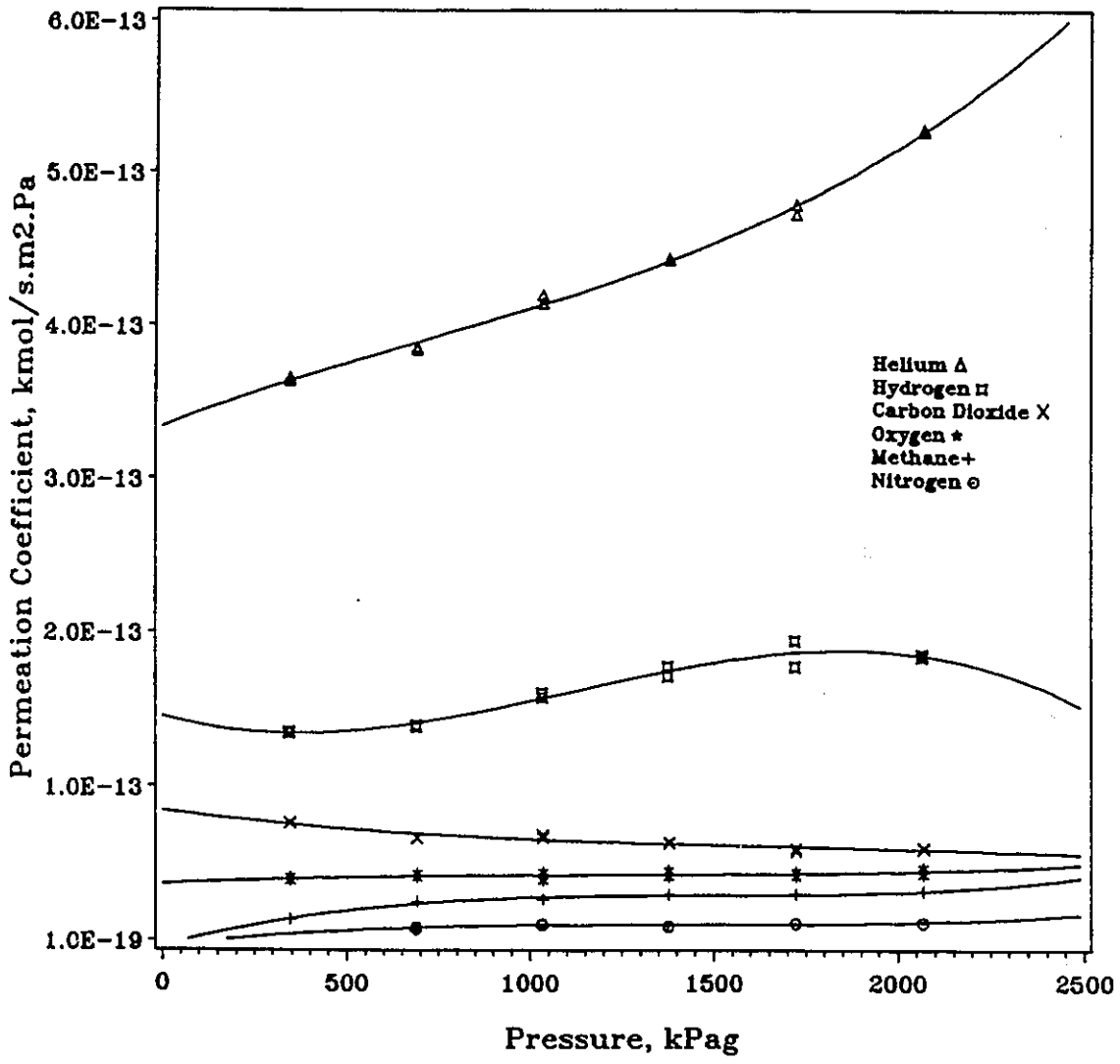

Figure 27: Permeation coefficient of pure gases versus pressure for membrane PA-19.

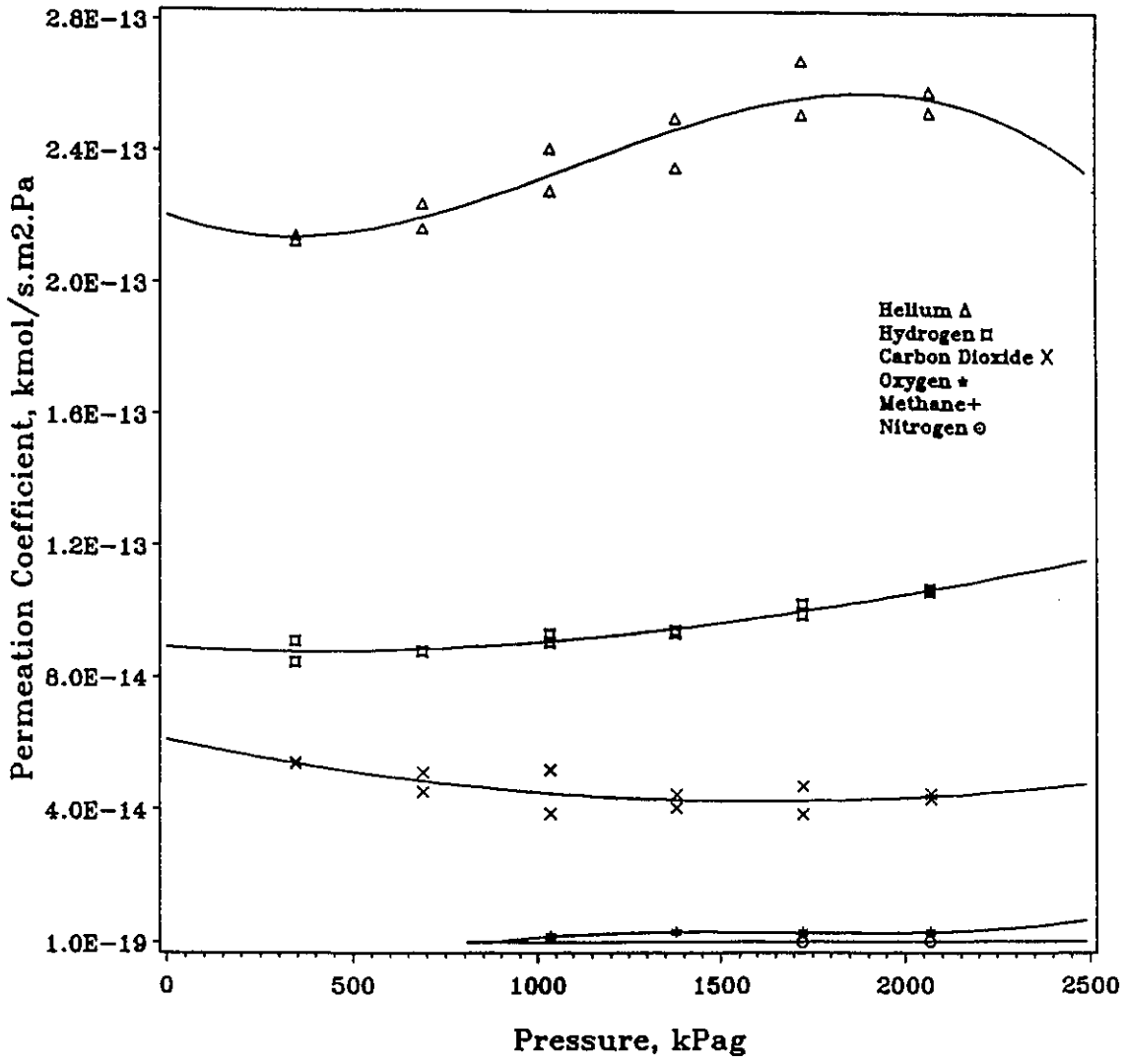

Figure 28: Permeation coefficient of pure gases versus pressure for laminated membrane PA-9.

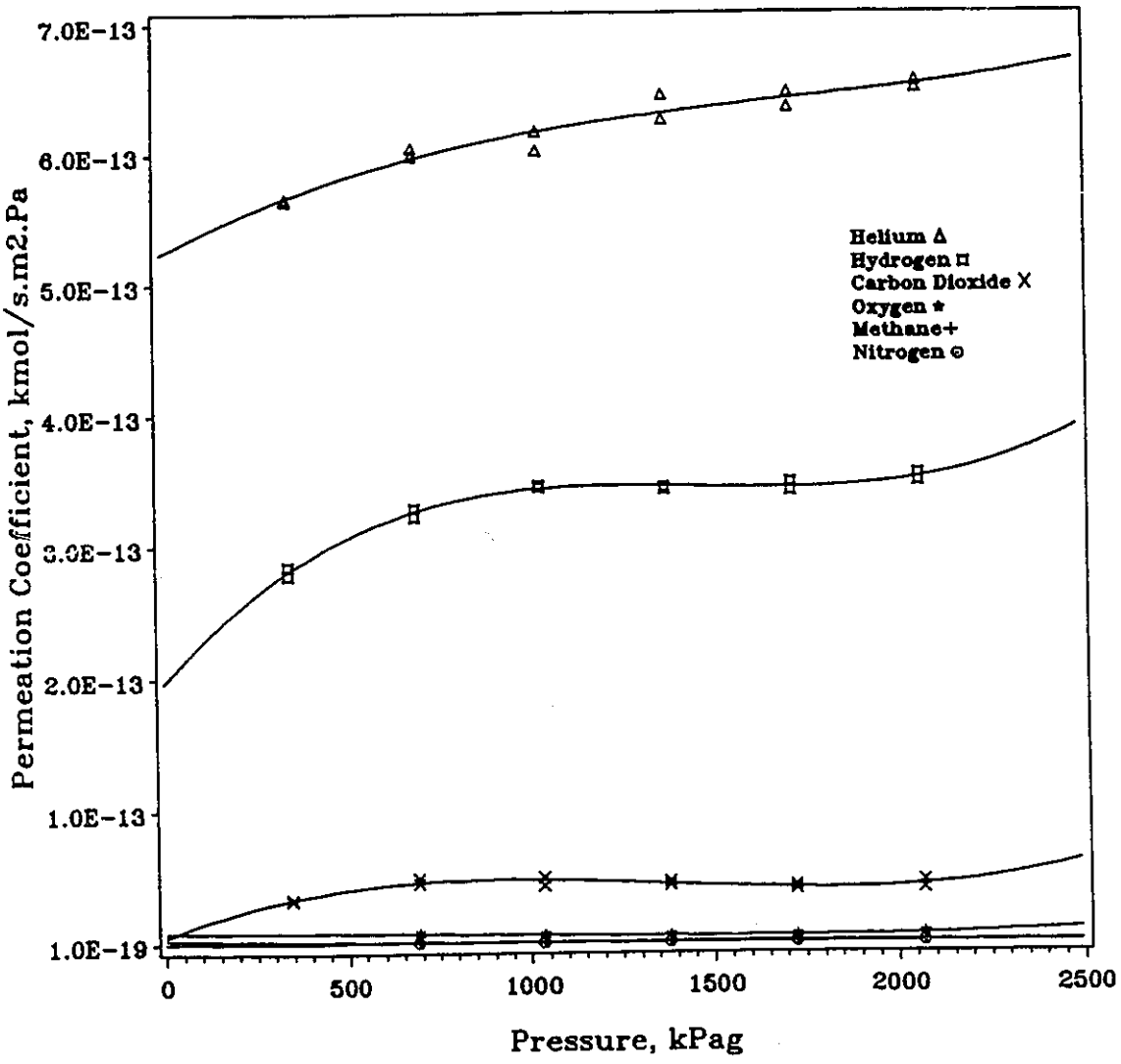

Figure 29: Permeation coefficient of pure gases versus pressure for laminated membrane PA-15.

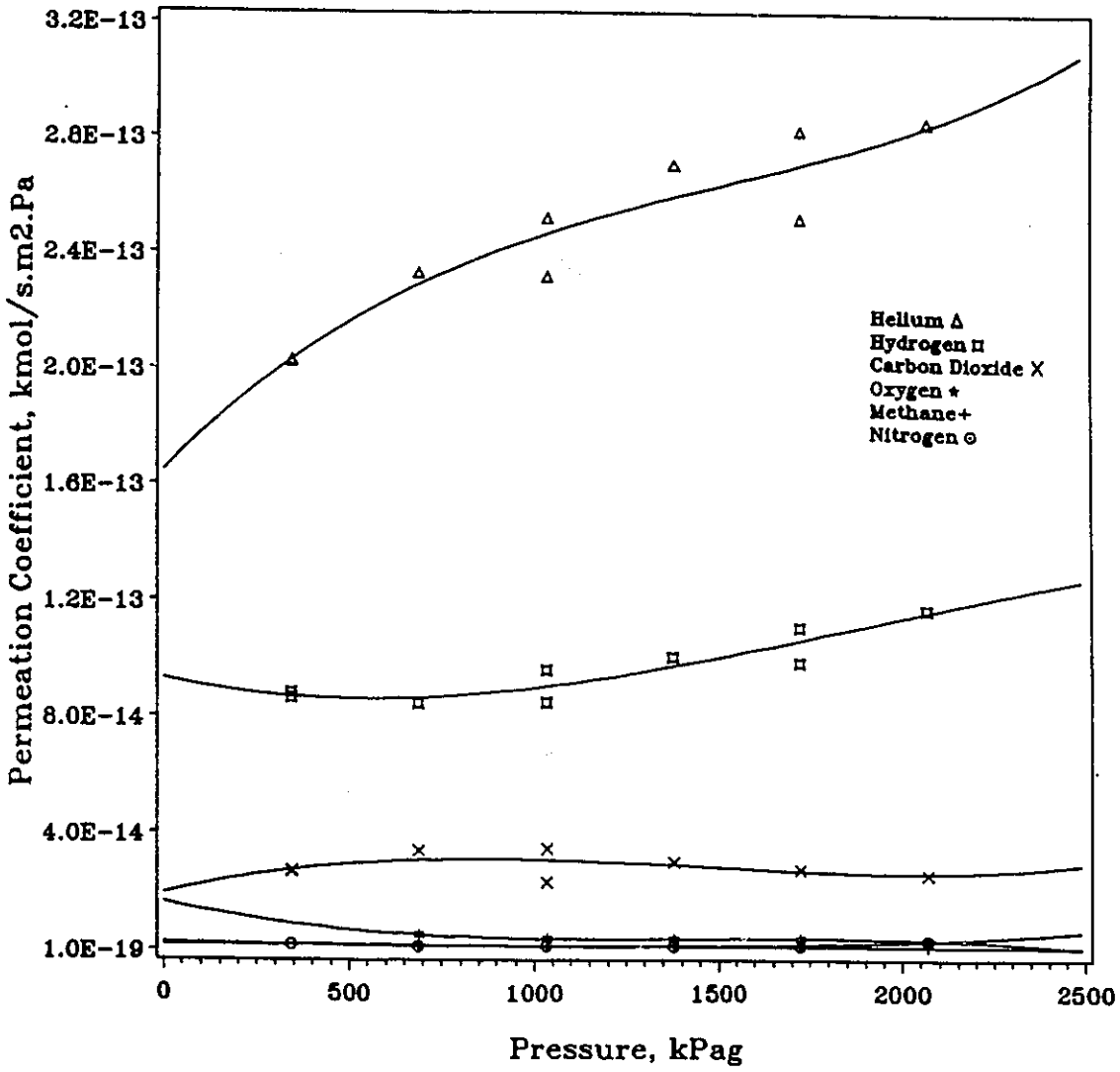

Figure 30: Permeation coefficient of pure gases versus pressure for laminated membrane PA-19.

Appendix C

Data Analysis

Table 23: SFPF parameters for membrane PA-9 (9 min. oven evap. time).

Gas	$\bar{R} \times 10^{10}$ m	$\sigma \times 10^{10}$ m	A_1 m^{-3}	A_2 $kmol/m^3.s.Pa^2$
He	7.9	1.3	0.13270E+19	0.80842E-09
H_2	5.8	1.2	0.16970E+19	0.10218E-08
CO_2	10.0	1.2	0.10076E+19	0.36003E-10
O_2	1.1	1.5	0.18963E+21	0.23609E-09
CH_4	2.0	1.3	0.22144E+20	0.53369E-09
N_2	1.0	1.6	0.15250E+21	0.28647E-09

Table 24: SFPF parameters for membrane PA-11 (11 min. oven evap. time).

Gas	$\overline{R} \times 10^{10}$ m	$\sigma \times 10^{10}$ m	A_1 m^{-3}	A_2 $kmol/m^3.s.Pa^2$
He	9.2	1.6	0.17673E+18	0.35615E-09
H_2	4.9	1.1	0.94488E+18	0.37920E-09
CO_2	3.2	1.4	0.94393E+19	0.24073E-09
O_2	2.8	1.4	0.58710E+19	0.17100E-09
CH_4	2.7	1.2	0.37585E+19	0.28157E-09
N_2	2.4	1.2	0.89111E+19	0.18001E-09

Table 25: SFPF parameters for membrane PA-13 (13 min. oven evap. time).

Gas	$\overline{R} \times 10^{10}$ m	$\sigma \times 10^{10}$ m	A_1 m^{-3}	A_2 $kmol/m^3.s.Pa^2$
He	4.3	1.5	0.12481E+20	0.17071E-08
H_2	4.4	1.2	0.60396E+19	0.20218E-08
CO_2	1.0	1.5	0.84186E+21	0.92061E-09
O_2	1.8	1.4	0.36222E+20	0.43873E-09
CH_4	1.6	1.2	0.61700E+20	0.90163E-09
N_2	2.3	1.2	0.17914E+20	0.47500E-09

Table 26: SFPF parameters for membrane PA-15 (15 min. oven evap. time).

Gas	$\overline{R} \times 10^{10}$ m	$\sigma \times 10^{10}$ m	A_1 m^{-3}	A_2 $kmol/m^3.s.Pa^2$
He	7.8	1.3	0.29800E+19	0.27024E-08
H_2	6.0	1.2	0.62186E+19	0.53652E-08
CO_2	1.0	1.5	0.21085E+22	0.28690E-08
O_2	1.2	1.8	0.19236E+21	0.15084E-08
CH_4	1.9	1.4	0.13203E+21	0.19833E-08
N_2	2.4	1.4	0.83258E+20	0.16665E-08

Table 27: SFPF parameters for membrane PA2-15 (15 min. oven evap. time).

Gas	$\overline{R} \times 10^{10}$ m	$\sigma \times 10^{10}$ m	A_1 m^{-3}	A_2 $kmol/m^3.s.Pa^2$
He	9.2	1.2	0.38801E+18	0.48718E-09
H_2	6.2	1.1	0.64775E+18	0.95149E-09
CO_2	1.7	1.1	0.12405E+21	0.45811E-09
O_2	1.8	1.3	0.53088E+20	0.37171E-09
CH_4	2.5	1.2	0.14686E+20	0.75634E-09
N_2	2.1	1.4	0.23140E+20	0.45758E-09

Table 28: SFPF parameters for membrane PA-17 (17 min. oven evap. time).

Gas	$\overline{R} \times 10^{10}$ m	$\sigma \times 10^{10}$ m	A_1 m^{-3}	A_2 $kmol/m^3.s.Pa^2$
He	8.8	1.2	0.80016E+18	0.10846E-08
H_2	6.3	1.01	0.10062E+19	0.14692E-08
CO_2	9.0	1.1	0.21583E+19	0.64864E-10
O_2	1.6	1.2	0.32523E+21	0.31959E-09
CH_4	1.4	1.5	0.88761E+20	0.97688E-09
N_2	1.5	1.1	0.40707E+22	0.44081E-09

Table 29: SFPF parameters for membrane PA-19 (19 min. oven evap. time).

Gas	$\overline{R} \times 10^{10}$ m	$\sigma \times 10^{10}$ m	A_1 m^{-3}	A_2 $kmol/m^3.s.Pa^2$
He	5.7	1.8	0.31561E+18	0.31003E-09
H_2	5.1	1.1	0.50848E+18	0.16370E-09
CO_2	9.2	1.2	0.41765E+18	-0.13554E-10
O_2	2.2	1.6	0.33024E+19	0.55908E-10
CH_4	2.8	1.01	0.96190E+18	0.81260E-10
N_2	4.2	1.01	0.16343E+18	0.18899E-10

Appendix D

Computer Programs

D.1 Pore Flow Program

D.1 Pore Flow Program

D.1.1 Program Listing

```
C     PROGRAM NAME IS :- POREBAX
C     **************************
C     October 6,1988
C     This is a modified version of the characterization program from
C     NRC where the regression is done on the equation Y=A(1)*X1+A(2)*X2
C     using the IMSL library subroutines DUNLSF, DU4LSF.
C     Numerical integration is done using the IMSL library subroutine
C     DQDAGS.
C               ****
C     THIS PROGRAM USES THE LOGNORMAL PORE SIZE DISTRIBUTION
C     THE FOLLOWING ARE THE DEFINITIONS OF THE VARIOUS VARIABLES:-
C     ===========================================================
C    1-M          =  No. of data points.
C    2-PAMB       =  Ambient pressure in ,Pa.
C    3-TAMB       =  Ambient temperature , K.
C    4-PSIG(I)    =  Pressure P ,(psig).
C    5-VOLMSD(I)  =  Volume V measured in time t at pressure P ,(cc)
C    6-TIME(I)    =  Time t, taken for volume V at pressure P ,(s)
C    7-VOLNTP(I)  =  Volume calculated at NTP, cc.
C    8-AG(I)      =  Permeability coefficient ,(kmol/s.cm2.atm.)
C    9-VFRATE(I)  =  Volume flow rate, (kmol/s.cm2.)
C   10-ATMG(I)    =  Gauge pressure , atm.
C   11-P2ABS(I)   =  Absolute pressure , Pa
C   12-AB(I)      =  permeability , cm3/s.cm2.cmHg.
C   13-BA(I)      =  Flux , kmol/s.
C   14-HRAD       =  Helium radius (1.25) , Angstrom
C   15-GASCON     =  Gas Constant = 8314.4 J/kmol.K
C   16-AVGNUM     =  Avogadro's Number = 0.602E27 molecule/kmol
C                    G1 UNITS ARE IN kmol.s/kg.m
C                    C1 UNITS ARE IN m/s
C                    G2 UNITS ARE IN kmol.s/m.kg
C     ------------------------------------------------------------------
      IMPLICIT  REAL*8 (A-H,O-Z)
      REAL*8    MOLVEL
      REAL*8    A(2),FVEC(6),FJAC(6,2),RPARAM(7),FCN
     1           ,LAMDA(10),FSCALE(6),XSCALE(2),XGUESS(2)
     2           ,X1(10),X2(10),Y(10),SSQQ
      DIMENSION X(10),COEF(5),PSIG(50),ATMG(10),AG(10),TIME(10),YC(10),
     1          VOLNTP(10),VOLMSD(10),P2ABS(10),VFRATE(10),AB(10),BA(10)
     2          ,XU1(10),XU2(10),G3(10),XOPT(10),ERPER(10),YTH(10),
     3          YOPT(10),SUMOPT(10),AVEP(10),X1OPT(10),X2OPT(10),
     4          UNITN(10),COLF(10),COLR(10)
      INTEGER   J,M,N,LDFJAC,COUNT,COUNT2,IPARAM(6),MT1,MT2
      CHARACTER*1 NAME1(40),NAME2(40),NAME3(40),TITLE(78),STITLE(78),
     1          FMLEG(78)
      EXTERNAL  F1TOT,F2TOT,F3TOT,F4TOT,F5TOT,FCN,DU4LSF,DUNLSF,UMACH
      COMMON    /ONE/ R,SIGMA
      COMMON    /TWO/ X1,X2,Y
      CALL XUFLOW(0)
      DATA      MT1,MT2/0,0/
      DATA      PI,GASCON,AVGNUM,HRAD/3.141593,8314.4,0.602252D27,1.25/
C     *************** HRAD VALUES ************************
C     HE  RADIUS=1.25          CH4 RADIUS=1.92             *
C     CO2 RADIUS=1.65          O2  RADIUS=1.73             *
C     N2  RADIUS=1.82          H2  RADIUS=1.445            *
C     ****************************************************
```

```
      DATA      RI,SIGMAI,DR,DSIGMA/1.00,1.001,0.25,0.10/
      DATA      NWRIT /2/
C     ------------------------------------------------------------------
      MT1    = 200
      DR     = 0.1D0
      MT2    = 30
      DSIGMA = 0.1D0
C     ------------------------------------------------------------------
    1 READ (10,*,END=9999) AMOLWT,NCELLS,C1,C2,C3,C4
      DO 9000 N1 = 1,NCELLS
      READ (10,106) (TITLE(I), I=1,78)
      READ (10,106)(STITLE(I), I=1,76)
      READ (10,*)    NTESTS
      DO 8000 N2 = 1,NTESTS
      READ (10,106) (FMLEG(I),I=1,78)
      READ (10,*) M,PAMB,TAMB
      READ (10,*) (PSIG(I),VOLMSD(I),TIME(I),I=1,M)
      JFK    = 1
      COUNT  = 1
      SSQ    = 1.0D28
      G1     = DSQRT(32.0*PI/9.0/AMOLWT/GASCON/TAMB)
      MOLVEL = DSQRT(8.0*GASCON*TAMB/PI/AMOLWT)
      G2     = PI/AMOLWT/MOLVEL
      MOLVEL = DSQRT(8.0D0*GASCON*TAMB/(PI*AMOLWT))
      UNITM  = AMOLWT / AVGNUM
      ETA    = (C1 + C2*(TAMB-273.15) + C3*(TAMB-273.15)**2 +
     1          C4*(TAMB-273.15)**3) / 1.0E06
      COLDIA = SQRT(MOLVEL*UNITM/(2.0*DSQRT(2.D0)*PI*ETA))
C     ------------------------------------------------------------------
      DO 1000 I  =1,M
      ATMG(I)    = PSIG(I)/14.696
      P2ABS(I)   = ATMG(I)+1.0
      VOLNTP(I)  = VOLMSD(I)*(273.15/TAMB)*(PAMB/101325.0)
C NRC AG(I)       = VOLNTP(I)/(TIME(I)*22.4D06*10.18*ATMG(I))
      AG(I)      = VOLNTP(I)/(TIME(I)*22.4D06*9.62113*ATMG(I))
      VFRATE(I)  = AG(I)*(P2ABS(I)-1.0)
      AB(I)      = AG(I)*22.4D06/76.0
C NRC BA(I)       = AG(I)*ATMG(I)*10.18
      BA(I)      = AG(I)*ATMG(I)*9.62113
      X(I)       = (101325.0*P2ABS(I)+PAMB)/2.0
      Y(I)       = AG(I)* 0.0986923*1.0E10
      AVEP(I)    = (101325.0*P2ABS(I)+PAMB)/2.0
      G3(I)      = PI*AVEP(I)/8.0/ETA/GASCON/TAMB
      UNITN(I)   = (AVGNUM/22.4) * (273.15/TAMB) * (AVEP(I)/101325.0)
      LAMDA(I)   = 1.0D10 / (DSQRT(2.D0) * PI * COLDIA**2 * UNITN(I))
      COLF(I)    = DSQRT(2.D0) * PI * COLDIA**2 * MOLVEL * UNITN(I)
      COLR(I)    = COLF(I) * UNITN(I) / 2.0
      XU1(I)     = 0.05*LAMDA(I)
      XU2(I)     = 50.0*LAMDA(I)
 1000 CONTINUE
      WRITE(2,51) TITLE,STITLE,FMLEG,M,PAMB,TAMB,AMOLWT,ETA,COLDIA,RI,
     1            SIGMAI,DR,DSIGMA,MT1,MT2,(PSIG(I),P2ABS(I)*101325.0,
     2            VOLMSD(I),TIME(I),VFRATE(I),AG(I),AB(I),BA(I),I=1,M)
      WRITE(2,52)
      WRITE(2,53) (P2ABS(I)*101.325,AG(I)*0.0986923,X(I),Y(I),I=1,M)
      WRITE(2,54)
      WRITE(2,25) (I,X(I)/1000.0,LAMDA(I),XU1(I),XU2(I),COLF(I),
     1             COLR(I),UNITN(I),I=1,M)
      WRITE(2,56)
      WRITE(3,151) TITLE,FMLEG
```

```
      C
   64       DO 7000 NOUT=1,MT1
   65       IF(NOUT.EQ.1) R = RI
   67       IF(NOUT.GT.1.AND.R.GE.1.00) R = R + DR
   69       IF(NOUT.GT.1.AND.R.LT.0.11) R = R * 10.0
   71       DO 6000 NIN =1,MT2
      C        IF (NIN.EQ.1) SIGMA = 1.0001
      C        IF (NIN.EQ.2) SIGMA = 1.001
   72       IF (NIN.EQ.1) SIGMA = 1.01
   74       IF (NIN.EQ.2) SIGMA = 1.00 + DSIGMA
   76       IF (NIN.GT.2) SIGMA = SIGMA + DSIGMA
   78       RMAX     = R*SIGMA**4
   79       RMIN     = R/SIGMA**4
   80       IF (RMIN.LE.HRAD) RMIN = HRAD
   82       IF (RMAX.LE.HRAD.OR.RMAX.GT.200.) GO TO 5500
   83       DO 2000 I=1,M
   84       Y1 = 0.0D0
   85       Y2 = 0.0D0
   86       Y3 = 0.0D0
   87       Y4 = 0.0D0
   88       Y5 = 0.0D0
   89       CALL DQDAGS (F4TOT , RMIN , RMAX , 0.0D0 ,1.0D-6, Y4 , EST)
   90       CALL DQDAGS (F5TOT , RMIN , RMAX , 0.0D0 ,1.0D-6, Y5 , EST)
   91       IF(RMIN.LT.XU1(I).AND.RMAX.LT.XU1(I)) GO TO 17
   92       IF(RMIN.GT.XU2(I).AND.RMAX.GT.XU2(I)) GO TO 12
   93       IF(RMIN.GT.XU1(I).AND.RMAX.GT.XU2(I)) GO TO 11
   94       IF(RMIN.LT.XU1(I).AND.RMAX.GT.XU2(I)) GO TO 10
   95       IF(RMIN.LT.XU1(I).AND.RMAX.LT.XU2(I)) GO TO 13
   96       IF(RMIN.GT.XU1(I).AND.RMAX.LT.XU2(I)) GO TO 14
   97    10 CALL DQDAGS (F1TOT , RMIN   , XU1(I) , 0.0D0 ,1.0D-6, Y1 , EST)
   98       CALL DQDAGS (F2TOT , XU1(I) , XU2(I) , 0.0D0 ,1.0D-6, Y2 , EST)
   99       CALL DQDAGS (F3TOT , XU2(I) , RMAX   , 0.0D0 ,1.0D-6, Y3 , EST)
  100       GO TO 16
  101    11 Y1 = 0.0D0
  102       CALL DQDAGS (F2TOT , RMIN , XU2(I) , 0.0D0 ,1.0D-6, Y2 , EST)
  103       CALL DQDAGS (F3TOT , XU2(I) , RMAX , 0.0D0 ,1.0D-6, Y3 , EST)
  104       GO TO 16
  105    12 Y1 = 0.0D0
  106       Y2 = 0.0D0
  107       CALL DQDAGS (F3TOT , RMIN , RMAX , 0.0D0 ,1.0D-6, Y3 , EST)
  108       GO TO 16
  109    13 Y3 = 0.0D0
  110       CALL DQDAGS (F1TOT , RMIN , XU1(I) , 0.0D0 ,1.0D-6, Y1 , EST)
  111       CALL DQDAGS (F2TOT , XU1(I) , RMAX , 0.0D0 ,1.0D-6, Y2 , EST)
  112       GO TO 16
  113    14 Y1 = 0.0D0
  114       Y3 = 0.0D0
  115       CALL DQDAGS (F2TOT , RMIN , RMAX , 0.0D0 ,1.0D-6, Y2 , EST)
  116       GO TO 16
  117    17 Y2 = 0.0D0
  118       Y3 = 0.0D0
  119       CALL DQDAGS (F1TOT , RMIN , RMAX , 0.0D0 ,1.0D-6, Y1 , EST)
  120       GO TO 16
  121    16 X1(I)    = G1*Y1+G2*Y2+G3(I)*Y3*1.0D-10
  122       X2(I)    = X(I)*Y4/Y5
  123  2000 CONTINUE
       C    ****************************************************************
       C      NONLINEAR REGRESSION ROUTINE ******DUNLSF
       C    1-The following starting values provide a rough fit :-
       C
```

```
124         XGUESS(1)   = 1.0D0
125         XGUESS(2)   = 1.0D0
          C ============================
126         XSCALE(1)   = 1.0D0
127         XSCALE(2)   = 1.0D0
128         FSCALE(1)   = 1.0D0
129         FSCALE(2)   = 1.0D0
130         FSCALE(3)   = 1.0D0
131         FSCALE(4)   = 1.0D0
132         FSCALE(5)   = 1.0D0
133         FSCALE(6)   = 1.0D0
134         N      = 2
135         LDFJAC = M
136         CALL DU4LSF (IPARAM,RPARAM)
137         RPARAM(4)=10.0D0*RPARAM(4)
138         RPARAM(6)=-200.0D2*RPARAM(6)
139         CALL DUNLSF (FCN,M,N,XGUESS,XSCALE,FSCALE,IPARAM,
              *              RPARAM,A,FVEC,FJAC,LDFJAC)
          C     ***************************************************************
140         SSQQ=DDOT(M,FVEC,1,FVEC,1)
141         IF (SSQQ.GT.SSQ) GO TO 5500
142         JK     = JFK
143         COUNT2= COUNT
144         ROPT   = R
145         SOPT   = SIGMA
146         A1OPT = A(1)
147         A2OPT = A(2)
148         ROMAX = R*SIGMA**4
149         ROMIN = R/SIGMA**4
150         SUM1   = 0.0
151         DO 3000 I = 1,M
152         X1OPT(I) = X1(I)
153         X2OPT(I) = X2(I)
154         YTH(I)    =  A(1)*X1(I)+A(2)*X2(I)
155         ERPER(I) = (Y(I)-YTH(I))*100.0/Y(I)
156         SUM1      = SUM1 + ERPER(I)**2
157         SUMOPT(I)= SUM1
158      3000 CONTINUE
159         SSQ       =   SSQQ
160      5500 JFK       = JFK   + 1
161         COUNT     = COUNT + 1
          C     PRINT*,JFK,COUNT
162      6000 CONTINUE
163      7000 CONTINUE
          C ------------------------------------------------------------------
164         WRITE (NWRIT,57) (I,X1OPT(I),X2OPT(I),Y(I),YTH(I),ERPER(I),
              1                    SUMOPT(I),I=1,M)
165         WRITE (NWRIT,58)
166         WRITE (NWRIT,59) COUNT2,ROPT,SOPT,ROMAX,ROMIN,1.0E30*A1OPT/1.0E10,
              1                    1.0E10*A2OPT/1.0E10,SSQ
167         WRITE (3,152) ROPT,SOPT,1.0E30*A1OPT/1.0E10,1.0E10*A2OPT/1.0E10
168      8000 CONTINUE
169      9000 CONTINUE
170         GO TO 1
          C ------------------------------------------------------------------
171       106 FORMAT (78A1)
172        51 FORMAT('1',T5,78A1/T5,78A1/T5,78A1///T5,'INPUT PARAMETERS :-'/T5,
             *16('=')/T5,'No. of data points',T35,'=',I14/T5,'Ambient pressure',
             *T35,'=',F14.0,2X,'Pa'/T5,'Ambient temperature',T35,'=',F14.2,2X,
             *'K'/T5,'Gas molecular wt',T35,'=',F14.5,2X,'kg/kmol'/T5,'Gas visco
```

```
     *sity',T35,'=',E14.7,2X,'kg/m.s'/T5,'Collision diameter',T35,
     *'=',E14.7,2X,'m'/T5,'Initial Radius Value',T35,'=',F14.2,2X,
     *'Angstrom'/T5,'Initial SIGMA value',T35,'=',F14.2,2X,'Angstrom'/
     *T5,'Increment in radius',T35,'=',F14.2,2X,'Angstrom'/T5,'Increment
     *in SIGMA',T35,'=',F14.2,2X,'Angstrom'/T5,'No. of radius iterations
     *',T35,'=',I14/T5,'No. of SIGMA Iterations',T35,'=',I14/T5,
     *56('-')///T5,'Table of Results'/T5,100('-')/T8,'Feed Pressure',
     *T30,'VOLUME',T40,'TIME',T50,'FLOW RATE',T65,'PERMEABILITY coeffici
     *ent',T95,'FLUX'/T5,23('-'),T65,25('-')/T5,'psig',T15,'Pa (abs.)'
     *,T30,'ml',T40,'s',T50,'kmol/s.cm2',T65,'kmol/',T80,'cm3/',
     *T95,'kmol/s'/T65,'s.cm2.atm',T80,'s.cm2.cmHg'/T5,100('-'),/
     *(T5,F5.1,T15,E12.5,T30,F7.4,T40,F5.1,T50,E12.5,T64,E12.5,
     *T80,E12.5,T93,E 2.5))
173      52 FORMAT (T5,100('-'))
174      53 FORMAT (//T5,'Table of Model Parameters'/T5,
     1     175('-')/T5,'Feed Pressure',T25,'PERMEABILITY',T45,'X Value',
     2T65,'Y Value'/T25,'Coefficient (AG)',T45,'Average Pressure',T65,
     3'AG*1.0E10'/T5,'kPa',T25,'kmol/s.m2.Pa',T45,'Pa',T65,
     4'kmol/s.m2.Pa'/T5,75('-')/(T5,F10.3,T25,E12.5,T45,
     5 E12.5,T65,F10.5))
175      54 FORMAT (T5,75('-'))
176      25 FORMAT('1',T5,'Kinetic-Molecular Gas Properties at the Average pre
     1ssure'/T5,87('-')/T5,'NO.',T10,'Average',T20,'MEAN',T30,
     2'Knudsen',T40,'Slip',T50,'COLLISION',T65,'COLLISION',T80,
     3'No. OF'/T10,'Pressure',T20,'Free Path',T30,'Limit',T40,
     3'Limit',T50,'Frequency',T65,'Rate',T80,'Molecules/'/
     4T80,'unit volume'/T10,'kPa',T20,'Angstrom',T30,'Angstrom',
     5T40,'Angstrom',T50,'coll./s',T65,'coll./m3.s',T80,'molecule/m3'
     6/T5,87('-')/(I6,T10,F7.2,T20,F7.1,T30,F6.1,T40,F7.0,T50,
     7E12.5,T65,E12.5,T80,E12.5))
177      56 FORMAT (T5,87('-'))
178      57 FORMAT (///T5,'TABLE OF PREDICTED RESULTS'/T5,73('-')/T5,'POINT
     1',T15,'X1(I)',T30,'X2',T40,'Yexp(I)',T50,'Ycalc(I)',T63,'ERPER',
     2T73,'SSQ'/T5,73('-')/(I7,T10,E12.5,T25,E12.5,T40,
     3E8.3,T50,E8.3,
     4T60,F8.2,T70,F8.2))
179      58 FORMAT (T5,73('-'))
180      59 FORMAT (/T31,'Search Final Results'/T31,20('=')//T11,'Combination
     1no for Min SSQ',T41,'=',I15/T11,'Average Radius',T41,'=',F15.2,2X
     2,'Angstrom'/T11,'Standard Deviation',T41,'=',F15.5,2X,'Angstrom'/T
     311,'Maximum Radius',T41,'=',F15.2,2X,'Angstrom'/T11,'Minimum Radiu
     4s',T41,'=',F15.4,2X,'Angstrom'/T11,'Parameter A(1)',T41,'=',E15.7,
     52X,'m**-3'/T11,'Parameter A(2)',T41,'=',E15.7,2X,'kmol/Pa2.s.m**3'
     6/T11,'Min. of Residuals SSQ',T41,'=',E15.7/T11,65('-')/
     7T11,'NOTE:-'/T17,'1- A1,A2 are divided by 1.0E10 to account for
     8the factor'/T20,'1.0E10 which was multiplied by the AG value'/
     9T17,'2- A1 is then multiplied by 1.0E30 while A2 by 1.0E10 to'
     1/T20,'get their values in the proper units'/T11,65('='))
181      60 FORMAT (//T11,'Optimum values of the regression routine are :-'/
     1T11,47('=')//T11,'Final NORM of the residuals',T41,'=',E15.7/
     2T11,'Number of function evaluations',T41,'=',I15/
     3T11,'Number of JACOBIAN evaluations',T41,'=',I15/
     4T11,'Exit parameter',T41,'=',I15/T11,'IOPT',T41,'=',I15/
     6T11,'IFLAG',T41,'=',I15/T11,40('-')/
     7T11,'Correlation matrix for the parameters'/T11,37('=')/
     8T11,40('-')/T11,'ROW',T25,'COLUMN',T40,'COLUMN'/T11,'NO.',T25,
     9'  (1)',T40,'  (2)'/T11,40('-')/(T11,I2,T20,E12.5,T35,E12.5))
182     151 FORMAT (T2,76A1/T2,76A1)
183     152 FORMAT (2F10.3,2E20.7)
184    9999 STOP
185          END
```

```
      C     ------------------------------------------------------------------
1           REAL FUNCTION F1TOT(X)
2           IMPLICIT REAL*8 (A-H,O-Z)
3           COMMON /ONE/R,SIGMA
4           PI    = 3.14159
5           F1TOT = (1.0/X) * (X**3/(DLOG(SIGMA)*DSQRT(2.0D0*PI)))*
              +DEXP((-1.0/(2.0*DLOG(SIGMA)**2))*(DLOG(X)-DLOG(R))**2)
6           RETURN
7           END

      C     ------------------------------------------------------------------
1           REAL FUNCTION F2TOT(X)
2           IMPLICIT REAL*8 (A-H,O-Z)
3           COMMON /ONE/R,SIGMA
4           PI    = 3.14159
5           F2TOT = (1.0/X) * (X**3/(DLOG(SIGMA)*DSQRT(2.0D0*PI)))*
              +DEXP((-1.0/(2.0*DLOG(SIGMA)**2))*(DLOG(X)-DLOG(R))**2)
6           RETURN
7           END

      C     ------------------------------------------------------------------
1           REAL FUNCTION F3TOT(X)
2           IMPLICIT REAL*8 (A-H,O-Z)
3           COMMON /ONE/R,SIGMA
4           PI    = 3.14159
5           F3TOT = (1.0/X) * (X**4/(DLOG(SIGMA)*DSQRT(2.0D0*PI)))*
              +DEXP((-1.0/(2.0*DLOG(SIGMA)**2))*(DLOG(X)-DLOG(R))**2)
6           RETURN
7           END

      C     ------------------------------------------------------------------
1           REAL FUNCTION F4TOT(X)
2           IMPLICIT REAL*8 (A-H,O-Z)
3           COMMON /ONE/R,SIGMA
4           PI    = 3.14159
5           F4TOT = (1.0/X) * (X**2/(DLOG(SIGMA)*DSQRT(2.0D0*PI)))*
              +DEXP((-1.0/(2.0*DLOG(SIGMA)**2))*(DLOG(X)-DLOG(R))**2)
6           RETURN
7           END

      C     ------------------------------------------------------------------
1           REAL FUNCTION F5TOT(X)
2           IMPLICIT REAL*8 (A-H,O-Z)
3           COMMON /ONE/R,SIGMA
4           PI    = 3.14159
5           F5TOT = (1.0/X) * (X/(DLOG(SIGMA)*DSQRT(2.0D0*PI)))*
              +DEXP((-1.0/(2.0*DLOG(SIGMA)**2))*(DLOG(X)-DLOG(R))**2)
6           RETURN
7           END

      C     ------------------------------------------------------------------
1           SUBROUTINE FCN(M,N,A,F)
2           INTEGER M,N,I
3           REAL*8 A(N),F(M)
4           REAL*8 X1(10),X2(10),Y(10)
5           COMMON/TWO/X1,X2,Y
6           DO 10 I = 1, M
7           F(I) = Y(I) - (A(1)*X1(I) + A(2)*X2(I))
8         10 CONTINUE
9           RETURN
10          END
```

D.1.2 Sample Data File

```
  4.0026     1
  0.1859030799990169D+02
  0.4274849525327286D-01
 -0.1075803754998549D-04
  0.2113335316347596D-08
MOUNTED : 16/03/89- PA-17    17 MIN IN OVEN (ISO/HEX)
-------------------------------------------------------
         1
HELIUM PERMEATION - AVG OF INCREASING AND DECREASING PRESS
  6  100514.4  296.15
   50. .5    67.4     100.  1.0   52.6
  150. 2.0   64.3     200.  2.5   53.5
  250. 3.0   48.5     300.  2.5   32.3
```

D.1.3 Execution File

```
&TRACE ALL
CP LINK TO 426032 191 225 RR
ACC 225 B/A
GLOBAL TXTLIB VLNKMLIB VFORTLIB IMSL1 IMSL2 IMSL3 IMSL4
GLOBAL LOADLIB VFLODLIB
CP SPOOL CONS PURGE
CP SPOOL PRT TO 426032 CONT
FORTVS POREBAX
LOAD POREBAX (CLEAR
FI 10 DISK SAMPLE DATA
FI 2 DISK OUTPUT LISTING (LRECL 110
FI 3 DISK OUTPUT1 LISTING
CPEX FIFO Q T
START
CPEX FIFO Q T
&STACK FIFO &BLANK
CPEX FIFO IND USER
&STACK FIFO &BLANK
EXECIO 1 PRINT (CC 1
EXECIO 7 PRINT
CP SPOOL PRT CLOSE NOCONT DIST POREBAX
CP SPOOL CONS STOP PURGE
EXEC PRINT OUTPUT LISTING AT CBYQMS
EXEC PRINT OUTPUT1 LISTING AT CBYQMS
EXEC SENDFILE OUTPUT LISTING A TO 426032 AT UOTTAWA
EXEC SENDFILE OUTPUT1 LISTING A TO 426032 AT UOTTAWA
&EXIT
```

D.1.4 Output Listing

MOUNTED : 16/03/89- PA-17 17 MIN IN OVEN (ISO/HEX)

HELIUM PERMEATION - AVG OF INCREASING AND DECREASING PRESS

INPUT PARAMETERS :-

No. of data points	=	6	
Ambient pressure	=	100514.	Pa
Ambient temperature	=	296.15	K
Gas molecular wt	=	4.00260	kg/kmol
Gas viscosity	=	0.1956786E-04	kg/m.s
Collision diameter	=	0.2187248E-09	m
Initial Radius Value	=	1.00	Angstrom
Initial SIGMA value	=	1.00	Angstrom
Increment in radius	=	0.10	Angstrom
Incrementin SIGMA	=	0.10	Angstrom
No. of radius iterations	=	100	
No. of SIGMA Iterations	=	30	

Table of Results

Feed Pressure		VOLUME	TIME	FLOW RATE	PERMEABILITY coefficient		FLUX
psig	Pa (abs.)	ml	s	kmol/s.cm2	kmol/ s.cm2.atm	cm3/ s.cm2.cmHg	kmol/s
50.0	0.44606E+06	0.5000	67.4	0.31495E-10	0.92569E-11	0.27284E-05	0.30301E-09
100.0	0.79080E+06	1.0000	52.6	0.80713E-10	0.11862E-10	0.34960E-05	0.77655E-09
150.0	0.11355E+07	2.0000	64.3	0.13205E-09	0.12938E-10	0.38132E-05	0.12705E-08
200.0	0.14803E+07	2.5000	53.5	0.19839E-09	0.14577E-10	0.42965E-05	0.19087E-08
250.0	0.18250E+07	3.0000	48.5	0.26261E-09	0.15437E-10	0.45499E-05	0.25266E-08
300.0	0.21697E+07	2.5000	32.3	0.32860E-09	0.16097E-10	0.47443E-05	0.31615E-08

Table of Model Parameters

Feed Pressure kPa	PERMEABILITY Coefficient (AG) kmol/s.m2.Pa	X Value Average Pressure Pa	Y Value AG*1.0E10 kmol/s.m2.Pa
446.062	0.91359E-12	0.27329E+06	0.00914
790.798	0.11706E-11	0.44566E+06	0.01171
1135.535	0.12768E-11	0.61802E+06	0.01277
1480.272	0.14387E-11	0.79039E+06	0.01439
1825.008	0.15235E-11	0.96276E+06	0.01524
2169.745	0.15886E-11	0.11351E+07	0.01589

Kinetic-Molecular Gas Properties at the Average pressure

NO.	Average Pressure kPa	MEAN Free Path Angstrom	Knudsen Limit Angstrom	Slip Limit Angstrom	COLLISION Frequency coll./s	COLLISION Rate coll./m3.s	No. OF Molecules/ unit volume molecule/m3
1	273.29	703.4	35.2	35171.	0.17793E+11	0.59504E+36	0.66884E+26
2	445.66	431.4	21.6	21568.	0.29016E+11	0.15824E+37	0.10907E+27
3	618.02	311.1	15.6	15553.	0.40238E+11	0.30431E+37	0.15125E+27
4	790.39	243.2	12.2	12161.	0.51461E+11	0.49773E+37	0.19344E+27
5	962.76	199.7	10.0	9984.	0.62683E+11	0.73849E+37	0.23563E+27
6	1135.13	169.4	8.5	8468.	0.73906E+11	0.10266E+38	0.27781E+27

TABLE OF PREDICTED RESULTS

POINT	X1(I)	X2	Yexp(I)	Ycalc(I)	ERPER	SSQ
1	0.84232E+00	0.25277E+07	.914E-02	.948E-02	-3.78	14.31
2	0.84232E+00	0.41220E+07	.117E-01	.112E-01	4.23	32.25
3	0.84069E+00	0.57163E+07	.128E-01	.129E-01	-1.24	33.78
4	0.80437E+00	0.73106E+07	.144E-01	.144E-01	0.15	33.81
5	0.68927E+00	0.89049E+07	.152E-01	.152E-01	0.40	33.97
6	0.57379E+00	0.10499E+08	.159E-01	.160E-01	-0.58	34.31

Search Final Results

Combination no for Min SSQ	=	2343	
Average Radius	=	8.80	Angstrom
Standard Deviation	=	1.20000	Angstrom
Maximum Radius	=	18.25	Angstrom
Minimum Radius	=	4.2438	Angstrom
Parameter A(1)	=	0.8001565E+18	m**-3
Parameter A(2)	=	0.1084613E-08	kmol/Pa2.s.m**3
Min. of Residuals SSQ	=	0.4030747E-06	

NOTE:-

1- A1,A2 are divided by 1.0E10 to account for the factor 1.0E10 which was multiplied by the AG value

2- A1 is then multiplied by 1.0E30 while A2 by 1.0E10 to get their values in the proper units

D.2 Resistance Program

D.2.1 Program Listing

```
C   PROGRAM NAME IS :-RESI4
C   ********************
C   The first half of this computer program calculates the unknowns,
C   R1', R2, R3, and ALPHA3 using the modified resistance model.
C
C   The second half is a simulation program where the pore area, A3
C   and the lamination thickness is varied, while keeping R2, ALPHA2,
C   A2, L2, and ALPHA3 the same and calc. R3 by mult. by A3OLD/A3NEW.
C
C         INPUT OF EXPERMENTAL VALUES
C  ****************************************************
C    1-A1       = film area of top layer (m2)
C    2-A2       = film area of bottom layer (m2)
C    3-L1       = thickness of top layer (m)
C    4-FLUXH2   = flux of h2 w/o lamination (mol/s.m2.Pa)
C    5-FLUXYY   = flux of other gas w/o lamination (mol/s.m2.Pa)
C    6-P1H2     = intrin. permeability of h2 on top layer (mol.m/m2.s.Pa)
C    7-P1YY     = intrin. permeability of other gas (mol.m/m2.s.Pa)
C    8-LUXH2    = flux of h2 with lamination (mol/s.m2.Pa)
C    9-LUXYY    = flux of other gas with lamination (mol/s.m2.Pa)
C   10-AA2      = ratio of intrinsic permeability for h2 and yy layer 2
C   11-YY       = is the other gas ie. N2, CO2, He, O2, CH4
C
C         CALCULATED VALUES
C  ****************************************************
C    1-A3       = area of aggregate pore in bottom layer (m2)
C    2-AA3      = ratio of intrinsic permeability for h2 and yy for pore
C    3-Rij      = resistance for region i and gas j (Pa.s/mol)
C
1       INTEGER ITMAX,N,NGAS,MM,I
2       PARAMETER (N=2)
C
3       INTEGER K,NOUT
4       REAL FCN,FNORM,R(N),XGUESS(N),A1,A2,L1,FLUXYY,FLUXH2,P1H2,
          1     P1YY,LUXH2,LUXYY,AA2,RH2,AA,AA1,RLH2,AAL,R1H2,A3,X1,X2,AA3,
          2     FCC,ERRREL,R3H2,Z3,RLH2A,L12,A32
5       CHARACTER*1 TITLE(78),STITLE(78)
6       COMMON /ONE/ R1H2,RLH2,AA1,AA2,AAL,AA3,R3H2
7       EXTERNAL FCN,NEQNF,UMACH,FCC
C
8       READ (10,*,END=9999)NGAS
9       DO 9000 N1 = 1,NGAS
C Assuming A2 is equal to the area of the cell, and specifying the
C thickness and intrinsic permeability of silicone rubber as given
C by the manufacture.
10        A1=     9.62112E-4
11        A2=     9.62112E-4
12        L1=     25.4E-6
13        P1H2=   16.872E-14
C For first approximation assume R3*alpha3 is equal to zero.
14        AA3=    0.0
C
15        READ (10,100) (TITLE(I), I=1,78)
16        READ (10,*) FLUXH2,LUXH2
17        READ (10,100) (STITLE(I), I=1,78)
18        READ (10,*) FLUXYY,LUXYY,AA2,P1YY
```

```
19          RH2=      (1/FLUXH2)*(1/A2)
20          AA=       FLUXH2/FLUXYY
21          AA1=      P1H2/P1YY
22          RLH2=     (1/LUXH2)*(1/A2)
23          AAL=      LUXH2/LUXYY
24          R1H2=     L1/(P1H2*A1)
        C
25          WRITE (3,110)TITLE,STITLE
26          WRITE (4,110)TITLE,STITLE
27          WRITE (6,110)TITLE,STITLE
28          WRITE (4,115)
        C
        C                       SET VALUES OF INITIAL GUESS
        C                       R(1')H2=1.0E14  R(2)=1.0E12
        C
29          DATA XGUESS/1.0E14,1.0E12/
30          ERRREL=0.0001
31          ITMAX=800
        C                      IMSL SUBROUTINE TO
        C                      SOLVE NONLINEAR EQUATIONS
32          CALL UMACH(2,NOUT)
33          CALL NEQNF (FCN,ERRREL,N,ITMAX,XGUESS,R,FNORM)
        C
34          R3H2 = (RH2*R(2)) / (R(2)-RH2)
35          AA3 = (AA*RH2*AA2*R(2)) / (AA2*R(2)*R3H2-AA*RH2*R3H2)
        C
36          A3  = L1 / (P1H2*R(1))
37          RYY = RH2*AA
38          RLYY = RLH2*AAL
39          R1YY = R1H2*AA1
40          R11Y = R(1)*AA1
41          R2YY = R(2)*AA2
42          R3YY = R3H2*AA3
        C
        C
43          MM=1
44      777 A3=Z3
45          ERRREL=0.0001
46          ITMAX=800
        C                      IMSL SUBROUTINE TO
        C                      SOLVE NONLINEAR EQUATIONS
47          CALL UMACH(2,NOUT)
48          CALL NEQNF (FCC,ERRREL,N,ITMAX,XGUESS,R,FNORM)
        C
49          R3H2 = (RH2*R(2)) / (R(2)-RH2)
50          AA3 = (AA*RH2*AA2*R(2)) / (AA2*R(2)*R3H2-AA*RH2*R3H2)
        C
51          Z3  = L1 / (P1H2*R(1))
52          MM=MM+1
        C       IF (ABS(Z3-A3).GT.(0.001*A3)) GO TO 777
53          IF (ABS(Z3-A3).GT.(0.00001*A3)) GO TO 777
54          RYY = RH2*AA
55          RLYY = RLH2*AAL
56          R1YY = R1H2*AA1
57          R11Y = R(1)*AA1
58          R2YY = R(2)*AA2
59          R3YY = R3H2*AA3
60          PRINT*,'      # OF ITERATIONS = ',MM
61          PRINT*,'ALPHA= ',AA
```

```
      PRINT*,'ALPHA1=',AA1
      PRINT*,'ALPHA2=',AA2
      PRINT*,'ALPHA3=',AA3
      PRINT*,'ALPHAL=',AAL
      PRINT*,'RH2=    ',RH2 ,'    RYY= ',RYY,'PA.S/MOL'
      PRINT*,'RLH2=   ',RLH2,'    RLYY= ',RLYY,'PA.S/MOL'
      PRINT*,'R(1)H2= ',R1H2,'    R(1)YY= ',R1YY,'PA.S/MOL'
      PRINT*,'R(1`)H2=',R(1),'    R(1`)YY= ',R11Y,'PA.S/MOL'
      PRINT*,'R(2)H2= ',R(2),'    R(2)YY= ',R2YY,'PA.S/MOL'
      PRINT*,'R(3)H2= ',R3H2,'    R(3)YY= ',R3YY,'PA.S/MOL'
      PRINT*,'AREA OF HOLE IN POLYAMIDE - A1`= A3 =',A3 ,'M2'
      PRINT*,'    '
      PRINT*,'A1=A2=',A1 ,'M2' ,'   L1=',L1 ,'M'
      PRINT*,'P1H2=',P1H2 ,'  P1YY=',P1YY,'MOL.M/SEC.M2.PA'
C
C   This part simulates membrane performance for varying substrate
C   porsities and lamination thicknesses.
C
      A32=0.1E-12
      DO 2000 II=1,18
      A33 = A32 * 2.5
      A32 = A33
      R33H2 = R3H2*(A3/A33)
      WRITE (3,120)A33
      L12 = 0.1E-6
      L1=0.0
      DO 1000 I=1,30
      R1H2=    L1/(P1H2*A1)
      R(1)=    L1/(P1H2*A33)
      RLH2=((R1H2+R(2)) * (R(1)+R33H2)) / (R1H2+R(2)+R(1)+R33H2)
      RLH2A=((AA1 * R1H2 + AA2 * R(2)) * (AA1 * R(1) + AA3 * R33H2)) /
     1(AA1*R1H2 + AA2*R(2) + AA1*R(1) + AA3*R33H2)
      AAL=RLH2A/RLH2
      LUXH2= (1/RLH2)*(1/A2)
      WRITE(4,130)A33,L1,AAL,LUXH2
      WRITE(3,140)L1,AAL,LUXH2,RLH2,R1H2,R(1),R(2),R33H2,RH2
      L1 = L12 * 1.25
      L12 = L1
 1000 CONTINUE
 2000 CONTINUE
C
 9000 CONTINUE
  100 FORMAT (78A1/78A1)
  110 FORMAT (///,T5,78A1,/,T5,78A1)
  115 FORMAT (/,2X,'A3',8X,'L1',9X,'ALPHA L',4X,'H2 FLUX')
  120 FORMAT (/,1X,'AREA OF HOLE IN POLYAMIDE = ',E12.5,' M2')
  130 FORMAT (1X,E10.3,3(1X,E10.5))
  140 FORMAT (/,1X,'L1=',E12.5,/,1X,
     1'ALPHAL=',F10.5,/,1X,'FLUX OF H2=',E12.5,/,1X,'RLH2=',E12.5,6X,
     2'R(1)H2=',E12.5,/,1X,'R(1`)H2=',E12.5,6X,'R(2)H2=',E12.5,/,1X,
     3'R(3)H2=',E12.5,6X,'RH2=',E12.5)
 9999 STOP
      END
```

```
C-----------------------------------------------------------------------
1       SUBROUTINE FCN (R,F,N)
2       INTEGER N
3       REAL R(N),F(N)
4       COMMON /ONE/ R1H2,RLH2,AA1,AA2,AAL
5       F(1)=((R1H2 + R(2)) * R(1)) / (R1H2 + R(2) + R(1)) - RLH2
6       F(2)=( (AA1 * R1H2 + AA2 * R(2)) * AA1 * R(1) ) /
          1(AA1*R1H2 + AA2*R(2) + AA1*R(1)) - RLH2*AAL
7       RETURN
8       END

C-----------------------------------------------------------------------
1       SUBROUTINE FCC (R,F,N)
2       INTEGER N
3       REAL R(N),F(N)
4       COMMON /ONE/ R1H2,RLH2,AA1,AA2,AAL,AA3,R3H2
5       F(1)=((R1H2+R(2)) * (R(1)+R3H2)) / (R1H2+R(2)+R(1)+R3H2) - RLH2
6       F(2)=((AA1 * R1H2 + AA2 * R(2)) * (AA1 * R(1) + AA3 * R3H2)) /
          1(AA1*R1H2 + AA2*R(2) + AA1*R(1) + AA3*R3H2) - RLH2*AAL
7       RETURN
8       END
```

D.2.2 Sample Data File

```
      2
MEMBRANE PA-19 AT A PRESSURE OF 2068 kPa
1.847E-10          1.185E-10
HYDROGEN / NITROGEN GAS
1.148E-11     3.226E-12      409.5          7.6693E-14
MEMBRANE PA-19 AT A PRESSURE OF 2068 kPa
1.847E-10          1.185E-10
HYDROGEN / CARBON DIOXIDE GAS
5.939E-11     2.514E-11      8.2            8.2828E-13
```

D.2.3 Execution File

```
FORTVS &1 (OPT(2)
GLOBAL TXTLIB VLNKMLIB VFORTLIB IMSL1 IMSL2 IMSL3 IMSL4 IMSLDLIB
LOAD &1 (CLEAR
GLOBAL LOADLIB VFLODLIB
FI 10 DISK SAMPLE DATA
FI 6 DISK OUTPUT LISTING  (LRECL 110
FI 4 DISK OUTPUT3 LISTING (LRECL 110
FI 3 DISK OUTPUT2 LISTING (LRECL 110
CP Q T
START
CP Q T
*COPY &1 OUTPUT A &1 LISTING A (APPEND
```

D.2.4 Output Listing

```
   MEMBRANE PA-19 AT A PRESSURE OF 2068 kPa
   HYDROGEN / NITROGEN GAS
      # OF ITERATIONS =           4
ALPHA=    16.0888367
ALPHA1=   2.19993973
ALPHA2=   409.500000
ALPHA3=   6.44168854
ALPHAL=   36.7327881
RH2=      0.562739177E+13     RYY=  0.905381790E+14 PA.S/MOL
RLH2=     0.877113586E+13     RLYY=  0.322188045E+15 PA.S/MOL
R(1)H2=   0.156473754E+12     R(1)YY=  0.344232821E+12 PA.S/MOL
R(1`)H2=  0.117923360E+15     R(1`)YY=  0.259424279E+15 PA.S/MOL
R(2)H2=   0.923733800E+13     R(2)YY=  0.378268990E+16 PA.S/MOL
R(3)H2=   0.143996916E+14     R(3)YY=  0.927583248E+14 PA.S/MOL
AREA OF HOLE IN POLYAMIDE - A1`= A3 = 0.127664771E-05 M2

A1=A2= 0.962112099E-03 M2   L1= 0.254000042E-04 M
P1H2= 0.168720018E-12   P1YY= 0.766929922E-13 MOL.M/SEC.M2.PA


   MEMBRANE PA-19 AT A PRESSURE OF 2068 kPa
   HYDROGEN / CARBON DIOXIDE GAS
      # OF ITERATIONS =           4
ALPHA=    3.10995007
ALPHA1=  0.203699231
ALPHA2=   8.19999981
ALPHA3=   1.48616695
ALPHAL=   4.71360302
RH2=      0.562739177E+13     RYY=  0.175009065E+14 PA.S/MOL
RLH2=     0.877113586E+13     RLYY=  0.413436404E+14 PA.S/MOL
R(1)H2=   0.156473754E+12     R(1)YY=  0.318735811E+11 PA.S/MOL
R(1`)H2=  0.359901080E+15     R(1`)YY=  0.733115685E+14 PA.S/MOL
R(2)H2=   0.882447797E+13     R(2)YY=  0.723607030E+14 PA.S/MOL
R(3)H2=   0.155325122E+14     R(3)YY=  0.230839057E+14 PA.S/MOL
AREA OF HOLE IN POLYAMIDE - A1`= A3 = 0.418295713E-06 M2

A1=A2= 0.962112099E-03 M2   L1= 0.254000042E-04 M
P1H2= 0.168720018E-12   P1YY= 0.828279990E-12 MOL.M/SEC.M2.PA
```